



Institute of Pure and Applied Sciences

International Journal of Advances
in Engineering and Pure Sciences

MARMARA JEPS



In the name of Rectorate of Marmara University, Rector
Prof. Dr. Mustafa KURT

In the name of Directory of Institute of Pure and Applied Sciences, Director
Prof. Dr. Bülent EKİCİ

Editor-in-Chief
Asst. Prof. Dr. Merve ER

Associate Editors
Prof. Dr. Bülent EKİCİ, Prof. Dr. Hayriye KORKMAZ

Editorial Boards

Dr. Aris Quantana NEDELCO,
Materials Science

Asst. Prof. Dr. Berçem KIRAN YILDIRIM,
Chemical Engineering

Asst. Prof. Dr. Beste TURANLI,
Bioengineering

Prof. Dr. İsmail USTA,
Textile Engineering

Prof. Dr. Kazım Yalçın ARĞA,
Bioengineering, Bioinformatics

Prof. Dr. Bülent AKKOYUNLU,
Physics

Dr. Mohammad ALSUNAIDI,
Electrical and Electronics Engineering

Prof. Dr. Mustafa ATMACA,
Mechanical Engineering-Energy

Assoc. Prof. Dr. ESRA ERKEN,
Environmental Engineering

Prof. Dr. Mustafa ÖZDEMİR,
Mechanical Engineering- System Dynamics and Mechanics

Assoc. Prof. Dr. Mustafa Taylan ŞENGÜL,
Mathematics

Assoc. Prof. Dr. Ömer KORÇAK,
Computer Science and Engineering

Assoc. Prof. Dr. Pınar ÇAĞLAYAN,
Biology

Asst. Prof. Dr. Rosa Maria FLORES,
Environmental Engineering

Dr. Sergey V. DOROZHKIN,
Bio-Materials (Ceramics)

Prof. Dr. Uğur YAHŞI,
Physics

Prof. Dr. Yahya BOZKURT,
Material Sciences

Assoc. Prof. Dr. Yeşim GÜRTUĞ,
Architectural and Civil Engineering

Publishing Editor
Oğuz Eren SÜSLÜ

Correspondance and Communication

Merve ER
Industrial Engineering, Faculty of
Engineering, M5-233 Maltepe
/ISTANBUL

Tel: +90 216 777 0 777
merve.er@marmara.edu.tr

Publisher

Marmara University Press
Göztepe Kampusu 34722
Kadıköy/ISTANBUL

Tel: +90 216 777 1408
yayinevi@marmara.edu.tr

Marmara Üniversitesi Rektörlüğü adına, *Rektör*
Prof. Dr. Mustafa KURT

Fen Bilimleri Enstitüsü Müdürlüğü adına, *Müdür*
Prof. Dr. Bülent EKİCİ

Editör

Dr. Öğr. Üyesi Merve ER

Yardımcı Editörler

Prof. Dr. Bülent EKİCİ, Prof. Dr. Hayriye KORKMAZ

Editörler Kurulu

Dr. Aris Quantana NEDELCOŞ,
Malzeme Bilimleri

Dr. Öğretim Üyesi Berçem KIRAN YILDIRIM,
Kimya Mühendisliği

Dr. Öğretim Üyesi Beste TURANLI,
Biyomühendislik

Prof. Dr. İsmail USTA,
Tekstil Mühendisliği

Prof. Dr. Kazım Yalçın ARĞA,
Biyomühendislik, Biyoinformatik

Prof. Dr. Bülent AKKOYUNLU,
Fizik

Dr. Mohammad ALSUNAİDİ,
Elektrik ve Elektronik Mühendisliği

Prof. Dr. Mustafa ATMACA,
Makine Mühendisliği- Enerji

Doç. Dr. ESRA ERKEN,
Environmental Engineering

Prof. Dr. Mustafa ÖZDEMİR,
Makine Mühendisliği- Sistem Dinamiği ve Mekaniği

Doç. Dr. Mustafa Taylan ŞENGÜL,
Matematik

Doç. Dr. Ömer KORÇAK,
Bilgisayar Bilimleri ve Mühendisliği

Doç. Dr. Pınar ÇAĞLAYAN,
Biyoloji

Dr. Öğretim Üyesi Rosa Maria FLORES,
Çevre Mühendisliği

Dr. Sergey V. DOROZHKIN,
Biyomalzemeler (Seramikler)

Prof. Dr. Uğur YAHŞI,
Fizik

Prof. Dr. Yahya BOZKURT,
Malzeme Bilimleri

Doç. Dr. Yeşim GÜRTUĞ,
Mimarlık ve İnşaat Mühendisliği

Yayın Editörü
Oğuz Eren SÜSLÜ

Yazışmalar ve İletişim

Merve ER

Endüstri Mühendisliği,
Mühendislik Fakültesi, M5-
233 Maltepe /İSTANBUL
Tel: +90 216 777 0 777
merve.er@marmara.edu.tr

Yayıncı

Marmara Üniversitesi Yayınevi
Göztepe Kampusu 34722
Kadıköy/İSTANBUL
Tel: +90 216 777 1408
yayinevi@marmara.edu.tr

İÇİNDEKİLER/ CONTENTS

Araştırma Makaleleri/ Research Articles

1. Küresel Bulanık Ortamda Çok Kriterli Karar Verme Yöntemleri ile Demir Çelik Sektöründe Tedarikçi Seçimi
Zeynep Simge BAYSAL, Berk AYVAZ, Muhammet CEYLAN
Sayfa/Page: 116 - 133
2. Synthesis, Structural Characterization and Temperature Effects on Chloroform Vapor Sensing Properties of ZnO Nanocrystals
Doruk YILDIZTEKİN, Fatih DUMLUDAĞ
Sayfa/Page: 134 - 139
3. Güneş Paneli Kusurlarının Derin Öğrenme Tabanlı Sınıflandırılması
Sebahattin Yiğit LERMİ, Tuğba Özge ONUR
Sayfa/Page: 140 - 149
4. Green Synthesis, Characterization and Antibacterial Activities of Silk Sericin Capped Zinc Oxide Nanoparticles
Aleyna TEMEL, Zehra GÜN GÖK
Sayfa/Page : 150 - 159
5. Enzymatic Bioregeneration of Activated Carbon by Laccase
Özgür AKTAŞ, Zeynep Merve TİRYAKİ, Işık ÇOBAN
Sayfa/Page : 160 - 172
6. Morphological and molecular diagnosis of the pine processionary moth in Marmara University Göztepe Campus
Semanur YAZICI, İrem Sülüm AYDOĞAN, Berfin Ece DALKIRAN, Hilal CODUR, Tunahan Irmak BAŞARAN, Barış GÖKALSIN, Nüzhet Cenk SESAL, Yavuz TURAN
Sayfa/Page : 173 - 177

Küresel Bulanık Ortamda Çok Kriterli Karar Verme Yöntemleri ile Demir Çelik Sektöründe Tedarikçi Seçimi

Supplier Selection in the Iron and Steel Industry with Multi-Criteria Decision Making Methods in a Spherical Fuzzy Environment

Zeynep Simge BAYSAL¹, Berk AYVAZ², Muhammet CEYLAN³

¹İstanbul Ticaret Üniversitesi, Mühendislik Fakültesi, Endüstri Mühendisliği Bölümü,

²İstanbul Ticaret Üniversitesi, Mühendislik Fakültesi, Endüstri Mühendisliği Bölümü,

³İstanbul Ticaret Üniversitesi, Mühendislik Fakültesi, Mekatronik Mühendisliği Bölümü, İstanbul, Türkiye

Öz

Şirketler tedarikçi seçimini gerçekleştirirken genel olarak satın alma ve rekabet stratejilerine uygun olarak belirlenmiş kriterlere dikkat etmektedirler. Fakat bu seçimi yaparken birçok zorlukla karşılaşıldığı, bu sebeple dikkat edilmesi gereken pek çok hususun bulunduğu bilinmektedir. Piyasada çok sayıda tedarikçi bulunmakta ve bu tedarikçiler içinden şirkete en uygun olanın seçilmesi amaçlanmaktadır. Tedarikçi seçim problemlerinin çözümünde genellikle Çok Kriterli Karar Verme (ÇKKV) yöntemleri uygulanmaktadır. Bahis konusu çalışmada, Avrupa Yeşil Mutabakatı kapsamında oluşturulan Sınırdaki Karbon Düzenleme Mekanizması'na tabi olan demir-çelik sektöründe faaliyet gösteren bir şirket için tedarikçi seçim problemi ele alınmıştır. Üç tedarikçinin performans değerlendirilmesi yapılarak söz konusu tedarikçiler 6 ana, 23 alt kriterde incelenmiştir. Çalışmada, Küresel Bulanık Analitik Hiyerarşi Prosesi, TOPSIS (Technique for Order Preference by Similarity to Ideal Solution) ve CODAS (Communication Disorders, Audiology and Swallowing) yöntemlerini içeren bir karar verme yaklaşımı yer almaktadır. Tedarikçilerin değerlendirilmesi sürecinde uzmanlar tarafından belirlenen kriterlerin ağırlıklarını hesaplamak için Küresel Bulanık AHP yöntemi kullanılmış olup, demir-çelik sektöründe tedarikçi seçimi aşamasında en önemli kriterin fiyat olduğu tespit edilmiştir. Küresel Bulanık TOPSIS yöntemi kullanılarak Tedarikçi 3; Küresel Bulanık CODAS yöntemiyle ise Tedarikçi 1'in en iyi alternatif olduğu belirlenerek tedarikçiler sıralanmıştır.

Anahtar Kelimeler: Çok Kriterli Karar Verme (ÇKKV); Küresel Bulanık Sayılar; AHP; TOPSIS; CODAS; Tedarikçi Seçimi

Abstract

When selecting suppliers, companies generally pay attention to criteria determined in accordance with their purchasing and competition strategies. However, it is known that many difficulties are encountered when making this choice, and therefore there are many issues that need to be taken into consideration. There are many suppliers in the market and the aim is to choose the one that is most suitable for the company among these suppliers. Multi-Criteria Decision Making (MCDM) methods are generally applied to solve supplier selection problems. In the study in question, the supplier selection problem for a company operating in the iron and steel industry that is subject to the Border Carbon Regulation Mechanism established within the scope of the European Green Deal is discussed. The performance evaluation of three suppliers was made and the suppliers in question were examined in 6 main and 23 sub-criteria. The study includes a decision-making approach that includes Spherical Fuzzy Analytical Hierarchy Process, TOPSIS (Technique for Order Preference by Similarity to Ideal Solution) and CODAS (Communication Disorders, Audiology and Swallowing) methods. During the evaluation of suppliers, the Spherical Fuzzy AHP method was used to calculate the weights of the criteria determined by the experts, and it was determined that the most important criterion was price in the supplier selection phase in the iron and steel industry. Supplier 3 selected with the Spherical Fuzzy TOPSIS method, and spherical fuzzy CODAS method, Supplier 1 was determined to be the best alternative and the suppliers were ranked.

Keywords: Multi-Criteria Decision Making (MCDM); Spherical Fuzzy Numbers; AHP; TOPSIS; CODAS; Supplier Selection

I. GİRİŞ

Günümüzde tedarikçi seçimi işletmelerin ticari faaliyetlerinin sürdürülmesi aşamasında büyük önem taşımaktadır. Tedarikçi seçimi, birbirine zıt sayısal veri içeren veya içermeyen birçok kriteri bulunan çok kriterli bir karar verme problemi olarak tanımlanmaktadır. Bu problemlerde ilgili firmaların isteklerine göre en uygun tedarikçilerin seçilmesi hedeflenmektedir. Hangi ürün veya hizmetin, hangi firmadan ne kadar alınacağını doğru bir şekilde belirlenmesi, müşteri memnuniyetinin artırılması ve firmaların rekabet yeteneğinin geliştirilmesini sağlamaktadır. Aynı sektörlerde yer alan firmalar arasında rekabet oluşmakta ve bu firmaların çetrefilli rekabet ortamında doğru bir tedarik zinciri yönetimi sağlayarak fark oluşturmaları gerekmektedir.

Son zamanlarda fosil yakıtların kullanılması, endüstriyel ve tarımsal etkinlikler sonucu meydana gelen iklim değişikliğinin olumsuz etkilerinin yoğun bir şekilde görülmesi tüm dünya için gelecek korkusu oluşturmaktadır. Küresel ısınma sebebiyle, gelişmekte ve gelişmiş ekonomilerde artan endüstriyel faaliyetlerin de sürdürülebilir olması gerekmektedir [1].

Söz konusu ticaret ortamında endüstriyel faaliyetlerini daha çevreci gerçekleştiren işletmelerin rekabet avantajı sağlaması öngörülmektedir. Adı sıkça duyulan iklim kriziyle mücadele kapsamında ülkeler ayrı ayrı hedeflerini, politikalarını ve yol haritalarını açıklamaktadır. Ülkemizin toplam ihracatının yaklaşık %41'ini gerçekleştirdiği Avrupa Birliği (AB) ise iklim kriziyle mücadele kapsamında Avrupa Yeşil Mutabakatı'nı (AYM) oluşturmuştur. Oluşturulan mutabakat kapsamında, AB'nin 2050 yılına kadar net sıfır emisyon hedefini tamamlayan ilk kıta olması, ekonomisinin yeniden şekillenmesi, sistemlerin ve tedarik zinciri yapısının sürdürülebilirlik ve yeşil dönüşüm kavramlarına uyumlu olacak şekilde yenilenmesi hedeflenmektedir. Aynı zamanda ticaret sisteminin değişmesi ve karbon emisyonunun azaltılmasına yönelik AB'de ikamet eden ithalatçı firmalara çeşitli kısıtlamaların getirilmesi öngörülmektedir.

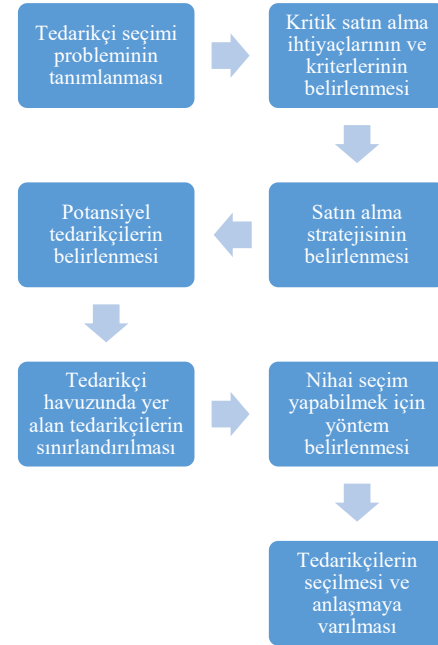
AYM kapsamında oluşturulan Sınırdan Karbon Düzenleme Mekanizması (SKDM) çerçevesinde AB'nin ithal ettiği ürünlerin karbon içeriğinin kontrol edilerek, ürünleri ithal eden firmadan belirli oranda karbon vergisi alınması planlanmaktadır [2]. 1 Ekim 2023 tarihi itibarıyla başlayan geçiş dönemi kapsamında karbon vergisine tabi olan 6 sektör (elektrik, gübre, demir-çelik, çimento, alüminyum ve hidrojen) olarak belirlenmiştir [3]. Geçiş döneminin bitmesinin ardından 2026 yılı itibarıyla diğer sektörler için de uygulanacaktır. Bu doğrultuda tüm sektörlerle yönelik tedarik zincirinin sürdürülebilir ve yeşile uyum göstermesinin iklim kriziyle mücadele kapsamında ve döngüsel ekonomi modelinde önemli rol oynayacaktır. Öte yandan, sürdürülebilir maksimum kar ve istihdam sağlamak global düzeyde yer alan işletmelerin en önemli amaçlarıdır. Firmaların mali açıdan güçlü olmalarının yalnızca satış performansına bağlı olmadığı, tedarik zinciri yönetim performansının da yukarıda bahsedilen amaçları yerine getirmek için direkt olarak etkilediği bilinmektedir. Firmaların faaliyet gösterdikleri sektörlerde ihtiyaç duydukları ürün ve hizmet alımlarında ortaya çıkan, tedarik zinciri ilişkisinde yer alan tedarikçilerin seçimi ve değerlendirilmesi elzemdir. Zaman içerisinde artış gösteren rekabet ortamı, maliyet ve ilişkilerin karmaşıklaşması gibi nedenlerin akabinde rasyonel kararların alınabilmesi için sezgiler, tecrübeler ve sınırlı bilgiler dışında karar sürecinin analitik olarak değerlendirilmesi gerekmektedir [4].

Tedarikçinin seçim kararı ve değerlendirme sürecinde çok sayıda kriter yer aldığı ve birbirleriyle çatışan bahis konusu kriterler arasından seçim yapılması gerektiği için karar verme problemleri karmaşık problemlerdir [5]. Bu karmaşık problemlerin çözümü aşamasında, pek çok becerikliliğe sahip tedarikçilerin içerisinde en efektif olanın seçilebilmesi için çok kriterli karar verme (ÇKKV) yöntemleri kullanılmaktadır. Söz konusu yöntemler sayesinde tedarikçilerin değerlendirilme süreçlerinde

birbirine çelişen nitel ve nicel kriterler kullanılarak tedarikçilerin kapsamlı bir şekilde kıyaslanması sağlanmaktadır.

İşletmelerin faaliyet gösterdikleri sektörlerdeki tedarikçilerin belirlenmesi için kullanılan kriterler firmaların gerekliliklerine bağlı olarak farklılık göstermektedir. Tedarikçi seçimi probleminde karar vericiler tarafından değerlendirilen en popüler kriterlerin; teslimat, servis, fiyat/maliyet, kalite, yönetim, teknoloji, üretim yeteneği, finans, esneklik, araştırma ve geliştirme, risk, güvenlik, ilişki ve çevre olduğu belirtilmektedir [6]. Literatür incelendiğinde tedarikçi seçim süreci yedi adımdan oluşmakta olup, Şekil 1'de yer almaktadır [7].

İlk aşamada problemin tanımlanması, tedarikçi seçim ihtiyacının olup olmaması belirlenmektedir. İkinci aşamada karar vericilerin ihtiyaçları neticesinde kriterler belirlenmektedir. Ardından niteliklerine göre potansiyel tedarikçilerin belirlenerek değerlendirilmesi ve nihai seçiminin gerçekleştirilmesi gerekmektedir.



Şekil 1. Tedarikçi Seçim Süreci

Bu çalışmada, son zamanlarda oldukça popüler olan SKDM'ye tabii olan demir-çelik sektörü baz alınarak, bu sektörde faaliyet gösteren çelik sacdan malzeme üreten bir şirket için tedarikçi seçim problemi ele alınmıştır. Buradaki kriter belirleme ve kriterlerin değerlendirilmesi işlemi 5 kişilik bir ekip tarafından yapılmıştır. Bahis konusu ekipte 2 mühendis ve 3 satın alma personeli yer almıştır. Çalışmada 3 farklı tedarikçi 6 ana, 23 alt kriter kapsamında değerlendirilmiştir. Her bir kriter uzmanların değerlendirmeleri ışığında detaylı incelenmiştir. Çalışmanın sonunda söz konusu şirket için en uygun tedarikçilerin değerlendirilmesi amaçlanmış olup, tedarikçi seçim probleminin çözülmesi için üç adet Çok Kriterli Karar Verme (ÇKKV) yöntemi kullanılmıştır. Seçim kriterlerinin ağırlıklarının belirlenebilmesi amacıyla Küresel Bulanık Analitik Hiyerarşi Prosesi yöntemi, tedarikçilerin

sıralanabilmesi aşamasında ise Küresel Bulanık TOPSIS ve Küresel Bulanık CODAS yöntemleri uygulanmıştır. Bu çalışma, beş bölümden oluşmuştur. İlk bölümde giriş yapılarak çalışma hakkında genel bilgiler verilmektedir. İkinci bölümde, literatür taramasına yer verilmektedir. Sonraki bölümde ise çok kriterli karar verme yöntemlerinden çalışmada uygulanan Küresel Bulanık AHP, TOPSIS ve CODAS yöntemlerinin metodolojisi sunulmaktadır. Dördüncü bölümde, bahsedilen yöntemler uygulanmakta ve tedarikçiler sıralanmaktadır. Beşinci bölümde ise sonuçlar ve bulgular yorumlanmaktadır. Yapılan değerlendirme sonucunda SKDM'ye tabi olan demir-çelik sektöründe tedarikçi seçimi aşamasında çevre ana kriteri başlığı altında bulunan karbon emisyonunun azaltılmasına yönelik belirlenen yeşil kriterlere pek önem verilmediği, en önemli kriterin fiyat unsuru olduğu tespit edilmiştir.

Çalışmada kullanılacak kriterlerin ve yöntemin belirlenmesine yönelik literatür taramasında 2003-2023 yılları arasında yapılan çalışmalar ve araştırmalar ele alınmıştır. Özellikle tedarikçi seçimi, yeşil tedarikçi seçimi, çok kriterli karar verme yöntemleri anahtar kelimeleri taranarak inceleme yapılmıştır.

Kahraman vd. (2003), yaptığı çalışmada Türkiye'de beyaz eşya üreticisi firma için tedarikçi seçimi problemini ele almıştır. Firmanın satın alma yöneticilerine görüşülmüş, anket uygulanmış ve kriterler belirlenmiştir. Uygulamada 3 ana kriter, 11 alt kriter belirlenerek 3 tedarikçi değerlendirilmiştir. Tedarikçilerin değerlendirilmesinde Bulanık AHP yöntemi kullanılmıştır. Soner ve Önüt, (2006) tarafından gerçekleştirilen çalışmada, havalandırma ve klima cihazları üreten bir işletmenin tedarikçi seçim problemini ele alınmıştır. Çalışmada AHP yöntemi ile 7 kriterleri değerlendirip, ELECTRE yöntemi kullanarak 5 tedarikçiyi sıralamışlardır. Tahriri vd. (2008) çalışmasında, Malezya'da bir çelik imalat şirketi için tedarikçi seçim problemini ele almış ve problemin çözümü için AHP yöntemini kullanmıştır. Çalışmada 6 ana kriter, 16 alt kriter belirlenmiş ve 4 tedarikçi değerlendirilmiştir. Büyüközkan & Çiftçi (2012) yapmış oldukları çalışmada, yeşil tedarikçi değerlendirmesi için hibrit Çok Kriterli Karar Verme Yöntemi kullanılmıştır. Uygulamada, bulanık ortamda DEMATEL, ANP ve TOPSIS yöntemleri kullanılmış, 19 kriter baz alınarak 5 tedarikçi değerlendirilmiştir. Çalışma, Türkiye'de öncü firmalardan biri olan Ford Otosan'da uygulanmıştır.

Arıkan ve Küçükçe (2013) çalışmalarında, satın alma faaliyetlerini sürdüren bir kamu kuruluşuna en uygun tedarikçinin seçilmesini hedeflemişlerdir. Kurumun tedarikçi seçiminde etkisi olacağı değerlendirilen kriterler anket çalışması sonucunda tespit edilen 6 ana kriter ve alt kriterler AHP yöntemi kullanılarak ağırlıklandırılmıştır. Yapılan çalışmada PROMETHEE II yöntemi kullanılarak 32 tedarikçi firma değerlendirilmiştir. Junior vd. (2014) yaptığı çalışmada, otomotiv üretim zincirinde yer alan bir firmanın tedarikçi seçim problemini ele alarak, problemin çözüm aşamasında Bulanık AHP-TOPSIS yöntemlerini uygulayarak 5 tedarikçiyi değerlendirmiştir. Yapılan çalışmada her iki yöntem karşılaştırılmıştır. Bronja (2015) çalışmasında, araba egzoz sisteminde kullanılacak alüminize edilmiş levha için tedarikçi seçimi gerçekleştirmiştir.

Kriterlerin ağırlıklandırılmasında Bulanık AHP yöntemi, tedarikçilerin sıralanmasında ise Bulanık TOPSIS yöntemini kullanarak, 10 kriter baz alınarak 6 tedarikçi değerlendirilmiştir. Yılmaz (2015) çalışmasında, bir firma için tedarikçi seçim problemini odaklanmıştır. Çalışmada Bulanık AHP ve Bulanık VIKOR bütünleşik yöntemi uygulanmıştır. Uygulamada fiyat, kalite, teslimat ve hizmet kalitesi kriterleri baz alınarak 3 tedarikçi değerlendirilmiştir. Kara ve Ecer (2016) çalışmasında, AHP ve VIKOR yöntemlerini kullanarak tedarikçi seçim problemini çözme amaçlamıştır. Yapılan çalışmada belirlenen ana kriterler; kalite, maliyet, profil, teslimat ve esneklik olarak verilmiştir. Bu kriterlerin 12 adet alt kriteri oluşturulmuştur. Çalışma sonucunda tüm kriterler içinde "teslimat" kriterinin en önemli olduğu tespit edilmiştir.

Tekez ve Bark (2016) çalışmasında, bir mobilya fabrikasının tedarikçi seçimi problemini çözmek için Bulanık TOPSIS yöntemi kullanılmıştır. Çalışmada 6 kriter baz alınarak 6 tedarikçi değerlendirilmiştir. Denizhan vd., (2017) yapmış olduğu çalışmada, makine imalatı sektöründe yeşil tedarikçi seçim problemini ele alarak 6 ana kriter altında 3 firmayı değerlendirmiştir. Bu değerlendirmeler esnasında AHP ve Bulanık AHP yöntemlerini uygulamıştır. Arslan ve Uysal (2017) tarafından yapılan çalışmada ağaç işleme sektöründe faaliyet gösteren bir işletmenin çok kriterli karar verme yöntemleri kullanılarak tedarikçi seçim probleminin çözümlenmesi amaçlanmıştır. Üç ham ağaç tedarikçisinin performanslarının değerlendirilmesi aşamasında ELECTRE yöntemi uygulanmıştır. Daldır ve Tosun (2018) yılında yapmış oldukları çalışmada bir işletme için yeşil tedarikçi seçimi için 3 ana kriter 12 alt kriter kullanarak, 2 uzman görüşüne başvurmuşlardır. Problemin çözümü için Bulanık WASPAS ve AHS yöntemlerini kullanmışlardır. Narayanan ve Jinesh (2018) senesinde yaptıkları çalışmada, bir döküm ünitesi için tedarikçi seçimi gerçekleştirmiştir. Problemin çözümü için SWARA ve TOPSIS yöntemleri kullanılarak 4 alternatif tedarikçi içinden en uygun olan seçilmiştir. Onat ve Kaçtıoğlu (2019) çalışmalarında, perakende sektöründe Tuzla'da depo faaliyetlerini sürdüren bir işletmenin tedarikçi seçim problemi ele alınmış olup; Çok Kriterli Karar Verme Yöntemlerinden Bulanık AHP ve Bulanık TOPSIS bütünleşik kullanılmıştır. Problemin çözümünde 5 ana kriter, 15 alt kriter belirlenmiş ve tedarikçileri 4 karar verici değerlendirmiştir. Madenoğlu (2019) yaptığı çalışma ile mobilya üretimi yapan bir firmanın yeşil tedarikçi seçim problemini ele almıştır. Çalışmadaki kriterlerin ağırlıklandırılması aşamasında Bulanık SWARA, yeşil tedarikçilerin sıralanması ve seçimi aşamasında Bulanık ARAS, Bulanık Gri İlişkisel Analiz, Bulanık TOPSIS, Bulanık VIKOR, yöntemleri kullanılmıştır. Doğan ve Akbal (2019), yaptıkları çalışmada bir üniversite hastanesinin tedarikçileri satın alma birim yöneticilerinin görüşleri alınarak 5 kriter kapsamında AHP yöntemi kullanılarak değerlendirilmiştir. Polat ve Kaçmaz (2019), çalışmalarında imalat sektöründe faaliyet gösteren Kocaeli'de yer alan bir endüstriyel makine imalat firmasının elektrik malzemelerini temin ettiği tedarikçiyi seçmesi amaçlanmıştır. Çalışmada 5 ana kriter, 17 alt kriter baz alınarak Bulanık AHP yöntemi kullanılarak tedarikçiler değerlendirilmiştir. Şekerci ve Yazıcıoğlu (2019), çalışmalarında gıda sektörüne yönelik pet şişe platformu adına yapılan tedarikçi seçim problemini ele almışlardır. Yapılan çalışmada literatür incelenerek en

çok tercih edilen kriterler belirlenerek tedarikçiler AHP yöntemi kullanılarak değerlendirilmiştir. Cezlan (2021) çok kriterli karar yöntemlerini kullanarak sağlık sektöründe yeşil tedarikçi seçimi üzerine bir çalışma gerçekleştirmiştir. Çalışmada 7 yeşil kriter ele alınmış ve söz konusu kriterler AHP yöntemi ile ağırlıklandırılmıştır. Ardından 3 tedarikçi TOPSIS yöntemi kullanılarak sıralanmış en uygun tedarikçi seçilmiştir. Unal ve Temur (2021) yeşil tedarikçi seçimi problemini ele alarak bir şirketin tedarikçilerini SF-AHP ile çözümlenmiştir. Yapılan çalışmanın sonuçlarında en önemli kriterin maliyet olduğu belirlenmiştir. Erbyık vd. (2021) tarafından yapılan çalışmada, otomotiv sektöründe yeşil tedarikçi seçimi problemi ele alınmış olup, 5 kriter altında 3 farklı tedarikçi anket yöntemi ile değerlendirilmiştir. Kriterlerin ağırlıklandırılması aşamasında SWARA yöntemi, tedarikçilerin sıralanması aşamasında ise ELECTRE yöntemi kullanılmıştır. Nebati vd. (2021) çalışmada, otobüs tedarikçisi seçimi problemini ele almış olup, ilk aşamada çok kriterli karar verme yöntemlerinden biri olan AHP yöntemi kullanarak kriter ağırlıklarını tespit etmiştir. Ardından Promethee yöntemi kullanılarak da en uygun tedarikçinin seçimi sağlanmıştır. Çalışmada 3 ana kriter, 9 alt kriter kullanılarak 3 tedarikçi değerlendirilmiştir. Afzali vd. (2022) çalışmalarında bir çelik firması için tedarikçi seçim problemini çözmeye odaklanmıştır.

Çalışmada, çok kriterli sürdürülebilir tedarikçi seçimi için Aralık Değerli Sezgisel Bulanık (IVIF) AHP ile genişletilmiş bulanık Kombinatif Mesafeye Dayalı Değerlendirmeye (CODAS) yöntemi kullanılmıştır. 3 ana kriter, 9 alt kriter belirlenerek 4 tedarikçi değerlendirilmiştir. Türkmen ve Demirel (2022) yapmış oldukları çalışmada, enerji sektöründe rol oynayan bir firma için tedarikçi seçimine odaklanmıştır. Çalışmada ÇKKV (Çok Kriterli Karar Verme) yöntemleri uygulanarak 2 karar verici, 4 alternatif tedarikçiyi 7 kriter altında incelemiştir. Kriterlerin önemini hesaplama aşamasında SWARA ve tedarikçilerin değerlendirilmesi aşamasında ise Bulanık COPRAS yöntemi kullanılmıştır. Zaralı (2022) yapmış olduğu çalışmada, alüminyum sektöründe faaliyet gösteren bir firmanın 3. parti tersine lojistik hizmet sağlayıcısının değerlendirmesi ve seçilmesi amacıyla küresel bulanık TOPSIS yöntemi uygulanmıştır. Nebati, Ayvaz ve Kuşakçı (2023), yapmış oldukları çalışmada savunma sanayiye yönelik en iyi ERP yazılım sağlayıcısına öncelik vermek amacıyla hibritleştirilmiş küresel bulanık AHP ve küresel bulanık CODAS yöntemlerini kullanmıştır.

Çalışmada kullanılacak yöntemin ve kriterlerin belirlenmesi aşamasında yukarıda belirtilen çalışmalar incelenmiş olup, Tablo 1’de özetlenmektedir

Tablo 1. Literatür Araştırması Özet Tablo

Referans	Araştırma Amacı	Yöntem	Araştırma Alanı
Erbıyık vd. [4]	Yeşil tedarikçi seçimi	SWARA - ELECTRE	Otomotiv sektörü
Onat ve Kaçtıoğlu [5]	Tedarikçi seçimi	Bulanık AHP - Bulanık TOPSIS	Perakende sektörü
Kahraman vd. [8]	Tedarikçi seçimi	Bulanık AHP	Beyaz eşya sektörü
Soner ve Öğüt [9]	Tedarikçi seçimi	AHP-ELECTRE	Havalandırma ve klima cihazları
Tahriri vd. [10]	Tedarikçi seçimi	AHP	Çelik sektörü
Büyüközkan ve Çiftçi [11]	Yeşil tedarikçi seçimi	Bulanık DEMATEL-ANP-TOPSIS	Otomotiv sektörü
Arıkan ve Küçükçe [12]	Tedarikçi seçimi	AHP – PROMETHEE II	Satın alma
Junior vd. [13]	Tedarikçi seçimi	Bulanık AHP – Bulanık TOPSIS	Otomotiv sektörü
Bronja [14]	Tedarikçi seçimi	Bulanık AHP – Bulanık TOPSIS	Araba egzozu için alüminize edilmiş levha
Yılmaz [15]	Tedarikçi seçimi	Bulanık AHP – Bulanık VIKOR	Endüstriyel fırın
Kara ve Ecer [16]	Tedarikçi seçimi	AHP – VIKOR	Tekstil sektörü
Tekez ve Bark [17]	Tedarikçi seçimi	Bulanık TOPSIS	Mobilya sektörü
Denizhan vd. [18]	Yeşil tedarikçi seçimi	AHP – Bulanık AHP	Makine imalatı sektörü
Arslan ve Uysal [19]	Tedarikçi seçimi	ELECTRE	Ahşap sektörü
Daldır ve Tosun [20]	Yeşil tedarikçi seçimi	Bulanık WASPAS – Bulanık AHS	Üretim

Tablo 1. Literatür Araştırması Özet Tablo (devamı)

Narayanan ve Jinesh [21]	Tedarikçi seçimi	SWARA - TOPSIS	Döküm sektörü
Madençoğlu [22]	Yeşil tedarikçi seçimi	Bulanık TOPSIS – VIKOR- ARAS- Bulanık Gri İlişkisel Analiz	Mobilya sektörü
Doğan ve Akbal [23]	Tedarikçi seçimi	AHP	Sağlık sektörü
Polat ve Kaçmaz [24]	Tedarikçi seçimi	Bulanık AHP	Endüstriyel makine imalat sektörü
Şekerci ve Yazıcıoğlu [25]	Tedarikçi seçimi	AHP	Gıda sektörü
Cezlan [26]	Yeşil tedarikçi seçimi	AHP - TOPSIS	Sağlık sektörü
Unal ve Temur [27]	Yeşil tedarikçi seçimi	SF AHP	İşletme
Nebati vd. [28]	Tedarikçi seçimi	AHP - PROMETHEE	Ulaşım sektörü
Afzali vd. [29]	Tedarikçi seçimi	IVIF AHP - CODAS	Çelik sektörü
Türkmen ve Demirel [30]	Tedarikçi seçimi	SWARA – Bulanık COPRAS	Enerji sektörü
Zaralı [31]	Tedarikçi seçimi	SF TOPSIS	Alüminyum sektörü
Nebati vd. [32]	ERP seçimi	SF AHP-CODAS	Bilişim sektörü

Kaynak taramasında demir çelik sektöründe tedarikçi seçimine ilişkin olarak küresel bulanık AHP, TOPSIS ve CODAS yaklaşımlarının bir arada bulunduğu bir çalışma tespit edilmemiş olmakla birlikte, demir-çelik sektöründe tedarikçi seçim problemine ilişkin hibrit çok kriterli karar verme yöntemleri kullanılarak yapılan bir çalışmaya da rastlanılmamıştır.

II. MATERYAL VE YÖNTEM

Bu bölümde kriterlerin ağırlıklandırılması ve tedarikçilerin sıralanması problemleri için kullanılacak üç yöntemin aşamalarına yer verilmektedir. İlk olarak Küresel Bulanık AHP yöntemi ardından TOPSIS ve CODAS yöntemi açıklanmaktadır.

2.1 Küresel Bulanık AHP Yöntemi

Küresel bulanık kümelerle birlikte kullanımı yaygın ÇKKV yöntemlerinden biri olan AHP yöntemi problem çözerken kriterler arasındaki ilişkiyi ikili karşılaştırma yöntemi kullanarak önem derecelerinin tespit edilmesini sağlamaktadır. Küresel AHP yönteminin uygulanması için gerekli aşamalar aşağıda sunulmaktadır.

Aşama 1: Problemin çözümlenmesine ilişkin olarak literatür ve alternatiflere göre kriterler belirlenerek hiyerarşik yapı oluşturulur.

Aşama 2: Kriterlerin birbirleriyle etkileşimlerinin analiz edilmesine yönelik oluşturulan ikili karşılaştırma matrisleri, karar verici uzmanlardan alınan bilgiler doğrultusunda Tablo 2’de gösterilen sözel terimler kullanılarak tanımlanır.

Tablo 2. Dilsel Ölçek, Puan İndeksleri ve Karşılık Gelen Küresel Bulanık Sayılar [33]

Sözel terimler	Score İndeksi (SI)	(u, v, π)
Kesinlikle daha fazla önemli (KFÖ)	9	(0.9,0.1,0.1)
Çok yüksek önemli (ÇYÖ)	7	(0.8,0.2,0.2)
Yüksek önemli (YÖ)	5	(0.7,0.3,0.3)
Biraz fazla önemli (BFÖ)	3	(0.6,0.4,0.4)
Eşit önemli (EÖ)	1	(0.5,0.5,0.5)
Biraz düşük önemli (BDÖ)	1/3	(0.4,0.6,0.4)
Düşük önemli (DÖ)	1/5	(0.3,0.7,0.3)
Çok düşük önemli (ÇDÖ)	1/7	(0.2,0.8,0.2)
Kesinlikle daha düşük önemli (KDÖ)	1/9	(0.1,0.9,0.1)

Aşama 3: Tüm kriterler sözel terimlere dönüştürülür ve küresel bulanık ikili karşılaştırma matrisleri oluşturulur.

$$A = \begin{bmatrix} 1 & \tilde{a}_{12} & \dots & \tilde{a}_{1n} \\ \tilde{a}_{21} & \dots & \dots & \vdots \\ \vdots & \vdots & \dots & \vdots \\ \tilde{a}_{n1} & \dots & \dots & 1 \\ \vdots & \vdots & \dots & \vdots \end{bmatrix} \quad (1)$$

Aşama 4. Oluşturulan ikili karşılaştırma matrislerinin tutarlılığı puan endeksleri kullanarak incelenir. λ_{max} ikili karşılaştırma karar matrisinin maksimum veya temel özdeğeridir. Yapılan hesaplama göre CR değerinin 0,1 değerinden küçük olması matrisin tutarlılığı olduğu anlamına gelmektedir. 0,1 değerinde büyük olması durumunda ise verilerin tutarsız olduğu ve uzmanların yeniden değerlendirilmesi gerektiği değerlendirilir.

Aşama 5. Küresel ağırlıklı aritmetik ortalama operatörü (SWAM) kullanılarak her bir kritere göre küresel bulanık AHP ağırlıkları hesaplanır.

$$SWAM_w = (w_1 \tilde{B}_{S1} + w_2 \tilde{B}_{S2} + \dots + w_n \tilde{B}_{Sn}) \\ = \left(\left[1 - \prod_{i=1}^n (1 - \mu_{\tilde{A}_{Si}}^2)^{w_i} \right]^{1/2}, \prod_{i=1}^n v_{\tilde{A}_{Si}}^{w_i}, \left[\prod_{i=1}^n (1 - \mu_{\tilde{A}_{Si}}^2)^{w_i} - \prod_{i=1}^n (1 - \mu_{\tilde{A}_{Si}}^2 - \pi_{\tilde{A}_{Si}}^2)^{w_i} \right]^{1/2} \right) \quad (2)$$

Aşama 6. Aşağıdaki denklemi kullanarak kriterlerin önem düzeylerinin belirlenmesi için küresel bulanık sayılardan net sayı değerlerinin elde edilmesi amacıyla berraklaştırma yapılır.

$$S(\tilde{w}_j^s) = \sqrt{100 * \left[\left(3\mu_{\tilde{A}_s} - \frac{\pi_{\tilde{A}_s}}{2} \right)^2 - \left(\frac{v_{\tilde{A}_s}}{2} - \pi_{\tilde{A}_s} \right)^2 \right]} \quad (3)$$

Aşama 7. AHP yönteminde ikili karşılaştırma matrislerinin normalizasyonu için her öğenin kendi sütun toplamına bölünmesi gerekmektedir. Eşitlik 4 kullanılarak normalizasyon işlemi gerçekleştirilir.

$$W_j = \frac{s(\tilde{w}_j^s)}{\sum_{i=1}^n s(\tilde{w}_i^s)} \quad (4)$$

Aşama 8. Ana ve alt kriterlerin global ağırlıkları hesaplanır. Bu aşamada alt kriterlerin normalize yerel ağırlıkları ile ana kriterlerin yerel ağırlıkları çarpılır. Yapılan işlemlerin sonunda tüm kriterlerin hesaplanan ağırlıkları toplamının 1 olması gerekmektedir.

2.2 Küresel Bulanık TOPSIS Metodu

TOPSIS yöntemi ÇKKV yöntemleri arasında en yaygın olarak kullanılan yöntemlerin başında gelmektedir. Kullanım alanının kapsamlı ve uygulama aşamalarının diğer yöntemlere kıyasla daha anlaşılır olmasıyla birlikte karar verilirken pozitif ideal çözüme en yakınlık sağlaması sebebiyle bulanık setlerde oldukça fazla kullanılan ÇKKV yöntemidir [34]. Bahis konusu yöntemin aşamaları aşağıda sıralanmaktadır.

Aşama 1. Karar verici uzmanlardan gelen cevaplar kullanılarak karar matrisinin Tablo 1'de yer alan dilsel değerlere göre oluşturulur.

Aşama 2. Karar verici uzmanların ilettiği cevaplar Eşitlik 2'de belirtilen SWAM operatörü ile birleştirilir.

Aşama 2.a. Karar verici uzman kişilerin değerlendirmeleri baz alınarak kriter ağırlıkları birleştirilir ve kriterlerin ağırlıkları toplamının 1'e eşit olması sağlanır.

Aşama 2.b. Karar vericilerin değerlendirmeleri sonucunda elde edilen birleştirilmiş küresel bulanık karar matrisi Eşitlik 5'te belirtildiği üzere oluşturulur.

$$D = (C_j(X_i))_{m \times n} = \begin{pmatrix} (\mu_{11}, v_{11}, \pi_{11}) & (\mu_{12}, v_{12}, \pi_{12}) & \dots & \dots & \dots & (\mu_{1n}, v_{1n}, \pi_{1n}) \\ (\mu_{21}, v_{21}, \pi_{21}) & (\mu_{22}, v_{22}, \pi_{22}) & \dots & \dots & \dots & (\mu_{2n}, v_{2n}, \pi_{2n}) \\ \dots & \dots & \dots & \dots & \dots & \dots \\ (\mu_{m1}, v_{m1}, \pi_{m1}) & (\mu_{m2}, v_{m2}, \pi_{m2}) & \dots & \dots & \dots & (\mu_{mn}, v_{mn}, \pi_{mn}) \end{pmatrix} \quad (5)$$

Aşama 3. Kriterlerin ağırlıkları ve alternatif derecelerinin belirlenmesinin ardından kümelenmiş ağırlıklı küresel bulanık karar matrisi oluşturulur.

Aşama 4. Aşağıdaki eşitlik kullanılarak toplu ağırlıklı karar matrisi bulanıklaştırılır.

$$\text{Score}((C_j(X_{iw}))) \\ = (\mu_{ijw} - \pi_{ijw})^2 - (v_{ijw} - \pi_{ijw})^2 \quad (6)$$

Aşama 5. Eşitlik 6 ile elde edilen puan değerlerine göre Eşitlik 7 ve Eşitlik 8 kullanılarak Küresel Bulanık Pozitif İdeal Çözüm (SF-PIS) belirlenmektedir. Aynı şekilde Eşitlik 9 ve Eşitlik 10 uygulanarak Küresel Bulanık Negatif İdeal Çözüm (SF-NIS) elde edilmektedir.

SF-PIS için:

$$X^* = \{C_j, \max_i < \text{Score}((C_j(X_{iw}))) > j \\ = 1, 2, \dots, n\} \quad (7)$$

$$X^* = \{ \langle C_1, (\mu_1^*, v_1^*, \pi_1^*) \rangle, \langle C_2, (\mu_2^*, v_2^*, \pi_2^*) \rangle \dots \} \\ \langle C_n, (\mu_n^*, v_n^*, \pi_n^*) \rangle \quad (8)$$

SF-NIS için:

$$X^- = \{C_j, \min_i < \text{Score}((C_j(X_{iw}))) > j \\ = 1, 2, \dots, n\} \quad (9)$$

$$X^- = \{ \langle C_1, (\mu_1^-, v_1^-, \pi_1^-) \rangle, \langle C_2, (\mu_2^-, v_2^-, \pi_2^-) \rangle \dots \} \\ \langle C_n, (\mu_n^-, v_n^-, \pi_n^-) \rangle \quad (10)$$

Aşama 6. Tedarikçi X_i ile SF-NIS ve SF-PIS arasındaki mesafelerin sırasıyla hesaplanması gerekmektedir. Bu adım için normalleştirilmiş Öklid mesafesi kullanılır.

SF-PIS için:

$$D(X_i, X^*) \\ = \sqrt{\frac{1}{2n} \sum_{i=1}^n (\mu_{X_i} - \mu_{X^*})^2 + (v_{X_i} - v_{X^*})^2 + (\pi_{X_i} - \pi_{X^*})^2} \quad (11)$$

SF-NIS için:

$$D(X_i, X^-) = \sqrt{\frac{1}{2n} \sum_{i=1}^n (\mu_{X_i} - \mu_{X^-})^2 + (v_{X_i} - v_{X^-})^2 + (\pi_{X_i} - \pi_{X^-})^2} \quad (12)$$

Aşama 7. SF-NIS'e olan maksimum mesafenin ve SF-PIS'e olan minimum mesafenin belirlenmesi gerekmektedir.

SF-PIS için:

$$D_{\min}(X_i, X^*) = \min_{1 \leq i \leq m} D(X_i, X^*) \quad (13)$$

SF-NIS için:

$$D_{\max}(X_i, X^-) = \max_{1 \leq i \leq m} D(X_i, X^-) \quad (14)$$

Aşama 8. Eşitlik 13 ve Etkinlik 14'te yer alan denklemlerden faydalanılmaktadır. Yakınlık oranının hesaplanması için Eşitlik 15 kullanılmaktadır.

$$\xi(X_i) = \frac{D(X_i, X^*)}{D_{\min}(X_i, X^*)} - \frac{D(X_i, X^-)}{D_{\max}(X_i, X^-)} \quad (15)$$

Adım 9: Alternatiflerin/tedarikçilerin optimal sıralama sırasının ve optimal alternatifin belirlenmesi gerekmektedir. Yukarıdaki denklem kullanılarak yakınlık oranının artan değerlerine göre alternatifler sıralanmaktadır.

2.3 Küresel Bulanık CODAS

Aşama 1. Karar matrisinin her bir karar verici için oluşturulması gerekir. Sözel terimleri kullanarak karar matrisleri oluşturulur.

Aşama 2. Karar vericilerden alınan cevaplar Eşitlik 2'de belirtilen SWAM operatörü ile birleştirilir.

Aşama 3. Bireysel karar matrislerine dayalı olarak toplu küresel bulanık karar matrisi Eşitlik 4'teki şekilde oluşturulur.

Aşama 4. Kümelenmiş ağırlıklı küresel bulanık karar matrisi hesaplanır. Kriter ağırlıkları ve alternatiflerin derecelendirmeleri belirlendikten sonra, çarpma operatörü ile birleştirilmiş ağırlıklı küresel bulanık karar matrisi oluşturulur.

Aşama 5. Eşitlik 16'da belirtildiği üzere puan fonksiyonunu (SCF) kullanarak toplu ağırlıklı karar matrisinin bulanıklaştırılması gerekir.

$$\begin{aligned} SCF(E_j(Y_{iw})) \\ = \left(\mu_{ij}^w - \frac{\pi_{ij}^w}{2} \right)^2 - \left(v_{ij}^w - \frac{\pi_{ij}^w}{2} \right)^2 \end{aligned} \quad (16)$$

Aşama 6. Beşinci adımdaki puanlara göre Küresel Bulanık Negatif İdeal Çözümün (SF-NIS) bulunması gereklidir. Karşılık gelen SF sayıları, net minimum puanlara göre belirlenmektedir.

$$\tilde{X}^- = \{C_j, \min_i \langle SCF(E_j(Y_{iw})) \rangle \mid j = 1, 2, 3, \dots, n\} \quad (17)$$

$$\left\{ \langle C_1, (\mu_1^-, v_1^-, \pi_1^-) \rangle, \langle C_2, (\mu_2^-, v_2^-, \pi_2^-) \rangle, \dots, \langle C_n, (\mu_n^-, v_n^-, \pi_n^-) \rangle \right\} \quad (18)$$

Aşama 7. \tilde{X}_i ve \tilde{X}^- alternatifleri arasındaki mesafeler hesaplanmalıdır. Bu adım için Eşitlik 19 ve Eşitlik 20'de yer alan normalleştirilmiş Öklid mesafesi ve küresel mesafe denklemleri kullanılır.

$$\begin{aligned} Dis_{Euc}(\tilde{X}_i, \tilde{X}^-) \\ = \sqrt{\frac{1}{2n} \sum_{i=1}^n (\mu_{X_i} - \mu_{X^-})^2 + (v_{X_i} - v_{X^-})^2 + (\pi_{X_i} - \pi_{X^-})^2} \end{aligned} \quad (19)$$

$$Dis_{Sph}(\tilde{X}_i, \tilde{X}^-) = \frac{1}{\pi n} \sum_{i=1}^n \arccos(\mu_{X_i} \times \mu_{X^-} + v_{X_i} \times v_{X^-} + \pi_{X_i} \times \pi_{X^-}) \quad (20)$$

Aşama 8. Eşitlik 22 aracılığıyla herhangi iki alternatif arasında göreceli değerlendirme matrisi (RA) oluşturulur.

$$RA = [h_{ip}]_{m \times m} \quad (21)$$

$$\begin{aligned} h_{ip} = & (Dis_{Euc_i} - Dis_{Euc_p}) \\ & + \left(\delta (Dis_{Euc_i} - Dis_{Euc_p}) \right. \\ & \left. \times (Dis_{Sph_i} - Dis_{Sph_p}) \right) \end{aligned} \quad (22)$$

Aşama 9. Her alternatifin değerlendirme puanlarının (H_i) azalan değerlerine göre sıralanması gerekmektedir. En yüksek (H_i)'ye sahip alternatif, alternatifler arasındaki en iyi seçimdir.

$$H_i = \sum_{p=1}^m h_{ip} \quad (23)$$

III. UYGULAMA

Çalışmanın bu bölümünde demir çelik sektöründe faaliyet gösteren, ihracat yapan bir şirket için tedarikçi seçim problemi ele alınmaktadır. Söz konusu şirketin, Paris İklim Anlaşması'nın imzalanmasının ardından, AB tarafından oluşturulan Avrupa Yeşil Mutabakatı kapsamında AB'ye ihraç edilen ürünlerin karbon emisyonlarının hesaplanması gerekmekte, ithalatçılardan karbon vergisi talep edilmektedir. Bu çerçevede, ithalatçının düşük karbon vergisi ödemesi veya ödememesi rekabet avantajı sağlamaktadır. Dolayısıyla ihraç edilen ürünleri oluşturan, üretim süreçlerine dahil edilen ürünlerin talep edildiği tedarikçilerin seçimi önemlidir.

Çalışmada firma için uygun tedarikçinin seçilmesi hedeflenmektedir. Bu problem için demir-çelik firmalarında çalışan belirlenmiş farklı kişilere, tedarikçi seçiminde dikkat edilen kriterler sorulmaktadır. Buradaki kriter belirleme işlemi 5 kişilik uzman bir ekip tarafından yapılmıştır. Yapılan değerlendirme sonunda 6 ana kriter ve 23 alt kriter belirlenmiş ve puanlanmıştır. Belirlenen kriterler Tablo 3'te sunulmaktadır.

Tablo 3. Demir Çelik Sektöründe Tedarikçi Seçimi Kapsamında Belirlenen Ana ve Alt Kriterler

	Ana Kriterler	Alt Kriterler
	Tedarikçi Seçim Kararı	Kalite (Ka)
Fiyat (Fi)		Taşıma maliyeti (Fi ₁) Fiyat opsiyonu (Fi ₂) Maliyet (Fi ₃) Paketleme (Fi ₄) Vadeli satış (Fi ₅)
Teslimat (Te)		Teslimat süresi (Te ₁) Teslimat güvenilirliği (Te ₂)
Çevre (Ce)		Eko tasarım (Ce ₁) Kaynak kullanımı (Ce ₂) Kirlilik kontrolü (Ce ₃) Çevre yönetim sistemleri (Ce ₄) Yeşil imaj (Ce ₅) Yeşil üretim (Ce ₆) Yeşil lojistik (Ce ₇) Geri dönüşüm oranı (Ce ₈)
İletişim (İİ)		Ulaşılabilirlik (İİ ₁) Şeffaflık (İİ ₂)
Kurumsal İtibar (Ki)		Tecrübe (Ki ₁) Referans (Ki ₂)

Beş uzmanın görüşlerinden oluşturulan ikili karşılaştırma matrisleri SWAM operatörü ile birleştirilerek, KVortak'a (ortak karar verici) ait karar matrisi oluşturulmuştur. Önce ana kriterlerin ardından alt kriterlerin ikili karşılaştırmaları yapılmış olup, ağırlıkları hesaplanmıştır.

Son olarak global ağırlıklar hesaplanmıştır. Ana ve alt kriterlere ilişkin birleştirilmiş karar matrisleri Tablo 4, Tablo 5, Tablo 6, Tablo 7, Tablo 8, Tablo 9, Tablo 10'da verilmiştir.

Tablo 4. Ana Kriterlere Ait Birleştirilmiş Karar Matrisi

	Ka	Fi	Te
Ka	(0.50, 0.50, 0.50)	(0.40, 0.49, 0.31)	(0.49, 0.41, 0.31)
Fi	(0.49, 0.40, 0.31)	(0.50, 0.50, 0.50)	(0.64, 0.30, 0.30)
Te	(0.41, 0.49, 0.31)	(0.30, 0.64, 0.30)	(0.50, 0.50, 0.50)
Ce	(0.34, 0.58, 0.31)	(0.36, 0.56, 0.33)	(0.37, 0.53, 0.31)
İİ	(0.41, 0.55, 0.41)	(0.34, 0.60, 0.32)	(0.43, 0.41, 0.28)
Ki	(0.28, 0.48, 0.18)	(0.35, 0.58, 0.35)	(0.41, 0.55, 0.41)

Tablo 4. Ana Kriterlere Ait Birleştirilmiş Karar Matrisi (devamı)

	Ce	İİ	Ki
Ka	(0.58, 0.34, 0.31)	(0.58, 0.41, 0.41)	(0.48, 0.28, 0.18)
Fi	(0.56, 0.36, 0.33)	(0.60, 0.34, 0.32)	(0.58, 0.35, 0.35)
Te	(0.53, 0.37, 0.31)	(0.45, 0.37, 0.24)	(0.58, 0.41, 0.41)
Ce	(0.50, 0.50, 0.50)	(0.57, 0.32, 0.28)	(0.40, 0.40, 0.24)
İİ	(0.32, 0.57, 0.28)	(0.50, 0.50, 0.50)	(0.40, 0.49, 0.31)
Ki	(0.36, 0.56, 0.32)	(0.46, 0.40, 0.30)	(0.50, 0.50, 0.50)

Tablo 5. Kalite Ana Kriterinin Alt Kriterlerine Ait Birleştirilmiş Karar Matrisi

	Ka₁	Ka₂	Ka₃	Ka₄
Ka₁	(0.50, 0.50, 0.50)	(0.49, 0.40, 0.32)	(0.36, 0.56, 0.33)	(0.37, 0.61, 0.34)
Ka₂	(0.40, 0.49, 0.32)	(0.50, 0.50, 0.50)	(0.36, 0.55, 0.30)	(0.36, 0.61, 0.36)
Ka₃	(0.54, 0.38, 0.35)	(0.53, 0.37, 0.32)	(0.50, 0.50, 0.50)	(0.34, 0.60, 0.32)
Ka₄	(0.61, 0.37, 0.34)	(0.61, 0.36, 0.36)	(0.60, 0.34, 0.32)	(0.50, 0.50, 0.50)

Tablo 6. Fiyat Ana Kriterinin Alt Kriterlerine Ait Birleştirilmiş Karar Matrisi

	F_{i1}	F_{i2}	F_{i3}
F_{i1}	(0.50, 0.50, 0.50)	(0.60, 0.27, 0.23)	(0.36, 0.56, 0.36)
F_{i2}	(0.27, 0.60, 0.23)	(0.50, 0.50, 0.50)	(0.55, 0.42, 0.42)
F_{i3}	(0.56, 0.36, 0.36)	(0.42, 0.55, 0.42)	(0.50, 0.50, 0.50)
F_{i4}	(0.39, 0.59, 0.39)	(0.36, 0.61, 0.36)	(0.37, 0.61, 0.37)
F_{i5}	(0.37, 0.58, 0.34)	(0.43, 0.55, 0.40)	(0.33, 0.61, 0.28)

Tablo 6. Fiyat Ana Kriterinin Alt Kriterlerine Ait Birleştirilmiş Karar Matrisi (devamı)

	F_{i4}	F_{i5}
F_{i1}	(0.59, 0.39, 0.39)	(0.58, 0.37, 0.34)
F_{i2}	(0.61, 0.36, 0.36)	(0.55, 0.43, 0.40)
F_{i3}	(0.61, 0.37, 0.37)	(0.61, 0.33, 0.28)
F_{i4}	(0.50, 0.50, 0.50)	(0.41, 0.46, 0.30)
F_{i5}	(0.46, 0.51, 0.30)	(0.50, 0.50, 0.50)

Tablo 7. Teslimat Ana Kriterinin Alt Kriterlerine Ait Birleştirilmiş Karar Matrisi

	Te_1	Te_2
Te_1	(0.50, 0.50, 0.50)	(0.55, 0.39, 0.33)
Te_2	(0.39, 0.55, 0.33)	(0.50, 0.50, 0.50)

Tablo 8. Çevre Ana Kriterinin Alt Kriterlerine Ait Birleştirilmiş Karar Matrisi

	Ce_1	Ce_2	Ce_3	Ce_4
Ce_1	(0.50, 0.50, 0.50)	(0.45, 0.53, 0.45)	(0.30, 0.62, 0.30)	(0.40, 0.49, 0.31)
Ce_2	(0.53, 0.45, 0.45)	(0.50, 0.50, 0.50)	(0.47, 0.44, 0.33)	(0.53, 0.45, 0.41)
Ce_3	(0.62, 0.30, 0.30)	(0.44, 0.47, 0.33)	(0.50, 0.50, 0.50)	(0.56, 0.39, 0.36)
Ce_4	(0.49, 0.40, 0.31)	(0.45, 0.53, 0.41)	(0.39, 0.56, 0.36)	(0.50, 0.50, 0.50)

Tablo 8. Çevre Ana Kriterinin Alt Kriterlerine Ait Birleştirilmiş Karar Matrisi (devamı)

	Ce_5	Ce_6	Ce_7	Ce_8
Ce_5	(0.50, 0.50, 0.50)	(0.49, 0.41, 0.31)	(0.43, 0.55, 0.43)	(0.41, 0.45, 0.26)
Ce_6	(0.41, 0.49, 0.31)	(0.50, 0.50, 0.50)	(0.35, 0.60, 0.35)	(0.45, 0.53, 0.45)
Ce_7	(0.55, 0.43, 0.43)	(0.60, 0.35, 0.35)	(0.50, 0.50, 0.50)	(0.65, 0.32, 0.32)
Ce_8	(0.45, 0.41, 0.26)	(0.53, 0.45, 0.45)	(0.32, 0.65, 0.32)	(0.50, 0.50, 0.50)

Tablo 9. İletişim Ana Kriterinin Alt Kriterlerine Ait Birleştirilmiş Karar Matrisi

	$İ_1$	$İ_2$
$İ_1$	(0.50, 0.50, 0.50)	(0.55, 0.43, 0.33)
$İ_2$	(0.43, 0.50, 0.33)	(0.50, 0.50, 0.50)

Tablo 10. Kurumsal İtibar Ana Kriterinin Alt Kriterlerine Ait Birleştirilmiş Karar Matrisi

	Ki_1	Ki_2
Ki_1	(0.50, 0.50, 0.50)	(0.46, 0.34, 0.20)
Ki_2	(0.34, 0.46, 0.20)	(0.50, 0.50, 0.50)

Birleştirilmiş matrislerin oluşturulmasının ardından kriterlere ilişkin küresel bulanık ağırlıklar SWAM operatörü kullanılarak hesaplanmış olup, skor fonksiyonu ile durulaştırılmıştır. Sütun toplamı sütun değerlerine bölünerek normalize edilmiş ve yerel ağırlıklar bulunmuştur. Bununla

birlikte, ana kriterler için hesaplanan ve Tablo 11’de yer alan normalize yerel ağırlıklar ve alt kriterlere ait normalize yerel ağırlıklar çarpılarak global ağırlıklar hesaplanmış, Tablo 12’de gösterilmiştir.

Tablo 11. Ana Kriterlere Ait Ağırlıklar

	<i>Küresel Bulanık Ağırlıklar</i>	<i>Berraklaştırılmış Ağırlıklar</i>	<i>Normalize Yerel Ağırlıklar</i>
Ka	(0.55, 0.45, 0.39)	14.45	0.184
Fi	(0.61, 0.42, 0.39)	16.23	0.206
Te	(0.51, 0.52, 0.39)	13.35	0.170
Ce	(0.47, 0.53, 0.37)	12.24	0.156
İl	(0.44, 0.57, 0.39)	11.26	0.143
Ki	(0.44, 0.56, 0.39)	11.12	0.141

Tablo 12. Alt Kriterlere Ait Ağırlıklar

	<i>Küresel Bulanık Ağırlıklar</i>	<i>Berraklaştırılmış Ağırlıklar</i>	<i>Normalize Yerel Ağırlıklar</i>	<i>Global Ağırlıklar</i>
<i>Kalite Ana Kriterinin Alt Kriterleri</i>				
Ka₁	(0.08, 0.12, 0.06)	2.13	0.193	0.036
Ka₂	(0.07, 0.13, 0.06)	1.84	0.167	0.031
Ka₃	(0.10, 0.10, 0.06)	2.79	0.254	0.047
Ka₄	(0.15, 0.07, 0.06)	4.25	0.386	0.031
<i>Fiyat Ana Kriterinin Alt Kriterleri</i>				
Fi₁	(0.54, 0.44, 0.38)	14.22	0.225	0.046
Fi₂	(0.52, 0.47, 0.40)	13.46	0.213	0.044
Fi₃	(0.55, 0.43, 0.39)	14.36	0.227	0.047
Fi₄	(0.41, 0.56, 0.39)	10.34	0.164	0.034
Fi₅	(0.42, 0.54, 0.38)	10.82	0.171	0.035
<i>Teslimat Ana Kriterinin Alt Kriterleri</i>				
Te₁	(0.35, 0.30, 0.28)	9.00	0.549	0.093
Te₂	(0.30, 0.35, 0.28)	7.39	0.451	0.077
<i>Çevre Ana Kriterinin Alt Kriterleri</i>				
Ce₁	(0.58, 0.60, 0.50)	14.84	0.123	0.019
Ce₂	(0.66, 0.53, 0.51)	16.95	0.140	0.022
Ce₃	(0.66, 0.50, 0.46)	17.24	0.142	0.022
Ce₄	(0.59, 0.58, 0.49)	15.00	0.124	0.019
Ce₅	(0.55, 0.62, 0.49)	13.85	0.114	0.018
Ce₆	(0.52, 0.65, 0.50)	13.13	0.108	0.017
Ce₇	(0.63, 0.58, 0.49)	16.28	0.134	0.021
Ce₈	(0.54, 0.63, 0.48)	13.81	0.114	0.018
<i>İletişim Ana Kriterinin Alt Kriterleri</i>				
İl₁	(0.33, 0.31, 0.28)	8.37	0.519	0.074
İl₂	(0.31, 0.33, 0.28)	7.75	0.481	0.069
<i>Kurumsal İletişim Ana Kriterinin Alt Kriterleri</i>				
Ki₁	(0.32, 0.28, 0.25)	8.13	0.535	0.076
Ki₂	(0.28, 0.32, 0.25)	7.07	0.465	0.066

3.1 Küresel Bulanık TOPSIS Uygulaması

Kriterlere ait ağırlıkların belirlenmesinin ardından, SF-TOPSIS yöntemi kullanılarak demir-çelik sektöründe faaliyet gösteren şirketin 3 tedarikçisi karar vericiler

tarafından değerlendirilmiştir. Karar vericilerden gelen cevaplara ilişkin küresel bulanık matrisler Tablo 13, Tablo 14 ve Tablo 15 ile belirtilmiştir.

Tablo 13. Uzman 1-Tedarikçilerin Değerlendirmesinin Küresel Bulanık Küme Karşılıkları

Tedarikçiler	Ka ₁	Ka ₂	Ka ₃	Ka ₄
Ted-1	(0.7, 0.3, 0.3)	(0.9, 0.1, 0.1)	(0.5, 0.5, 0.5)	(0.5, 0.5, 0.5)
Ted-2	(0.7, 0.3, 0.3)	(0.7, 0.3, 0.3)	(0.9, 0.1, 0.1)	(0.9, 0.1, 0.1)
Ted-3	(0.5, 0.5, 0.5)	(0.5, 0.5, 0.5)	(0.7, 0.3, 0.3)	(0.9, 0.1, 0.1)
	Fi ₁	Fi ₂	Fi ₃	Fi ₄
Ted-1	(0.3, 0.7, 0.3)	(0.5, 0.5, 0.5)	(0.3, 0.7, 0.3)	(0.3, 0.7, 0.3)
Ted-2	(0.5, 0.5, 0.5)	(0.5, 0.5, 0.5)	(0.7, 0.3, 0.3)	(0.5, 0.5, 0.5)
Ted-3	(0.5, 0.5, 0.5)	(0.5, 0.5, 0.5)	(0.5, 0.5, 0.5)	(0.3, 0.7, 0.3)
	Fi ₅	Te ₁	Te ₂	Ce ₁
Ted-1	(0.5, 0.5, 0.5)	(0.7, 0.3, 0.3)	(0.7, 0.3, 0.3)	(0.7, 0.3, 0.3)
Ted-2	(0.3, 0.7, 0.3)	(0.7, 0.3, 0.3)	(0.7, 0.3, 0.3)	(0.9, 0.1, 0.1)
Ted-3	(0.3, 0.7, 0.3)	(0.9, 0.1, 0.1)	(0.9, 0.1, 0.1)	(0.5, 0.5, 0.5)
	Ce ₂	Ce ₃	Ce ₄	Ce ₅
Ted-1	(0.7, 0.3, 0.3)	(0.7, 0.3, 0.3)	(0.7, 0.3, 0.3)	(0.7, 0.3, 0.3)
Ted-2	(0.9, 0.1, 0.1)	(0.9, 0.1, 0.1)	(0.9, 0.1, 0.1)	(0.7, 0.3, 0.3)
Ted-3	(0.9, 0.1, 0.1)	(0.5, 0.5, 0.5)	(0.5, 0.5, 0.5)	(0.5, 0.5, 0.5)
	Ce ₆	Ce ₇	Ce ₈	İ ₁
Ted-1	(0.7, 0.3, 0.3)	(0.5, 0.5, 0.5)	(0.9, 0.1, 0.1)	(0.7, 0.3, 0.3)
Ted-2	(0.9, 0.1, 0.1)	(0.5, 0.5, 0.5)	(0.9, 0.1, 0.1)	(0.5, 0.5, 0.5)
Ted-3	(0.7, 0.3, 0.3)	(0.7, 0.3, 0.3)	(0.7, 0.3, 0.3)	(0.7, 0.3, 0.3)
	İ ₂	Ki ₁	Ki ₂	
Ted-1	(0.7, 0.3, 0.3)	(0.7, 0.3, 0.3)	(0.7, 0.3, 0.3)	
Ted-2	(0.5, 0.5, 0.5)	(0.9, 0.1, 0.1)	(0.9, 0.1, 0.1)	
Ted-3	(0.7, 0.3, 0.3)	(0.7, 0.3, 0.3)	(0.7, 0.3, 0.3)	

Tablo 14. Uzman 2-Tedarikçilerin Değerlendirmesinin Küresel Bulanık Küme Karşılıkları

Tedarikçiler	Ka ₁	Ka ₂	Ka ₃	Ka ₄
Ted-1	(0.5, 0.5, 0.5)	(0.5, 0.5, 0.5)	(0.5, 0.5, 0.5)	(0.5, 0.5, 0.5)
Ted-2	(0.5, 0.5, 0.5)	(0.5, 0.5, 0.5)	(0.7, 0.3, 0.3)	(0.7, 0.3, 0.3)
Ted-3	(0.7, 0.3, 0.3)	(0.7, 0.3, 0.3)	(0.7, 0.3, 0.3)	(0.7, 0.3, 0.3)
	Fi ₁	Fi ₂	Fi ₃	Fi ₄
Ted-1	(0.5, 0.5, 0.5)	(0.3, 0.7, 0.3)	(0.7, 0.3, 0.3)	(0.1, 0.9, 0.1)
Ted-2	(0.5, 0.5, 0.5)	(0.5, 0.5, 0.5)	(0.5, 0.5, 0.5)	(0.5, 0.5, 0.5)
Ted-3	(0.5, 0.5, 0.5)	(0.7, 0.3, 0.3)	(0.5, 0.5, 0.5)	(0.5, 0.5, 0.5)
	Fi ₅	Te ₁	Te ₂	Ce ₁
Ted-1	(0.3, 0.7, 0.3)	(0.5, 0.5, 0.5)	(0.3, 0.7, 0.3)	(0.7, 0.3, 0.3)
Ted-2	(0.7, 0.3, 0.3)	(0.5, 0.5, 0.5)	(0.3, 0.7, 0.3)	(0.7, 0.3, 0.3)
Ted-3	(0.7, 0.3, 0.3)	(0.9, 0.1, 0.1)	(0.5, 0.5, 0.5)	(0.7, 0.3, 0.3)
	Ce ₂	Ce ₃	Ce ₄	Ce ₅
Ted-1	(0.7, 0.3, 0.3)	(0.7, 0.3, 0.3)	(0.7, 0.3, 0.3)	(0.7, 0.3, 0.3)
Ted-2	(0.7, 0.3, 0.3)	(0.7, 0.3, 0.3)	(0.7, 0.3, 0.3)	(0.7, 0.3, 0.3)
Ted-3	(0.9, 0.1, 0.1)	(0.7, 0.3, 0.3)	(0.7, 0.3, 0.3)	(0.7, 0.3, 0.3)
	Ce ₆	Ce ₇	Ce ₈	İ ₁
Ted-1	(0.7, 0.3, 0.3)	(0.3, 0.7, 0.3)	(0.7, 0.3, 0.3)	(0.7, 0.3, 0.3)
Ted-2	(0.7, 0.3, 0.3)	(0.3, 0.7, 0.3)	(0.7, 0.3, 0.3)	(0.5, 0.5, 0.5)
Ted-3	(0.7, 0.3, 0.3)	(0.3, 0.7, 0.3)	(0.7, 0.3, 0.3)	(0.5, 0.5, 0.5)
	İ ₂	Ki ₁	Ki ₂	
Ted-1	(0.9, 0.1, 0.1)	(0.7, 0.3, 0.3)	(0.5, 0.5, 0.5)	
Ted-2	(0.9, 0.1, 0.1)	(0.7, 0.3, 0.3)	(0.7, 0.3, 0.3)	
Ted-3	(0.5, 0.5, 0.5)	(0.5, 0.5, 0.5)	(0.7, 0.3, 0.3)	

Tablo 15. Uzman 3-Tedarikçilerin Değerlendirmesinin Küresel Bulanık Küme Karşılıkları

Tedarikçiler	Ka ₁	Ka ₂	Ka ₃	Ka ₄
Ted-1	(0.7, 0.3, 0.3)	(0.7, 0.3, 0.3)	(0.9, 0.1, 0.1)	(0.9, 0.1, 0.1)
Ted-2	(0.3, 0.7, 0.3)	(0.5, 0.5, 0.5)	(0.5, 0.5, 0.5)	(0.7, 0.3, 0.3)
Ted-3	(0.7, 0.3, 0.3)	(0.7, 0.3, 0.3)	(0.7, 0.3, 0.3)	(0.3, 0.7, 0.3)
	Fi ₁	Fi ₂	Fi ₃	Fi ₄
Ted-1	(0.5, 0.5, 0.5)	(0.5, 0.5, 0.5)	(0.3, 0.7, 0.3)	(0.3, 0.7, 0.3)
Ted-2	(0.7, 0.3, 0.3)	(0.7, 0.3, 0.3)	(0.7, 0.3, 0.3)	(0.5, 0.5, 0.5)
Ted-3	(0.5, 0.5, 0.5)	(0.5, 0.5, 0.5)	(0.7, 0.3, 0.3)	(0.7, 0.3, 0.3)
	Fi ₅	Te ₁	Te ₂	Ce ₁
Ted-1	(0.3, 0.7, 0.3)	(0.3, 0.7, 0.3)	(0.7, 0.3, 0.3)	(0.7, 0.3, 0.3)
Ted-2	(0.5, 0.5, 0.5)	(0.5, 0.5, 0.5)	(0.7, 0.3, 0.3)	(0.7, 0.3, 0.3)
Ted-3	(0.3, 0.7, 0.3)	(0.7, 0.3, 0.3)	(0.9, 0.1, 0.1)	(0.7, 0.3, 0.3)
	Ce ₂	Ce ₃	Ce ₄	Ce ₅
Ted-1	(0.9, 0.1, 0.1)	(0.9, 0.1, 0.1)	(0.9, 0.1, 0.1)	(0.5, 0.5, 0.5)
Ted-2	(0.9, 0.1, 0.1)	(0.9, 0.1, 0.1)	(0.9, 0.1, 0.1)	(0.5, 0.5, 0.5)
Ted-3	(0.9, 0.1, 0.1)	(0.9, 0.1, 0.1)	(0.9, 0.1, 0.1)	(0.5, 0.5, 0.5)
	Ce ₆	Ce ₇	Ce ₈	İ ₁
Ted-1	(0.9, 0.1, 0.1)	(0.3, 0.7, 0.3)	(0.9, 0.1, 0.1)	(0.3, 0.7, 0.3)
Ted-2	(0.9, 0.1, 0.1)	(0.3, 0.7, 0.3)	(0.9, 0.1, 0.1)	(0.7, 0.3, 0.3)
Ted-3	(0.9, 0.1, 0.1)	(0.5, 0.5, 0.5)	(0.9, 0.1, 0.1)	(0.9, 0.1, 0.1)
	İ ₂	Ki ₁	Ki ₂	
Ted-1	(0.5, 0.5, 0.5)	(0.5, 0.5, 0.5)	(0.7, 0.3, 0.3)	
Ted-2	(0.5, 0.5, 0.5)	(0.5, 0.5, 0.5)	(0.7, 0.3, 0.3)	
Ted-3	(0.3, 0.7, 0.3)	(0.5, 0.5, 0.5)	(0.9, 0.1, 0.1)	

Uzmanlar tarafından verilmiş olan cevaplara ilişkin oluşturulan karar matrisi Tablo 16 ile gösterilmiştir.

Tablo 16. Cevaplara İlişkin Oluşturulan Karar Matrisi

Tedarikçiler	Ka ₁	Ka ₂	Ka ₃	Ka ₄
Ted-1	(0.65, 0.38, 0.38)	(0.76, 0.35, 0.35)	(0.72, 0.42, 0.42)	(0.72, 0.42, 0.42)
Ted-2	(0.54, 0.54, 0.38)	(0.56, 0.49, 0.41)	(0.76, 0.35, 0.35)	(0.79, 0.25, 0.25)
Ted-3	(0.65, 0.38, 0.38)	(0.65, 0.38, 0.38)	(0.70, 0.30, 0.30)	(0.74, 0.48, 0.25)
	Fi ₁	Fi ₂	Fi ₃	Fi ₄
Ted-1	(0.45, 0.58, 0.45)	(0.45, 0.58, 0.45)	(0.50, 0.62, 0.30)	(0.25, 0.79, 0.25)
Ted-2	(0.58, 0.45, 0.45)	(0.58, 0.45, 0.45)	(0.65, 0.38, 0.38)	(0.50, 0.50, 0.50)
Ted-3	(0.50, 0.50, 0.50)	(0.58, 0.45, 0.45)	(0.58, 0.45, 0.45)	(0.54, 0.54, 0.38)
	Fi ₅	Te ₁	Te ₂	Ce ₁
Ted-1	(0.38, 0.65, 0.38)	(0.54, 0.54, 0.38)	(0.62, 0.50, 0.30)	(0.70, 0.30, 0.30)
Ted-2	(0.54, 0.54, 0.38)	(0.58, 0.45, 0.45)	(0.62, 0.50, 0.30)	(0.79, 0.25, 0.25)
Ted-3	(0.50, 0.62, 0.30)	(0.86, 0.19, 0.19)	(0.83, 0.31, 0.31)	(0.65, 0.38, 0.38)
	Ce ₂	Ce ₃	Ce ₄	Ce ₅
Ted-1	(0.79, 0.25, 0.25)	(0.79, 0.25, 0.25)	(0.79, 0.25, 0.25)	(0.65, 0.38, 0.38)
Ted-2	(0.86, 0.19, 0.19)	(0.86, 0.19, 0.19)	(0.86, 0.19, 0.19)	(0.65, 0.38, 0.38)
Ted-3	(0.90, 0.10, 0.10)	(0.76, 0.35, 0.35)	(0.76, 0.35, 0.35)	(0.58, 0.45, 0.45)
	Ce ₆	Ce ₇	Ce ₈	İ ₁
Ted-1	(0.79, 0.25, 0.25)	(0.38, 0.65, 0.38)	(0.86, 0.19, 0.19)	(0.62, 0.50, 0.30)
Ted-2	(0.86, 0.19, 0.19)	(0.38, 0.65, 0.38)	(0.86, 0.19, 0.19)	(0.58, 0.45, 0.45)
Ted-3	(0.79, 0.25, 0.25)	(0.54, 0.54, 0.38)	(0.79, 0.25, 0.25)	(0.76, 0.35, 0.35)
	İ ₂	Ki ₁	Ki ₂	
Ted-1	(0.76, 0.35, 0.35)	(0.65, 0.38, 0.38)	(0.65, 0.38, 0.38)	
Ted-2	(0.72, 0.42, 0.42)	(0.76, 0.35, 0.35)	(0.79, 0.25, 0.25)	
Ted-3	(0.54, 0.54, 0.38)	(0.58, 0.45, 0.45)	(0.79, 0.25, 0.25)	

Karar matrisindeki değerleri kriterlere ilişkin elde edilen global ağırlıklar ve SWAM operatörü kullanılarak cevaplar birleştirilmekte olup, Tablo 17’de gösterilmektedir.

Tablo 17. Ağırlıklı Birleştirilmiş Matris

Tedarikçiler	Ka ₁	Ka ₂	Ka ₃	Ka ₄
Ted-1	(0.14, 0.97, 0.10)	(0.16, 0.97, 0.10)	(0.18, 0.96, 0.14)	(0.23, 0.94, 0.17)
Ted-2	(0.11, 0.98, 0.09)	(0.11, 0.98, 0.09)	(0.20, 0.95, 0.12)	(0.26, 0.91, 0.11)
Ted-3	(0.14, 0.97, 0.10)	(0.13, 0.97, 0.09)	(0.17, 0.95, 0.09)	(0.24, 0.95, 0.10)
	Fi ₁	Fi ₂	Fi ₃	Fi ₄
Ted-1	(0.10, 0.98, 0.11)	(0.10, 0.98, 0.11)	(0.12, 0.98, 0.08)	(0.05, 0.99, 0.07)
Ted-2	(0.14, 0.96, 0.13)	(0.13, 0.97, 0.12)	(0.16, 0.96, 0.11)	(0.10, 0.98, 0.12)
Ted-3	(0.11, 0.97, 0.13)	(0.13, 0.97, 0.12)	(0.14, 0.96, 0.13)	(0.11, 0.98, 0.09)
	Fi ₅	Te ₁	Te ₂	Ce ₁
Ted-1	(0.07, 0.98, 0.08)	(0.18, 0.94, 0.14)	(0.19, 0.95, 0.11)	(0.11, 0.98, 0.06)
Ted-2	(0.11, 0.98, 0.09)	(0.19, 0.93, 0.18)	(0.19, 0.95, 0.11)	(0.14, 0.97, 0.06)
Ted-3	(0.10, 0.98, 0.07)	(0.34, 0.86, 0.11)	(0.30, 0.91, 0.16)	(0.10, 0.98, 0.08)
	Ce ₂	Ce ₃	Ce ₄	Ce ₅
Ted-1	(0.15, 0.97, 0.06)	(0.15, 0.97, 0.06)	(0.14, 0.97, 0.06)	(0.10, 0.98, 0.07)
Ted-2	(0.17, 0.96, 0.06)	(0.17, 0.96, 0.06)	(0.16, 0.97, 0.05)	(0.10, 0.98, 0.07)
Ted-3	(0.19, 0.95, 0.03)	(0.14, 0.98, 0.09)	(0.13, 0.98, 0.08)	(0.09, 0.99, 0.08)
	Ce ₆	Ce ₇	Ce ₈	İ ₁
Ted-1	(0.13, 0.98, 0.06)	(0.06, 0.99, 0.06)	(0.15, 0.97, 0.05)	(0.19, 0.95, 0.11)
Ted-2	(0.15, 0.97, 0.05)	(0.06, 0.99, 0.06)	(0.15, 0.97, 0.05)	(0.17, 0.94, 0.16)
Ted-3	(0.13, 0.98, 0.06)	(0.09, 0.99, 0.07)	(0.13, 0.98, 0.06)	(0.25, 0.92, 0.15)
	İ ₂	Ki ₁	Ki ₂	
Ted-1	(0.24, 0.93, 0.10)	(0.20, 0.93, 0.14)	(0.19, 0.94, 0.13)	
Ted-2	(0.22, 0.94, 0.15)	(0.25, 0.92, 0.15)	(0.25, 0.91, 0.11)	
Ted-3	(0.15, 0.96, 0.15)	(0.18, 0.94, 0.16)	(0.25, 0.91, 0.11)	

Ağırlıklı Birleştirilmiş Matrisin durulaştırma işlemi, Eşitlik 5’te belirtilen skor fonksiyonu sayesinde gerçekleştirilmiştir. Ardından negatif ideal çözüm (NIS) ve pozitif ideal çözüm (PIS) noktaları hesaplanmıştır. Tablo 18’de belirtilen durulaştırılmış matrisler incelendiğinde mavi değerler PIS

noktalarını, pembe değerler NIS noktalarını tanımlamaktadır. SWAM operatörüne bağlı skor fonksiyonu ile durulaştırma işlemi ve SF-PIS ile SF-NIS noktaları Tablo 19’da yer almaktadır.

Tablo 18. Skor fonksiyonu Kullanılarak Durulaştırma

Tedarikçiler	Ka ₁	Ka ₂	Ka ₃	Ka ₄	Fi ₁	Fi ₂	Fi ₃
Ted-1	-0,749	-0,749	-0,667	-0,667	-0,742	-0,749	-0,811
Ted-2	-0,789	-0,786	-0,682	-0,682	-0,699	-0,708	-0,706
Ted-3	-0,749	-0,770	-0,720	-0,720	-0,694	-0,708	-0,698
	Fi ₄	Fi ₅	Te ₁	Te ₂	Ce ₁	Ce ₂	Ce ₃
Ted-1	-0,890	-0,817	-0,640	-0,701	-0,832	-0,816	-0,814
Ted-2	-0,742	-0,790	-0,563	-0,701	-0,824	-0,813	-0,811
Ted-3	-0,795	-0,839	-0,506	-0,548	-0,815	-0,818	-0,791
	Ce ₄	Ce ₅	Ce ₆	Ce ₇	Ce ₈	İ ₁	İ ₂
Ted-1	-0,833	-0,831	-0,843	-0,862	-0,837	-0,706	-0,668
Ted-2	-0,831	-0,831	-0,842	-0,862	-0,837	-0,612	-0,617
Ted-3	-0,812	-0,822	-0,843	-0,843	-0,838	-0,586	-0,658
	Ki ₁	Ki ₂					
Ted-1	-0,615	-0,644					
Ted-2	-0,582	-0,629					
Ted-3	-0,609	-0,629					

Tablo 19. SF-PIS ve SF-NIS Noktaları

	Ka₁	Ka₂	Ka₃	Ka₄
SF-PIS	(0.11, 0.98, 0.09)	(0.11, 0.98, 0.09)	(0.17, 0.95, 0.09)	(0.24, 0.95, 0.10)
SF-NIS	(0.14, 0.97, 0.10)	(0.16, 0.97, 0.10)	(0.18, 0.96, 0.14)	(0.23, 0.94, 0.17)
	Fi₁	Fi₂	Fi₃	Fi₄
SF-PIS	(0.10, 0.98, 0.11)	(0.10, 0.98, 0.11)	(0.12, 0.98, 0.08)	(0.05, 0.98, 0.09)
SF-NIS	(0.11, 0.97, 0.13)	(0.13, 0.97, 0.12)	(0.14, 0.96, 0.13)	(0.10, 0.98, 0.12)
	Fi₅	Te₁	Te₂	Ce₁
SF-PIS	(0.10, 0.98, 0.07)	(0.18, 0.94, 0.14)	(0.19, 0.95, 0.11)	(0.11, 0.98, 0.06)
SF-NIS	(0.11, 0.98, 0.09)	(0.34, 0.86, 0.11)	(0.30, 0.91, 0.16)	(0.10, 0.98, 0.08)
	Ce₂	Ce₃	Ce₄	Ce₅
SF-PIS	(0.19, 0.95, 0.03)	(0.15, 0.97, 0.06)	(0.14, 0.97, 0.06)	(0.10, 0.98, 0.07)
SF-NIS	(0.17, 0.96, 0.06)	(0.14, 0.98, 0.09)	(0.16, 0.97, 0.05)	(0.09, 0.99, 0.08)
	Ce₆	Ce₇	Ce₈	İl₁
SF-PIS	(0.13, 0.98, 0.06)	(0.06, 0.99, 0.06)	(0.13, 0.98, 0.06)	(0.19, 0.95, 0.11)
SF-NIS	(0.15, 0.97, 0.05)	(0.09, 0.99, 0.07)	(0.15, 0.97, 0.05)	(0.25, 0.92, 0.15)
	İl₂	Ki₁	Ki₂	
SF-PIS	(0.24, 0.93, 0.10)	(0.20, 0.93, 0.14)	(0.19, 0.94, 0.13)	
SF-NIS	(0.22, 0.94, 0.15)	(0.25, 0.92, 0.15)	(0.25, 0.91, 0.11)	

Eşitlik 7 kullanılarak SF-PIS mesafesi, Eşitlik 8 uygulanarak ise SF-NIS mesafesi hesaplanmıştır. Hesaplanan SF-PIS mesafe değerlerinden minimum SF-PIS ile olan en kısa mesafe ($D_{min}(X_i, X^*)$) Eşitlik 9 kullanılarak elde edilmiştir.

Bununla birlikte, SF-NIS mesafelerinin maksimumunu tanımlayan SF-NIS ile olan en uzun mesafe ($D_{max}(X_i, X^-)$) Eşitlik 10 ile tespit edilmiştir.

Tablo 20. SF-PIS ve SF-NIS Uzaklıkları

	$D(X_i, X^*)$	$D(X_i, X^-)$	$D(X_i, X^*)$	$D(X_i, X^-)$
Ted-1	0,020	0,043	0,006	0,020
Ted-2	0,028	0,039	0,014	0,017
Ted-3	0,044	0,023	0,020	0,007

Son aşamada demir çelik sektöründe faaliyet gösteren 3 tedarikçi arasında sıralama gerçekleştirmek için Eşitlik 11 kullanılarak alternatiflerin göreceli yakınlıkları ölçülmektedir.

Yapılan hesaplamalar neticesinde en yüksek değere sahip tedarikçi seçilir.

Tablo 21. Tedarikçilerin Yakınlık Katsayıları ve Sıralaması

	Yakınlık Oranları	Sıralama
Ted-1	0,684	3
Ted-2	0,587	2
Ted-3	0,345	1

Tablo 21’de görüldüğü üzere, küresel bulanık TOPSIS yöntemi sonucunda alternatifler Tedarikçi 3 > Tedarikçi 2 > Tedarikçi 1 olacak şekilde sıralanmıştır.

3.2 Küresel Bulanık CODAS Uygulaması

Çalışmanın devamında diğer çok kriterli karar verme yöntem olarak Küresel Bulanık CODAS yöntemi uygulanmıştır.

Tablo 13, Tablo 14 ve Tablo 15’te verilen değerlendirme sonuçları baz alınarak, Tablo 16’da oluşturulan karar matrisi ve Tablo 17’de yer alan SWAM operatörü ile meydana gelen birleştirilmiş matrisi verileri kullanılarak oluşturulan ağırlıklı matrisler Eşitlik 16’da belirtilen skor fonksiyonu kullanılarak Tablo 22’de görüldüğü üzere durulaştırma gerçekleştirilmiştir.

Tablo 22. Skor Fonksiyonu ile Durulaştırma

Tedarikçiler	Ka ₁	Ka ₂	Ka ₃	Ka ₄	Fi ₁	Fi ₂	Fi ₃
Ted-1	-0,832	-0,830	-0,777	-0,708	-0,841	-0,846	-0,876
Ted-2	-0,867	-0,866	-0,774	-0,683	-0,804	-0,811	-0,798
Ted-3	-0,832	-0,848	-0,792	-0,773	-0,809	-0,811	-0,803
	Fi ₄	Fi ₅	Te ₁	Te ₂	Ce ₁	Ce ₂	Ce ₃
Ted-1	0,717	0,047	-0,708	0,776	-0,051	-0,841	0,853
Ted-2	0,675	0,072	-0,683	0,700	0,019	-0,804	0,800
Ted-3	0,684	0,088	-0,773	0,793	0,010	-0,809	0,808
	Ce ₄	Ce ₅	Ce ₆	Ce ₇	Ce ₈	İ ₁	İ ₂
Ted-1	-0,012	-0,846	0,841	0,003	-0,876	0,907	-0,025
Ted-2	0,005	-0,811	0,783	0,023	-0,798	0,818	-0,013
Ted-3	-0,001	-0,811	0,800	0,010	-0,803	0,820	-0,014
	Ki ₁	Ki ₂					
Ted-1	-0,936	0,912					
Ted-2	-0,843	0,845					
Ted-3	-0,872	0,863					

Tablo 22’de yer alan değerlere göre Küresel Bulanık Negatif İdeal Çözüme (SF-NIS) karşılık gelen SF sayıları, net minimum puanlara göre belirlenmektedir. SF-NIS değerleri Tablo 23’te yer almaktadır.

Tablo 23. Küresel Bulanık Negatif İdeal Çözüm Değerleri (SF-NIS)

Ka ₁	Ka ₂	Ka ₃	Ka ₄
(0.11, 0.98, 0.09)	(0.11, 0.98, 0.09)	(0.17, 0.95, 0.09)	(0.24, 0.95, 0.10)
Fi ₁	Fi ₂	Fi ₃	Fi ₄
(0.10, 0.98, 0.11)	(0.10, 0.98, 0.11)	(0.12, 0.98, 0.08)	(0.10, 0.98, 0.12)
Fi ₅	Te ₁	Te ₂	Ce ₁
(0.07, 0.98, 0.08)	(0.34, 0.86, 0.11)	(0.19, 0.95, 0.11)	(0.11, 0.98, 0.06)
Ce ₂	Ce ₃	Ce ₄	Ce ₅
(0.15, 0.97, 0.06)	(0.17, 0.96, 0.06)	(0.14, 0.97, 0.06)	(0.10, 0.98, 0.07)
Ce ₆	Ce ₇	Ce ₈	İ ₁
(0.15, 0.97, 0.05)	(0.06, 0.99, 0.06)	(0.15, 0.97, 0.05)	(0.17, 0.94, 0.16)
İ ₂	Ki ₁	Ki ₂	
(0.24, 0.93, 0.10)	(0.20, 0.93, 0.14)	(0.25, 0.91, 0.11)	

Ağırlıklı Öklid uzaklık değerleri (ÖÜD) Eşitlik 19 bulunmuş ve Tablo 24’te belirtilmiştir. yardımcıyla, küresel uzaklık (KU) ise Eşitlik 20 yardımcı ile

Tablo 24. Ağırlıklı Küresel ve Öklid Uzaklık Değerleri

	Küresel Uzaklık	Öklid Uzaklığı
Ted-1	5.892	0.037
Ted-2	6.093	0.033
Ted-3	6.041	0.033

Eşitlik 21 kullanılarak Tablo 25’te belirtilen görelî önem matrisi elde edilmiştir.

Tablo 25. Görelî Önem Değerleri Matrisi

	Ted-1	Ted-2	Ted-3
Ted-1	0.000	0.004	0.004
Ted-2	-0.004	0.000	0.000
Ted-3	-0.004	0.000	0.000

Eşitlik 23’ün yardımcıyla tedarikçilerin skor değerleri hesaplanmış Tablo 26’da gösterilmiştir.

Tablo 26. Tedarikçilerin skor değerleri

	Skor değerleri	Sıralama
Ted-1	0.0086	1
Ted-2	-0.0038	2
Ted-3	-0.0048	3

Tablo 26'da küresel bulanık CODAS yöntemi kullanılarak yapılan hesaplamayla alternatiflerin skor değerleri tespit edilmiştir. Elde edilen skor değerleri büyükten küçüğe doğru sıralanmaktadır. Uygulamada, küresel bulanık CODAS yöntemi kullanılarak yapılan Tedarikçi sıralaması ise; Tedarikçi 1 > Tedarikçi 2 > Tedarikçi 3 olacak şekilde gerçekleşmiştir.

3.2.1 Duyarlılık Analizi

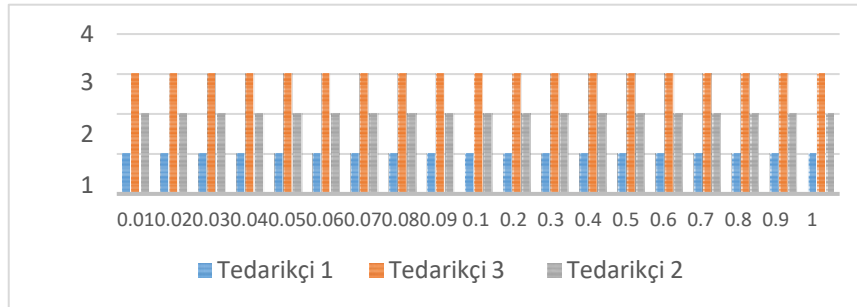
Elde edilen sonuçların sağlamlığının test edilmesi amacıyla duyarlılık analizi yapılmaktadır. CODAS'ın ince ayar gerektiren en hayati parametresi eşik parametresi τ 'dir [35]. Yukarıdaki hesaplamalar $\tau=0,02$ kullanılarak yapılmıştır. Sonuçlar üzerindeki etkisini değerlendirmek için alternatiflerin değerlendirme puanlarını ve sıralamalarını 0,01 ile 1,00 arasında değişen 14 farklı τ değeri için hesaplanmıştır. Tablo 27'de değişen değerlerine sahip sıralama sonuçları gösterilmektedir

Tablo 27. Her Tedarikçi İçin Farklı τ Değerlerine Sahip Değerlendirme Puanları

Tedarikçiler	0.01	0.02	0.03	0.04	0.05	0.06	0.07	0.08	
Ted-1	0.009	0.009	0.009	0.009	0.009	0.009	0.009	0.009	
Ted-2	-0.004	-0.004	-0.004	-0.004	-0.004	-0.004	-0.004	-0.004	
Ted-3	-0.005	-0.005	-0.005	-0.005	-0.005	-0.005	-0.005	-0.005	
Tedarikçiler	0.09	0.1	0.2	0.3	0.4	0.5	0.6	0.7	
Ted-1	0.009	0.009	0.009	0.009	0.009	0.009	0.009	0.009	
Ted-2	-0.004	-0.004	-0.004	-0.004	-0.004	-0.004	-0.004	-0.004	
Ted-3	-0.005	-0.005	-0.005	-0.005	-0.005	-0.005	-0.005	-0.005	
Tedarikçiler	0.8	0.9	01						
Ted-1	0.009	0.009	0.009						
Ted-2	-0.004	-0.004	-0.004						
Ted-3	-0.005	-0.005	-0.005						

Tablo 27'de görüldüğü gibi tedarikçi sıralamaları değişen τ değerlerine göre değişmemiştir. Duyarlılık analizi sonuçları Şekil 2'de görselleştirilmiştir. Üç alternatifin tümünün sıralaması sabittir. Sonuç olarak, gerçekleştirilen duyarlılık analizi sonuçlarının, önerilen SF-CODAS'ın tedarikçi seçim problemi için yüksek

sağlamlığını gösterdiği söylenebilir. Üç alternatif Tedarikçi 1 > Tedarikçi 2 > Tedarikçi 3 şeklinde sıralanmıştır. Böylece Tedarikçi 1 demir çelik sektöründe faaliyet gösteren firma için en iyi tedarikçi olarak değerlendirilmiştir.



Şekil 2. τ Değerlerinin Sıralamaya Etkisi

IV. SONUÇ

Bu çalışmada, demir-çelik sektöründe faaliyet gösteren çelik sacdan malzeme üreten bir şirket için tedarikçi seçim problemi ele alınmıştır. Buradaki kriter belirleme ve kriterlerin değerlendirilmesi aşamasında demir çelik sektöründe faaliyet gösteren işletmelerde görev alan 5 kişilik uzman bir kadronun değerlendirmesinden faydalanılmıştır. Bahis konusu ekipte 2 mühendis ve 3 satın alma personeli yer almıştır. Literatürde yer alan bilgiler incelenmiş ve demir çelik sektöründe çalışan farklı uzmanlardan alınan bilgiler ışığında kriterler belirlenmiştir. Belirlenen 6 ana, 23 alt kriter kriter kapsamında 3 farklı tedarikçi değerlendirilmiştir. Her bir kriter uzmanların değerlendirmeleri ışığında detaylı incelenmiştir. Belirlenen kriterlerin ağırlıklandırılması aşamasında Küresel Bulanık AHP yöntemi kullanılmıştır. Ardından tedarikçilerden demir-çelik sac temin eden bir şirketin iş yürüttüğü 3 tedarikçi değerlendirilerek

sıralanmıştır. Paris İklim Anlaşması'nın 2015 yılında imzalanması neticesinde AB tarafından oluşturulan Avrupa Yeşil Mutabakatı imzalanmıştır. Bu doğrultuda, Avrupa Yeşil Mutabakatı kapsamında çıkarılan Sınırdaki Karbon Düzenleme Mekanizması, AB tarafından ithal edilen öncelikli 6 sektör için (demir-çelik, alüminyum, gübre, çimento, elektrik ve hidrojen) karbon emisyonlarının hesaplanarak raporlanması gerekmektedir. Bu kapsamda AB'de ithalatçı konumunda bulunan firmaların demir-çelik ürünü tedarik ettiğinde, ihracatçıların ürünlerinin emisyon miktarlarının düşük olması önem arz etmektedir. Dolayısıyla, çalışmada tedarikçi seçim kriterlerinde çevre ana kriteri kapsamında yeşil kriterlere de yer verilmiştir.

Yapılan çalışmada ana kriterler baz alındığında demir-çelik sektöründe tedarikçi seçimi aşamasında en önemli kriterin fiyat olduğu görülmüştür. Daha sonra sırasıyla kalite, teslimat

çevre ve iletişim kriterlerinin önem teşkil ettiği, en etkisiz kriterin ise kurumsal itibar olduğu tespit edilmiştir. Hali hazırda çevre kriterine gerekli önem verilmediği görülmüş olup, SKDM'nin uygulanması ile Türkiye ihracatına yaklaşık %16 oranında katkı sağlayan demir-çelik sektöründe çevre kriterlerine gerekli önemin gösterilmesinin fayda sağlayacağı değerlendirilmiştir. Yapılan kriter ağırlıklandırılması sonrasında bir firma özelinde tedarikçiler SF-TOPSIS ve SF-CODAS yöntemleri kullanılarak kıyaslanmıştır. CODAS yöntemi ile gerçekleştirilen hesaplama neticesinde alternatiflerin skor değerleri belirtilmektedir. Buna göre, küresel bulanık TOPSIS yöntemi ile tedarikçiler Tedarikçi 3 > Tedarikçi 2 > Tedarikçi 1 olarak; küresel bulanık CODAS yöntemi sonucunda ise alternatifler Tedarikçi 1 > Tedarikçi 2 > Tedarikçi 3 olacak şekilde sıralanmıştır.

Gelecek çalışmalarda daha farklı çok kriterli karar verme yöntemleri kullanılabilir ve diğer yöntemlerden elde edilen sonuçlarla bir kıyaslama yapılabilir. Buna ek olarak ilerleyen çalışmalarda daha fazla uzmandan görüş alınarak kriterler çeşitlendirilebilir. Çalışmamızın sonucu olarak demir-çelik sektöründe tedarikçi seçimi yapan karar vericilerin çevre ana kriteri altında incelemiş olduğu yeşil kriterleri sağlayan tedarikçiler ile çalışmasının, SKDM'nin getirecek olduğu mali yükümlülüklerden kaçınmak bakımından da önemli olduğu değerlendirilmektedir.

KAYNAKLAR

- [1] Ageron, B., Gunasekaran, A., & Spalanzani, A. (2012). Sustainable Supply Management: An Empirical Study. *International Journal of Production Economics*, 140, 168-182.
- [2] Ertunga, E. İ., & Seyhun, Ö. K., (2022). Sınırdaki Karbon Düzenleme Mekanizması ve Türkiye'nin İhracatına Olası Etkileri. *Ege Stratejik Araştırmalar Dergisi*, Cilt 13, Sayı 1, 2022, ss. 1-13
- [3] T.C. Ticaret Bakanlığı (2023). Avrupa Yeşil Mutabakatı. <https://ticaret.gov.tr/dis-iliskiler/yesil-mutabakat/avrupa-yesil-mutabakatı>
- [4] Erbiyık, H., Kabakçı, G. A., & Erdil, A., (2021). Electre Yöntemi ile Otomotiv Sektöründe Tedarikçi Seçimi: Yeşil Tedarikçi Seçimi Uygulaması, *Avrupa Bilim ve Teknoloji Dergisi Özel Sayı 24*, S. 421-429, Nisan 2021.
- [5] Onat, A., & Kaçtıoğlu, S. (2020). Bulanık AHP ve Bulanık TOPSIS Yöntemi İle Tedarikçi Seçimi: Perakende Sektöründe Bir Uygulama. *İstanbul Ticaret Üniversitesi Fen Bilimleri Dergisi*, 19(37), 65-79.
- [6] Ho, W., Xu, X. & Dey, P. K. (2010). Tedarikçi Değerlendirmesi ve Seçimi için Çok Kriterli Karar Verme Yaklaşımları: Bir Literatür Taraması. *Avrupa Yönetim Araştırmaları Dergisi*, 202, 16-24.
- [7] Mendoza, A., (2007). Effective methodologies for supplier selection and order quantity allocation, *The Pennsylvania State University The Graduate School, Doctor of Philosophy*, 174 p.
- [8] Kahraman, C., Cebeci, U. and Ulukan Z., (2003). Multi-criteria supplier selection using Fuzzy AHP, *Logistics Information Management*, volume 16, p. 382-394.
- [9] S. Soner & S. Önüt. (2006) Çok Kriterli Tedarikçi Seçimi: Bir ELECTRE-AHP Uygulaması. *Sigma Mühendislik ve Fen Bilimleri Dergisi*, 24:4, 110-120.
- [10] Tahriri, F., Osman, M. R., Ali, A., Yusuff, R., Esfandiary, A. (2008). AHP approach for supplier evaluation and selection in a steel manufacturing company. *Journal of Industrial Engineering and Management (JIEM)*, ISSN 2013-0953, OmniaScience, Barcelona, Vol. 1, Iss. 2, pp. 54-76, <https://doi.org/10.3926/jiem.v1n2.p54-76>
- [11] Büyüközkan, G., & Çiftçi, G. (2012). A novel hybrid MCDM approach based on fuzzy Dematel, fuzzy ANP and fuzzy TOPSIS to evaluate green suppliers. *Expert Systems with Applications*, 39, 3000-3011.
- [12] Arıkan, F., & Küçükçe, Y. (2013). Satın Alma Faaliyeti İçin Bir Tedarikçi Seçimi- Değerlendirme Problemi ve Çözümü. *Gazi Üniversitesi Mühendislik Mimarlık Fakültesi Dergisi*, 27(2).
- [13] Junior, F. R. L., Osiro, L. & Carpinetti, L. C. R. (2014). A comparison between Fuzzy AHP and Fuzzy TOPSIS methods to supplier selection. *Applied Soft Computing*, 21, 194-209.
- [14] Bronja, H. (2015). Two-phase selection procedure of aluminized sheet supplier by applying fuzzy AHP and fuzzy TOPSIS methodology, *Tehnicki vjesnik - Technical Gazette* 22(4):821-828. <https://doi.org/10.17559/TV-20140203122653>
- [15] Yılmaz, E. (2015). Bulanık AHP-VIKOR Bütünleşik Yöntemi ile Tedarikçi Seçimi. *Marmara Üniversitesi İktisadi ve İdari Bilimler Dergisi*, 33(2), 331-354.
- [16] Kara, İ., & Ecer, F. (2016). Ahp-VIKOR Entegre Yöntemi ile Tedarikçi Seçimi: Tekstil Sektörü Uygulaması. *Dokuz Eylül Üniversitesi Sosyal Bilimler Enstitüsü Dergisi*, 18(2), 255-272.
- [17] Tekez, E., & Bark, N. (2016). Mobilya Sektöründe Bulanık TOPSIS Yöntemi ile Tedarikçi Seçimi. *Sakarya University Journal of Science*, 20(1), 55-63
- [18] Denizhan, B., Yalçın, A. Y., Berber, Ş. (2017). Analitik Hiyerarşi Proses ve Bulanık Analitik Hiyerarşi Proses Yöntemleri Kullanılarak Yeşil Tedarikçi Seçimi Uygulaması, *Nevşehir Bilim ve Teknoloji Dergisi*, 6(1), ss. 63-78.
- [19] Arslan, H. M., (2017). Electre I Yöntemi ile En Uygun Tedarikçinin Belirlenmesi: Ahşap Sektörü Uygulaması, *Düzce Üniversitesi Sosyal Bilimler Enstitüsü Dergisi*, Yıl: 7, Sayı: 1.
- [20] Daldır, İ., & Tosun, Ö. (2018). Bulanık WASPAS İle Yeşil Tedarikçi Seçimi, *Uludağ Üniversitesi Mühendislik Fakültesi Dergisi*, 23(4), ss. 193-208.
- [21] Narayanan, Arun K. & Jinesh, N. (2018) Application of SWARA and TOPSIS Methods for Supplier Selection in a Casting Unit, *International Journal of Engineering Research & Technology (IJERT)*, Vol. 7 Issue 05, May-2018, 2278-0181
- [22] Madenoğlu, F., S. (2019). Green Supplier Selection In Fuzzy Multi Criteria Decision Making Environment, *Business & Management Studies: An International Journal*, 7(4), ss. 1850-1869.
- [23] Doğan, N. Ö., & Akbal, H. (2019). Sağlık Sektöründe Tedarikçi Seçim Kararının AHP Yöntemi ile İncelenmesi: Bir Üniversite Hastanesi Örneği. *Manisa Celal Bayar Üniversitesi Sosyal Bilimler Dergisi*, 17(4),440-456. <https://doi.org/10.18026/cbayarsos.664380>
- [24] Korkusuz Polat, T. & Kaçmaz, Ö. (2019). Supplier Selection Application with Fuzzy AHP in Machine Manufacturing Factory. Presented at the 4th International Symposium on Innovative Approaches in

- Engineering and Natural Sciences (ISAS WINTER-2019 (ENS)), Samsun, Turkey, Nov 22, 2019. SETSCI Conference Proceedings, 2019, 9, Page (s): 37-41, <https://doi.org/10.36287/setsoci.4.6.017>
- [25] Şekerçi, A. Z., & Yazıcıoğlu, O. (2019). Ahp Yöntemi İle Tedarikçi Seçimi: Gıda Sektöründe Bir Uygulama. *Al Farabi Uluslararası Sosyal Bilimler Dergisi*, 3(2), 23-41.
- [26] Cezlan, E. Ç. (2022). Çok ölçütlü karar verme yöntemleri ile yeşil tedarikçi seçimi: Sağlık sektöründe bir uygulama. *Lojistik Dergisi*, 55, 39-52.
- [27] Unal, Y., & Temur, G. T. (2022). Sustainable supplier selection by using spherical fuzzy AHP. *Journal of Intelligent & Fuzzy Systems*, 42 (1), 593-603. <https://doi.org/10.3233/JIFS-219214>
- [28] Nebati, E., Yürük, H., & Kenar, Z. (2021). Bir Otobüs İşletmesi İçin Tedarikçi Seçimi. *Trafik ve Ulaşım Araştırmaları Dergisi*, 4(1), 1-14.
- [29] Afzali, M., Afzali, A. & Pourmohammadi, H. (2022). An interval-valued intuitionistic fuzzy-based CODAS for sustainable supplier selection. *Soft Computing*, 1-22
- [30] Ay Türkmen, M. & Demirel, A. (2022). SWARA Ağırlıklı Bulanık COPRAS Yöntemi ile Tedarikçi Seçimi, *Alanya Akademik Bakış*, 6(1), Sayfa No. 1739-1756.
- [31] Zaralı, F. (2022). Third Part Reverse Logistics Service Provider Selection Using the Spherical Fuzzy TOPSIS Method. *Erciyes Üniversitesi Fen Bilimleri Enstitüsü Fen Bilimleri Dergisi*, 38(2), 268-279.
- [32] Nebati, E. E., Ayvaz, B., Kuşakcı A. O. (2023). ERP System Evaluation in the Defense Industry: A Hybridized Spherical Fuzzy AHP-Codas Approach, *International Journal Of Information Technology & Decision Making*, cilt.19, sa.2, ss.1-42, 2023
- [33] Gündoğdu, F. K., & Kahraman, C. (2019). A novel fuzzy TOPSIS method using emerging interval-valued spherical fuzzy sets. *Engineering Applications of Artificial Intelligence*, 85, 307–323.
- [34] Kocakaya, K.; Engin, T.; Tektaş, M. ve Aydın, U. (2021). Türkiye’de Bölgesel Havayolları için Uçak Tipi Seçimi: Küresel Bulanık AHP-TOPSIS Yöntemlerinin Entegrasyonu. *Akıllı Ulaşım Sistemleri ve Uygulama Dergisi*, 4(1), 27-58.
- [35] Ghorabae, M. K., Zavadskas, E. K., Turskis, Z., & Antucheviciene, J. (2016). A new combinative distance-based assessment (CODAS) method for multi-criteria decision-making. *Economic Computation & Economic Cybernetics Studies & Research*, 50(3), 25-44.

Synthesis, Structural Characterization and Temperature Effects on Chloroform Vapor Sensing Properties of ZnO Nanocrystals

Doruk YILDIZTEKİN¹ , Fatih DUMLUDAĞ¹ 

¹Marmara University, Faculty of Science, Department of Physics, 34722, Kadıköy/İstanbul, TÜRKİYE

Abstract

In this study, nanocrystalline ZnO were synthesized onto glass substrates by using sol-gel method. Structural characterizations were performed by XRD, SEM and AFM techniques. Potential application of nanocrystal ZnO as chloroform sensor was investigated. Response of the fabricated thin films of the ZnO nanocrystals towards chloroform vapor was investigated depending on gas concentration (750-15000 ppm) between the temperatures of 22–150 °C in nitrogen ambient. Gas flow rates were controlled by using flow controller and flow meters. All the measurement system was computerized.

XRD results revealed that thin film of the ZnO nanocrystals on the glass substrate was in crystal form and can be characterized by 036-1451 JCPDS number. Crystallite sizes of the ZnO nanocrystals were determined both by SEM images and the Scherrer equation. The crystallite sizes were calculated between 27.9 – 50.4 nm using the Scherrer equation. The sensors showed reversible response towards the chloroform vapor in the measured temperature and gas concentration range. Response time and sensitivity values of the sensors towards the chloroform vapor were also calculated. The increase in temperature caused to increase in sensitivity values. The best sensitivity values were obtained at 150 °C.

Keywords: XRD, SEM, AFM, Sensor, Chloroform, Nano.

I. INTRODUCTION

Volatile organic compounds (VOCs) are organic liquids and can be found indoor air due to wood polishes, paints, adhesives and so on. VOCs vapor are hazardous and can cause long-term health and environmental problems even at ppm concentration levels. Chloroform (CHCl₃) is one of the VOCs and colorless liquid. Previously, chloroform was used as an inhalation anesthetic in surgeries, but it is not used in this way, nowadays. It was reported that by the ATSDR (Agency for Toxic Substances and Disease Registry) in a group of 1502 people (exposure less than 22 500 ppm), dose-related bradycardia developed in 8% of the peoples, and cardiac arrhythmia developed in 1.3% of the peoples [1]. A number of studies, using different sensing materials, were reported to sense the chloroform vapor previously due to importance of the sensing the chloroform vapor [2, 3, 4].

Some electrical parameters such as resistance and impedance of some metal oxide semiconductors changes when the materials exposed to gases. ZnO based gas sensors are used frequently in order to detect toxic and harmful gases because of its physicochemical properties [5, 6]. ZnO is a wide band gap metal oxide material and takes place between semiconductors and ionic materials [7, 8]. Several techniques have been reported to deposit doped and undoped ZnO films such as vapor condensation, thermal evaporation, spray pyrolysis, magnetron sputtering, metal organic chemical vapor deposition, and sol-gel [9, 10, 11, 12, 13].

ZnO based sensors are usually operated at elevated temperatures but it has been studied rarely at low temperatures below 200 °C and even at room temperature [14]. In this study ZnO nanocrystal structures have synthesized onto the glass substrate using sol-gel method. Digitated gold electrodes were deposited onto the nanocrystalline film in thermal evaporation system then the sensor was tested towards chloroform vapor at different gas concentrations and temperatures. The sensors were found reversible. Sensitivity of the sensors increased with increasing temperature. The best sensitivity values were obtained at 150 °C.

II. MATERIALS and METHOD

Glass substrates were cleaned using general cleaning procedures in order to synthesize ZnO nanocrystals onto glass substrates. To do this, the glass substrates were washed with isopropyl alcohol, acetone and DI-water in

ultrasonic cleaner with 15 minutes periods at 50 °C. The cleaned glass substrates were then dried by nitrogen blow and heated at 90 °C for one hour.

Thin films of ZnO were deposited onto the cleaned glass substrates using sol-gel spin coating route. Precursor solution was first prepared. To prepare the precursor solution 10 cc methanol was used as solvent. Appropriate amount of zinc acetate dihydrate ($\text{Zn}(\text{CH}_3\text{COO})_2 \cdot 2\text{H}_2\text{O}$) is slowly added to solvent while the solvent is mixed by using magnetic stirrer at 700 rpm and left to stir for 5 minutes. After that 0.4 cc diethanolamine (DEA) ($\text{HN}(\text{CH}_2\text{CH}_2\text{OH})_2$) and 0.5 cc of DI-water water was added drop by drop. The solution was then left to stir for 3 hours. The solution was spin coated at 2000 rpm onto the glass substrate by using spinner MODEL 6700 SERIES followed by annealing at 125 °C for 15 minutes. The solution was deposited onto the glass substrate 12 times by using the procedure explained above. Final annealing was performed at 600 °C for 2.5 hours.

Chemical sensors are devices that convert a chemical state into an electrical signal. In order to get electrical signal corresponding to chemical state, a suitable transducer is required to detect a gas molecule. ZnO nanocrystals deposited glass substrates were placed into thermal evaporation system in order to fabricate transducer. 20 couples interdigitated gold electrodes (IDE) were deposited onto the ZnO nanocrystal film in high vacuum ambient (10^{-6} mbar) by using a shadow mask. Thickness of the gold electrodes was kept at 2000 Å by using film thickness monitor. Schematic diagram of the IDE was presented in Figure 1.

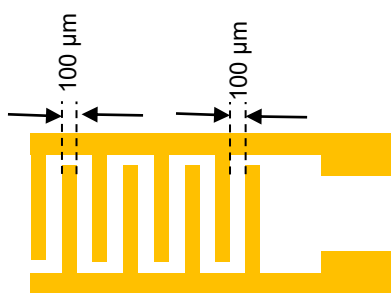


Figure 1. Schematic diagram of the transducer

Structural characterizations of the ZnO nanocrystals were performed by XRD, SEM, and AFM techniques. XRD measurements were performed by using Bruker D8 Advance with characteristic wavelength of 1.54059 Å. SEM and AFM images were obtained by using Digital Instruments NanoScope IV, and Philips XL 30 S, respectively. Crystallite size of the ZnO nanocrystals were calculated by using Scherrer formula (Equation 1).

$$L = \frac{K\lambda}{\beta \cos \theta} \quad (1)$$

where, L is the crystallite size, K is the dimensionless shape factor, (0.94), λ is the wavelength of the x-ray in nm, β is the full width half maximum of the peak (FWHM) in radians, and θ is the Bragg angle in radians.

The fabricated ZnO nanocrystals-based sensor was placed in homemade Teflon gas test chamber in order to determine response of the sensor towards chloroform vapor. The chamber was placed in a sealed chemical hood. Chloroform vapor were produced in washing bottle filled with extra pure grade chloroform from MERCK. Concentration of the vapor was calculated using Antoine equation. High purity nitrogen gas used as carrier gas and total flow rate was kept at 100 cc/min. Flow rates were controlled by using the MKS gas flow controller and gas flowmeters. Gas sensing measurements were performed depending on gas concentration at different temperatures between 22 °C - 150 °C. Sensitivity and response time values of the sensors, which is defined as the time it takes to reach 90% of the total change in measured gas concentration, were also calculated.

III. RESULTS and DISCUSSION

3.1. Structural Characterization

Structure of the ZnO were studied by XRD, SEM and AFM techniques. Figure 2 shows XRD pattern of the ZnO structure deposited onto glass substrates. The results revealed that the ZnO films were in crystal form. XRD results are matched with the pattern of ZnO JCPDS number 036-1451. Crystallite size of the ZnO nanocrystals were calculated by using Scherrer formula (Equation 1). The calculations revealed that the crystallite size varies between 27.9 – 50.4 nm. The 2θ degrees given in the XRD pattern were presented in Table 1.

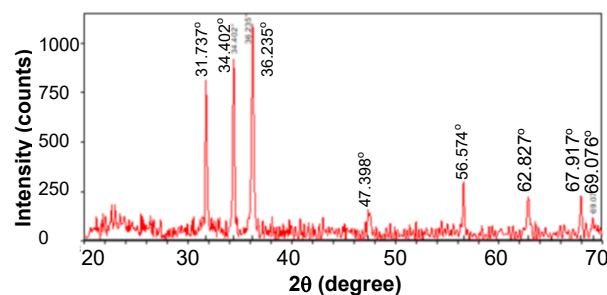


Figure 2. XRD pattern of the synthesized nanocrystalline ZnO film.

Table 1. 2θ degrees obtained from XRD pattern of the synthesized ZnO nanocrystals.

2θ values of the peaks (in degrees)	31.737	34.402	36.235	47.398	56.574	62.827	67.917	69.076
Miller Indices	(100)	(002)	(101)	(102)	(110)	(103)	(112)	(201)

SEM images of the ZnO nanocrystals with ($\times 20000$) and ($\times 50000$) magnification which is deposited onto glass substrate were shown in Figure 3. The image was obtained by using SEM operated at 15 kV. As can be seen from the Figure the particles are distributed homogeneously and the particles have a round shape. Different crystallite sizes were observed in SEM images, and their sizes varied between 24.8 – 101.0 nm. This may be because some particles within the particle may have agglomerated over time. As a result, it can be seen that the average ZnO nanocrystallite size calculated from the XRD data with the Scherrer formula is also supported by the SEM image.

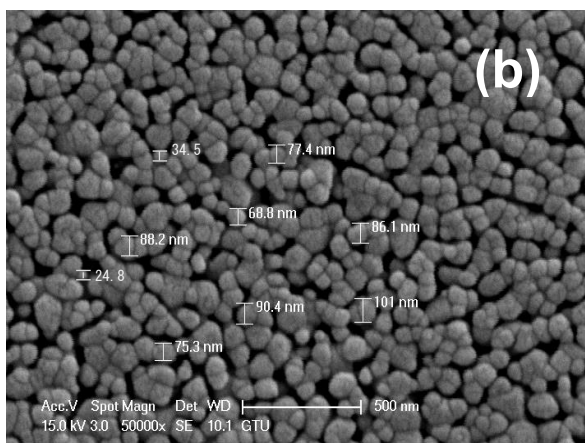
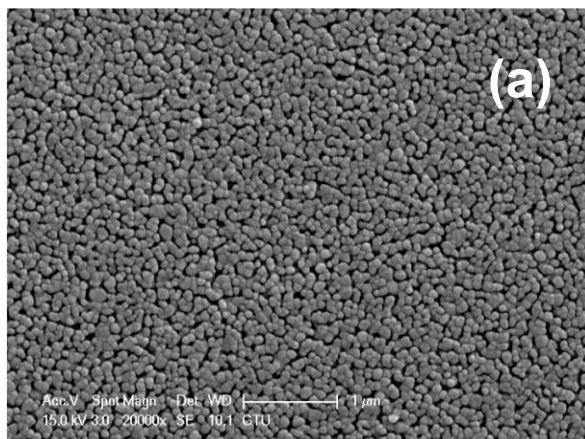
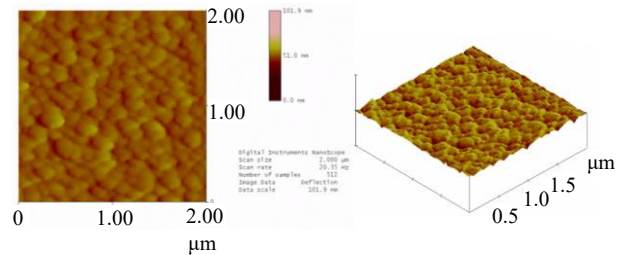
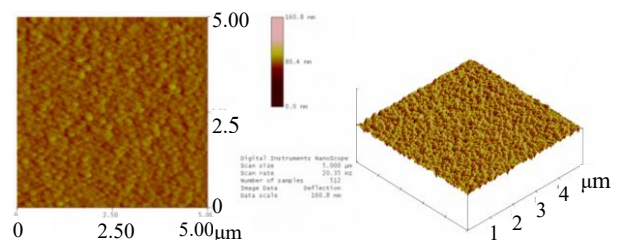


Figure 3. SEM images of the synthesized nanocrystalline ZnO film deposited onto glass substrate. (a) magnification ($\times 20000$) (b) magnification ($\times 50000$)

3D AFM images of the ZnO nanocrystal film of $2 \mu\text{m} \times 2 \mu\text{m}$ and $5 \mu\text{m} \times 5 \mu\text{m}$ size were presented in Figure 4. From the AFM images roughness was determined about 4.30 nm by the AFM software program.



(a)



(b)

Figure 4. 3D AFM images of the synthesized nanocrystalline ZnO film deposited onto glass substrate

(a) $2 \mu\text{m} \times 2 \mu\text{m}$ (b) $5 \mu\text{m} \times 5 \mu\text{m}$.

3.2. Gas Sensing Properties

Gas sensing measurements were conducted in homemade Teflon gas test chamber. Chloroform vapor and nitrogen gas were used as target gas and carrier gas, respectively. In order to test the sensor towards chloroform vapor, the gas sensing measurements were performed depending on gas concentration (750, 2 250, 3 750, 7 500, and 15 000 ppm) at different temperatures between $22 \text{ }^\circ\text{C}$ – $150 \text{ }^\circ\text{C}$. Chloroform vapor were produced in washing bottle filled with extra pure grade chloroform from MERCK. Gas concentrations were calculated by using Antoine equation given below (Equation 2).

$$\text{Log}_{10}P = A - \frac{B}{(T + C)} \quad (2)$$

where P is the vapor pressure in bar, T is the temperature in Kelvin, A , B , and C are vapor depended parameters. Response of the sensor were examined by recording the current values, which is passing through the sensor, as a function of time (Current-time ($I-t$)) at different gas concentrations and temperatures. Figure 5a shows the real-time response of the ZnO based sensor towards chloroform vapor at room temperature.

By examining the Figure 5a, before the chloroform vapor (target gas) exposure to sensor, current passing through the sensor nearly remains same under the flow of nitrogen gas (carrier gas). There is no remarkable change in current before the sensor is exposed towards to chloroform vapor. After the target gas flow turned on, the current begins to increase and then rate of increase slows down. In the 300 seconds time interval, the sensor response does not reach to saturation. After the target gas flow turned off, the current begins to decrease and current passing through the sensor decreases nearly to the initial current value during the sensor exposed to carrier gas. It was observed that total time needed to decrease the initial current value takes greater than 300 seconds. Because of this behavior it can be concluded that the response of the sensor were reversible. As it is well known, adsorption process occur while a sensor exposed to a target gas molecules. During this process if an electron is transferred from the target gas to n-type sensing material of the sensor, the conductivity of the sensing material is increased (physisorption). The increase in conductivity cause an increase in current passing through the sensor [15, 16]. We may conclude that the increase in current passing thorough the our sensor arises from the electron transfer from chloroform to ZnO film due to adsorption process. Another observation is that the change in current passing through the sensor is increased with an increase in gas concentration from 750 ppm to 15000 ppm. We may conclude that change in current increases with increasing gas concentration, since the number of electrons transferred from the target gas to sensing material is proportional to target gas concentration [15, 16, 17].

Response of the sensor at elevated temperatures were presented in Figure 5b (at 100 °C) and Figure 5c (at 150 °C). The sensor showed similar behavior with that of the response at room temperature. The sensor also showed reversible behavior at all measured temperature range and gas concentrations.

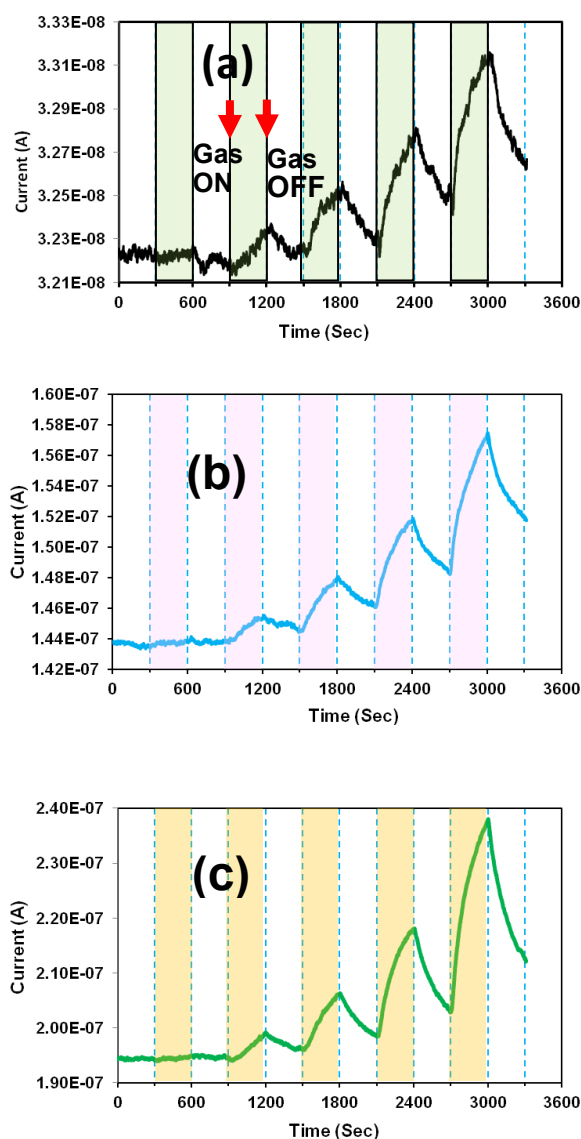


Figure 5. Response of the ZnO nanocrystal film towards chloroform vapor at (a) 22 °C (room temperature, RT) (b) 100 °C (c) 150 °C.

Response time values (τ_{90}) of the sensors was defined as the time it takes to reach 90% of the total change in current in the measured gas concentration. Calculated response time values of the sensors as a function of chloroform vapor concentrations were presented in Figure 6. By examining the Figure 6 it can be seen clearly that, in general, increase in gas concentration caused to decrease in response time values.

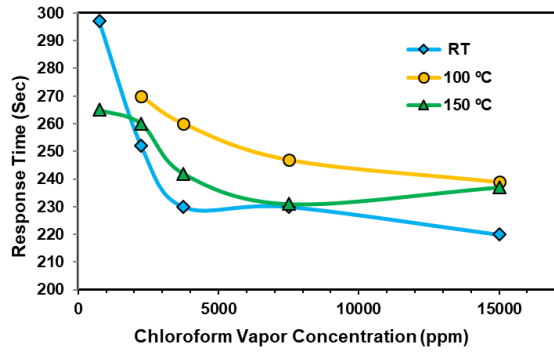


Figure 6. Response time values of the ZnO nanocrystal film as a function of gas concentration at indicated temperatures.

Sensitivity is defined as:

$$S = \left[\frac{\Delta I}{I_o} \right] \quad (3)$$

where I_o is the current passing through the sensor at the time the sensor exposed to target gas, ΔI is the change in current passing through the sensor corresponding to gas concentration.

Sensitivity values of the sensors were presented in Figure 7. The results showed that sensitivity of the ZnO nanocrystal film increased with increasing chloroform vapor concentration. Additionally, increment in temperature caused an increase in sensitivity also.

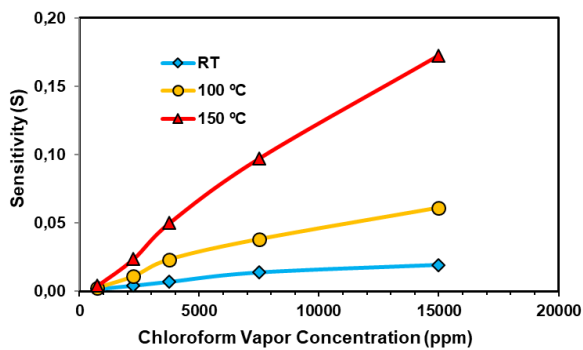


Figure 7. Sensitivity of the ZnO nanocrystal film as a function of gas concentration at indicated temperatures.

IV. CONCLUSION

ZnO nanocrystals were fabricated onto glass substrates. The XRD pattern revealed that the ZnO films were in crystal form and matched with the pattern of ZnO JCPDS number 036-1451. The

crystallite sizes of ZnO nanocrystals were determined by the Scherrer formula, varying between 27.9 – 50.4 nm. Gas sensing measurements showed that the ZnO based sensors can be used as chloroform vapor sensor successfully between the chloroform vapor concentrations of 750 – 15 000 ppm even at room temperature. The results were also showed that sensitivity of the sensors were increased with increasing temperature from 22 °C to 150 °C. Sensing mechanism of the sensors can be explained by electron exchange between the ZnO nanocrystals and chloroform vapor while the adsorption occurs on the surface of the ZnO. Since ZnO shows n-type semiconducting property we can conclude that an electron is transferred from chloroform to ZnO film and that causes an increase in dc conductivity of the ZnO film (physisorption). The best sensitivity values were obtained at 150 °C.

ACKNOWLEDGMENT

This work was supported by Research Fund of Marmara University with the project number: FYL-2022-10636. The authors gratefully acknowledge the Marmara University Commission of Scientific Research Projects (BAPKO) for this partial financial support.

REFERENCES

- [1] <https://www.atsdr.cdc.gov/ToxProfiles/tp6-c2.pdf>
- [2] Çimen, Y., Ermiş, E., Dumludağ, F., Özkaya, A.R., Salih, B. ve Bekaroğlu, Ö. (2014). Synthesis, characterization, electrochemistry and VOC sensing properties of novel ball-type dinuclear metallophthalocyanines. *Sensors and Actuators B* 202 1137–1147.
- [3] Franco, M.A., Conti, P.P., Andre, R.S. ve Correa, D.S. (2022) A review on chemiresistive ZnO gas sensors. *Sensors and Actuators Reports.*, 4 100100.
- [4] Ren, X., Xu, Z., Liu, D., Li, Y., Zhang, Z. ve Tang, Z. (2022) Conductometric NO₂ gas sensors based on MOF-derived porous ZnO nanoparticles. *Sensors and Actuators B: Chemical.*, 357 131384.
- [5] Kang, Y., Yu, F., Zhang, L., Wang, W., Chen, L. ve Li, Y. (2021) Review of ZnO-based nanomaterials in gas sensors. *Solid State Ionics.*, 360, 115544.
- [6] Zhang, J., Wang, S., Wang, Y., Xu, M., Xia, H., Zhang, S., Huang, W., Guo, X. ve Wu, S. (2009) ZnO hollow spheres: Preparation, characterization, and gas sensing properties. *Sensors and Actuators B.*, 139 411–417.
- [7] Kim, K.K., Kim, H.S., Hwang, D.K., Lim, J.H. ve Park, S.J. (2003) Realization of p-type ZnO thin films via phosphorus doping and thermal

- activation of the dopant. *Applied Physics Letters.*, vol. 83 (1) 63–65.
- [8] Srivastava, A.K., Chakraborty, B.R. ve Chandra, S. (2009) Crystallographically oriented nanorods and nanowires of rf magnetron- sputtered zinc oxide. *Journal of Nanomaterials.*, vol. 2009, Article ID 310360.
- [9] Grassi, M., Soares, D.A.W., De Queiroz, A.A.A., Bressiani, A.H.A. ve Bressiani, J.C., (2004) Organometallic chemical vapor deposition of compound semiconductors. *Materials Science and Engineering B.*, vol. 112, no. 2-3, pp. 179–181.
- [10] Al Asmar, R., Ferblantier, G., Maily, F., Gall-Borrut, P. ve Foucaran, A. (2005) Effect of annealing on the electrical and optical properties of electron beam evaporated ZnO thin films. *Thin Solid Films.*, vol. 473, no. 1, 49–53.
- [11] Kang, D. J., Kim, J.S., Jeong, S.W., Roh, Y., Jeong, S.H. ve Boo, J.H. (2005) Structural and electrical characteristics of R.F. magnetron sputtered ZnO films. *Thin Solid Films.*, vol. 475, no. 1-2, 160–165.
- [12] Cheng, X.L., Zhao, H., Huo, L.H., Gao, S. ve Zhao, J.G. (2004) ZnO nanoparticulate thin film: preparation, characterization and gas-sensing property. *Sensors and Actuators B.*, vol. 102, no. 2, 248–252.
- [13] Brockey, N.M. ve S. Genesan. (2004) ZnO thin films by MOCVD. *III-Vs Review.*, vol. 17, no. 7, 23–25.
- [14] Wang, L., Kang, Y., Liu, X., Zhang, S., Huang, W. ve Wang, S. (2002) ZnO nanorod gas sensor for ethanol detection. *Sensors and Actuators B.*, 162, 237-243.
- [15] Şenoğlu S., Özer M., Dumludağ F., Acar N., Salih B., Bekaroğlu Ö., (2020) Synthesis, characterization, DFT study, conductivity and effects of humidity on CO₂ sensing properties of the novel tetrakis-[2-(dibenzylamino)ethoxyl] substituted metallophthalocyanines, *Sensors and Actuators B: Chemical*, vol. 310, 127860
- [16] Köksoy B., Aygün M., Çapkın A., Dumludağ F., Bulut M., (2018) Electrical and gas sensing properties of novel cobalt(II), copper(II), manganese(III) phthalocyanines carrying ethyl 7-oxy-4,8-dimethylcoumarin-3-propanoate moieties, *Journal of Porphyrins and Phthalocyanines*, vol. 22, 1-16
- [17] Yasemin Ç., Emel E., Dumludağ F., Özkaya A., Salih B., Bekaroğlu Ö., (2014) Synthesis, characterization, electrochemistry and VOC sensing properties of novel ball-type dinuclear metallophthalocyanines, *Sensors and Actuators B: Chemical*, vol. 202, 1137-1147

Güneş Paneli Kusurlarının Derin Öğrenme Tabanlı Sınıflandırılması

Classification of Solar Panels Defects Based on Deep Learning

Sebahattin Yiğit LERMİ¹, Tuğba Özge ONUR¹

¹Zonguldak Bülent Ecevit Üniversitesi, Mühendislik Fakültesi, Elektrik-Elektronik Mühendisliği Bölümü,
Zonguldak, Türkiye

Öz

Yenilenebilir enerji kaynaklarının çevreye ve ekolojiye verdiği zararlar, yenilenebilir enerji kaynaklarına olan ilginin artmasına neden olmaktadır. Fotovoltaik (FV) enerji üretimi, temiz ve sürdürülebilir enerji üretimi için mükemmel enerji alternatiflerinden biridir. Fotovoltaik paneller üzerindeki kar, toz, gölge, kuş pisliği, mekaniksel ve fiziksel arıza gibi etkenler enerji üretimindeki verimi azaltmaktadır ve bu yüzden panel bakımı düzenli olarak yapılmalıdır. Bakımlar manuel olarak yapıldığında hatalar olmakta ve uzun zaman almaktadır. Bu nedenle güneş paneli kusurları son zamanlarda geliştirilen görüntü işleme ve derin öğrenme algoritmaları kullanılarak tespit edilebilmektedir. Bu çalışmada, derin öğrenme tekniği kullanılarak güneş panelleri üzerinde hasar tespiti sınıflandırması yapılmıştır. Çalışma iki aşamadan oluşmaktadır. İlk aşama, ön işleme aşamasıdır ve bu aşamada veri seti yetersiz olması nedeniyle veri çoğaltma teknikleri kullanılarak arttırılmıştır. İkinci aşama olan eğitim aşamasında ise çoğaltılan veri seti önerilen derin öğrenme modeliyle eğitilmiştir. Eğitim sonucunda önerilen modelin 7 farklı kusurun sınıflandırılmasında %96.56 başarı elde ettiği gözlemlenmiştir.

Anahtar Kelimeler: Derin öğrenme, Güneş panelleri, Fotovoltaik, Veri çoğaltma, Sınıflandırma

Abstract

The damage caused by non-renewable energy sources to the environment and ecology causes an increase in interest in renewable energy sources. Photovoltaic (PV) energy production is one of the well known energy alternatives for clean and sustainable energy production. Factors such as snow, dust, shadow, bird droppings, mechanical and physical failure on photovoltaic panels reduce the efficiency in energy production, and therefore panel maintenance should be done regularly. When maintenance is performed manually, errors occur and it takes a long time. Therefore, solar panel defects can be detected using recently developed image processing and deep learning algorithms. In this study, a damage detection classification was carried out on solar panels using the deep learning technique. Our study consists of two stages. The first stage is the pre-processing stage. At this stage, the data set is increased using data augmentation techniques due to insufficient data set. In the second stage, the training stage, the replicated data set was trained with the proposed deep learning model. As a result of the training, it was observed that the proposed model achieved %96.56 success in classifying 7 different defects.

Keywords: Deep learning, Solar panels, Photovoltaics, Data augmentation, Classification

I. GİRİŞ

Yenilenebilir enerji kaynaklarının tükenmesi ve çevreye verdikleri zarar, başta güneş enerjisi olmak üzere yenilenebilir enerji kaynaklarına olan ilginin artmasına neden olmuştur. Uluslararası Enerji Ajansı (UEA), 2030 ve 2040 yılına kadar dünyanın elektrik üretiminde yenilenebilir enerji oranının sırasıyla %30 ve %50'ye ulaşabileceğini, FV gücünün ise bu payın %10 ve %20'sini oluşturacağını öngörmektedir [1]. FV teknolojisi son yıllarda hızlı bir şekilde büyümüştür. 2008'den 2011'e kadar yalnızca Kanada'da güneş FV elektriği kurulu kapasitesi yıllık yaklaşık %150 artış göstererek 2011'de 495 MW'a ulaşmıştır [2]. FV sistemler genellikle güneş enerjisi üretimi sağlar. FV sistemlerinin ucuz kurulum maliyetleri, güvenli enerji üretimi, sessiz çalışması ve çevre dostu olması gibi faydaları da dikkat çekmektedir [3, 4].

Son yıllarda FV sistemlerine olan ilginin artması FV üreticilerinin sayısında artışa yol açmıştır. Bu nedenle FV güç üreten sistemlerin dayanıklılığının üretici tarafından garanti edilmesi gerekmektedir. Her ne kadar üretici 25 yıl sonra FV sisteminin çıkış gücünün %80'ini maksimum güç noktasında (MGN) garanti etse de FV sisteminin çıkış performansı zamanla kademeli olarak düşmektedir [5]. FV sistemlerdeki verim düşüşü bozulmalara ve çevresel etkenlere bağlıdır. Tozlanma, karlanma, kuş pisliği, gölgelenme, mekaniksel ve fiziksel hasarlar gibi etkenler panellerin performansını ciddi ölçüde olumsuz etkilemektedir ve bu yüzden panel bakımları düzenli olarak yaptırılmalıdır. Panel kusurunu insan gözüyle saptamak hatalara neden olabileceği gibi zaman ve maliyet açısından da kayıplara yol açmaktadır. Bu sorunların giderilebilmesi için günümüzde kullanımı giderek artan derin öğrenme ve görüntü işleme teknolojileri önerilmektedir.

1.1. İlgili Çalışmalar

Güneş panelleri üzerindeki kusurları saptama ve sınıflandırma konusunda çalışmalar FV modüllerin verimliliği için büyük önem taşımaktadır. Son yıllarda FV panel arızalarının anomalilerini sınıflandırmak için çeşitli çalışmalar yapılmıştır.

Korkmaz ve Açıkgöz fotovoltaik paneller üzerindeki anormallikleri tespit edebilmek ve sınıflandırmak için önerdikleri yöntemi transfer öğrenme stratejisine bağlı çok ölçekli bir evrişimli sinir ağı (ESA) olarak tasarlamışlardır. Veri kümesindeki dengesiz sınıf dağılımı sorununu çözmek için veri büyüme ve aşırı örnekleme tekniği kullanarak ağ performansını arttırmışlardır. Çalışmalarında 11 farklı fotovoltaik panel kusuru (çatlama, sıcak nokta gibi) kullanarak 11 anormali türünü sınıflandırmada %93,51 doğruluk elde etmişlerdir. Elde edilen sonuçların fotovoltaik panellerdeki kusurları bulmak ve sınıflandırmak için yeterli olduğu gözlenmiştir [6].

Espinosa ve arkadaşları yaptıkları çalışmalarda FV kusurları tespit etmek için anlamsal bölümlendirme ve görüntüleri sınıflandırmak için evrişimli sinir ağlarını kullanan otomatik hata sınıflandırma yöntemi önermektedir. Bu çalışma kusurlu ve kusursuz tanımlanan 2 çıkış sınıfı ve kolayca tespit edilemeyen arıza, çatlak, gölge ve toz yok şeklinde 4 çıkış sınıfı için deneysel sonuçları göstermektedir. Önerilen yöntemle 2 çıkış sınıfı için %75 ve 4 sınıf için %70 doğruluk oranına ulaşılmıştır [7].

Kaycı ve arkadaşları çalışmalarında, termal kamera yerleştirilmiş dronla elde edilen güneş paneli termal görüntülerini hücre, modül ve panel arızalarının tespitinde kullanmışlardır. Edinilen görüntüler ile modül kusuru, hücre kusuru ve panel kusuru içeren veri seti hazırlanmıştır. Veri seti YOLOv3 derin öğrenme tabanlı yapay sinir ağıyla eğitilmiştir. Eğitim sonucunda hücre arızaları %98, modül arızaları %89 ve panel arızaları %77 başarıyla saptanmıştır [8].

Pierdicca ve arkadaşları çalışmalarında, FV hücresi bozulmasını tahmin etmek için derin evrişimli sinir ağları (DESA) kullanmaya yönelik yeni bir yöntem önermişlerdir. Bu çalışmada ilk kez termal kızılötesi sensöre sahip bir dronedan alınan bilgiler kullanılmıştır. Bozulma sorununu göstermek ve bu çalışmada önerilen çözümü kapsamlı bir şekilde değerlendirmek için, toplanan fotovoltaik görüntüler veri kümesi üzerinde deneyler yapılmıştır. Eğitilen ağı başarı oranı %70 olarak bulunmuştur [9].

Li ve arkadaşları tarafından yapılan çalışmada, büyük boyutlu fotovoltaik panel alanlarının denetimi sırasında panellerin durumunu gözlemleyebilmek için derin öğrenme tabanlı kusur tespiti kullanan bir yöntem oluşturulmuştur. Oluşturulan bu sistemde kullanılan derin öğrenme tekniği ESA tabanlı bir yapıdır. Çalışma sonucunda toz, kapsülleme, delaminasyon, ızgara hattı

aşınması, salyangoz izleri ve sararma hataları tespit edilmiş ve ortalama %97.9 doğruluk oranı elde edilmiştir. Önerilen yöntemin VGG16 ve geleneksel yöntemlerden daha başarılı olduğu gözlenmiştir [10].

Wei ve arkadaşları tarafından güneş panellerinde sıcak nokta ve yansıtıcı bölge arızalarının teşhis edilebilmesi için iki yaklaşım önerilmiştir. Sıcak noktaların algılanması için Hough çizgi dönüşümünü ve Canny operatörünü, reflektör arızalarının tespit edilmesinde ise derin öğrenme yöntemini kullanmışlardır. Çalışma sonucunda geleneksel görüntü işleme ve daha hızlı bölge tabanlı evrişimli sinir ağları başarı oranları sırasıyla %89,96 ve %95,15 olarak elde edilmiştir [11].

Herraz ve arkadaşları çalışmalarında, güneş panellerindeki kusurları bulmak için insansız hava aracına monte edilen termografik kameradan yararlanılan yeni bir teknik önermişlerdir. Yapılan çalışmada sıcak noktaların tespit edilmesinde ve yeniden konumlandırılmasında kullanılacak panellerin yerinin tespit edilmesi amacıyla yeni bir yöntem sunulmuştur. İki yeni bölge tabanlı evrişimli sinir ağına birleştirilmesiyle güçlü bir tespit çerçevesi geliştirmişlerdir. Otomatik veri toplama ve işleme, denetim sırasında kusurların tespit edilmesini sağlamaktadır. Elde edilen sonuçlar, yaklaşımın %91,67 hassasiyetle ve %99,02'den fazla doğrulukla güneş takip cihazlarının ve göreceli sıcak bölgelerinin otomatik lokalizasyonu için uygun olduğunu göstermektedir [12].

Venkatesh ve arkadaşları insansız hava araçlarından (İHA) elde edilen hava görüntülerinin yardımıyla derin öğrenmeye dayalı fotovoltaik modüllerdeki arıza tespitini sunmaktadır. Veri setlerini VGG16 ile eğitmişler ve yanık izleri, delaminasyon, renk bozulması, fiziksel hasar, sağlam ve salyangoz izi gibi kusurları sınıflandırmada başarılı olduğu gözlenmiştir. Sonuçlar, modelin tüm FV kusurlarını sınıflandırmada %95,40 gibi yüksek bir sınıflandırma doğruluğuna ulaştığını göstermektedir [13].

Xie ve arkadaşları fotovoltaik kızılötesi hedef anomali tespit sistemi önermektedir. FV panel kusurlarının İHA tarafından tespitinin doğruluğunu arttırmak için Sobel ve Canny operatörlerini birleştirmişlerdir. Yatay ve dikey özellikleri çıkarmak için Sobel operatörü, dikey ve yatay kenar özelliklerini hesaplamak ve doldurmak için Canny operatörü kullanılmıştır. Eş zamanlı olarak görüntünün ayırt edici özelliklerini öğrenmek için algoritmaya derin öğrenme uygulanmıştır. Çalışmalar sonucunda model %90,91 oranında sınıflandırma başarısı elde etmiştir [14].

Díaz ve arkadaşları İHA üzerine monte edilmiş termal kamerayla fotovoltaik panelleri için otomatik bir kusur tespit yöntemi önermektedir. Güneş paneli arızalarının tespitinde klasik ve derin öğrenmeye dayalı iki yöntem

kullanılmaktadır. Öncelikle, bazı ön işleme teknikleri kullanılarak termal görüntünün düşük kontrastı düzeltilir. Daha sonra, kenar algılama, segmentasyon ve segment sınıflandırması uygulanır. İkinci yöntem, üç farklı ön işleme işlemine tabi tutulmuş görüntülerle eğitilmiş derin öğrenmeye dayanmaktadır. İlk yöntem sonucu %98,3, ikinci yöntem sonucu %98,9 doğruluğa ulaşmıştır [15].

Akram ve arkadaşları izole edilmiş derin öğrenme ve model geliştirme-transfer derin öğrenme teknikleriyle kızılötesi görüntülerdeki fotovoltaik modül kusurlarının otomatik olarak tespit edilmesi üzerine çalışmışlardır. Veri setleri normal çalışan ve arızalı modüllerin kızılötesi görüntülerini içermektedir. Başlangıçta transfer öğrenimi için fotovoltaik hücrelerin elektrolüminesans (EL) görüntülerinden oluşan bir veri kümesi oluşturmuşlar ve ardından kızılötesi görüntülerden oluşan bir veri kümesi kullanmışlardır. Önerilen yaklaşımla ortalama %99,23'lük bir doğruluk elde edilmiştir [16].

Kurukuru ve arkadaşları termografi ve makine öğrenimi tabanlı FV modülü arıza sınıflandırması üzerine çalışmışlardır. Hasar görmüş panellerden alınan çeşitli termal görüntülerin özelliklerini, doku özelliği analizinin değiştirilmiş bir versiyonunu kullanarak incelemişlerdir. Kusur sınıflandırıcısını oluşturmak için, alınan özellikler bir yapay sinir ağı (YSA) sınıflandırıcısı kullanılarak eğitilmiştir. Oluşturulan yöntem %93,4 eğitim verimliliği ve %91,7 test verimliliği göstermiştir [17].

Zaki ve arkadaşları derin öğrenme tabanlı FV sistem için hata sınıflandırma çalışması yapmışlardır. Yaptıkları çalışmada, öncelikle FV modelin en uygun beş özelliğini çıkarmak için bir algoritma önermişler ve bunun MATLAB simülasyon modeline yardımcı olacağını düşünmüşlerdir. İkinci olarak, derin öğrenme kullanılarak FV sistemlerdeki hataların sınıflandırılmasına yönelik yeni bir yaklaşım önermişlerdir. Bu yöntem, bilgisayardaki performansı ve sınıflandırma doğruluğunu artıran otomatik özellik çıkarma özelliğine sahiptir. Son olarak, kullanılan ESA modelinin teorik ve pratik doğrulaması için çeşitli atmosferik koşullara dayalı olarak normal ve altı arıza örneği seçmişlerdir. Önerilen ESA modeli, eğitim ve test süreçleri için simülasyon testlerinde sırasıyla %98,3 ve %98,9, deneysel testlerde ise %96,76 ve %97,41 civarında ortalama sınıflandırma doğruluğu elde etmiştir [18].

Deitsch ve arkadaşları, EL görüntülerinde arızalı fotovoltaik modül hücrelerinin otomatik sınıflandırılması adlı çalışmalarında FV hücrelerdeki sorunları tespit edebilmek amacıyla 2 farklı yaklaşım ortaya sunmuşlardır. Yaklaşımlar, donanım gereksinimleri nedeniyle farklılık göstermektedir. Donanım açısından verimli olan, Destek Vektör Makinesi (DVM) kullanılarak sınıflandırılmaya dayanmaktadır. Daha fazla donanım gerektiren yöntem

ise ESA'yı kullanmaktadır. Her iki yaklaşım da 1968 farklı hücre üzerinde eğitilmiştir. ESA başarı oranı %88,42 ve DVM başarı oranı %82,44'tür [19].

Tang ve arkadaşları EL görüntüleri kullanılarak fotovoltaik modülün derin öğrenme tabanlı otomatik kusur tespiti isimli çalışmalarında 2 farklı adımla EL görüntülerini derin öğrenmeye dayalı kusur tespitini sunmuşlardır. Önerilen çalışmada ilk adım kısıtlı sayıdaki EL görüntüyü yüksek kalitede arttırmak, ikinci adım ise elde edilen görüntüler ile otomatik sınıflandırma yapan bir model ortaya koymaktır. EL görüntü oluşturma yöntemi, Çekişmeli Üretici Ağ (ÇÜA) özelliklerini geleneksel görüntü işleme teknolojileriyle birleştirmektedir. EL görüntülerinden derin özelliklerin çıkarılmasında, ESA kullanılmaktadır. Önerilen model diğer çözümlerle karşılaştırıldığında, FV modülü denetiminin doğruluğunu ve verimliliğini önemli ölçüde artırabilir. Önerilen model %83'lük başarı oranına sahiptir [20].

Sunulan literatür taramasından görüldüğü üzere, güneş panellerindeki hasarların tespiti için son dönemde birçok çalışma yapılmıştır. Ancak yapılan çalışmalarda yaklaşımların hiçbiri çok sınıflı hasarları kısa bir sürede yüksek doğrulukta sınıflandıramamaktadır. Güneş panelleri üzerindeki hasarların erken tespit ve müdahale edilebilmesi, veriminin artması için oldukça önemlidir. Bu çalışmada, güneş panelleri üzerindeki hasarların hızlı ve otomatik bir şekilde tespit edilebilmesi için görüntü işleme ve derin öğrenme tabanlı arıza tespit yöntemi önerilmiştir. Önerilen yöntem, ön işleme ve ESA tabanlı oluşturulan derin öğrenme mimarisine sınıflandırma aşamaları olmak üzere 2 aşamadan oluşmaktadır. Bu çalışma kapsamında farklı iklim şartlarında elde edilen görüntüler, model performansının iyileştirilmesi ve veri setinin yetersiz olması nedeniyle veri çoğullama teknikleri ile (yakınlaştırma, simetrisini alma, görüntüyü belirli açılarla döndürme, gürültü ekleme ve parlaklık değiştirme) artırılmıştır. Önerilen yöntem 7 farklı panel kusurunu yüksek doğrulukta sınıflandırabilmektedir.

II. MATERYAL VE METOD

2.1. Veri Seti

Bu çalışma kapsamında kullanılan veri seti, açık erişimli Kaggle [21] web sitesinden elde edilmiştir.

2.2. Ön İşleme

Veri setinde Tablo 1'de görüldüğü üzere toplam 988 adet farklı görüntü vardır. Her görüntü 0-6 arası sınıflandırılmıştır. Kuş Pislği olan paneller 1, Temiz olan paneller 2, Tozlu olan paneller 3, Elektriksel Hasarlı paneller 4, Fiziksel Hasarlı paneller 5, Gölgelemiş paneller 6, Karlı paneller 7 olarak sınıflandırılmıştır.

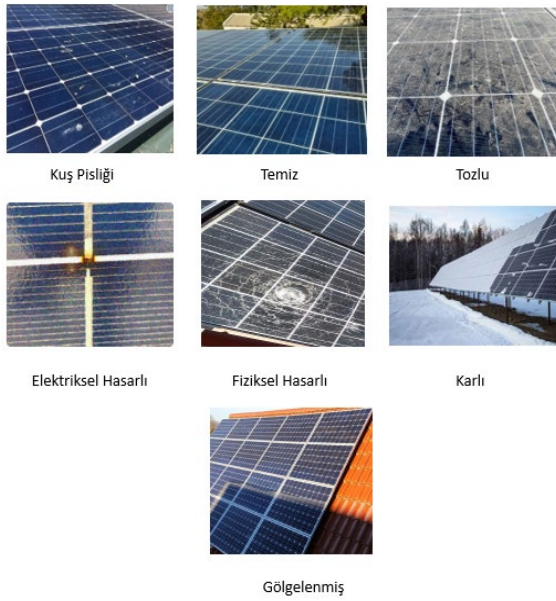
Tablo 1 Orijinal veri seti

Sınıf	Panel Durumu	Görüntü Sayısı
0	Kuş Pisiği	200
1	Temiz	202
2	Tozlu	220
3	Elektriksel	98
4	Hasarlı	66
5	Fiziksel	66
6	Hasarlı	66
5	Karlı	122
6	Gölgelenmiş	80

Tablo 2 Çoğaltılmış veri seti

Sınıf	Panel Durumu	Görüntü Sayısı
0	Kuş Pisiği	820
1	Temiz	1040
2	Tozlu	920
3	Elektriksel	850
4	Hasarlı	830
5	Fiziksel	830
6	Hasarlı	830
5	Karlı	917
6	Gölgelenmiş	720

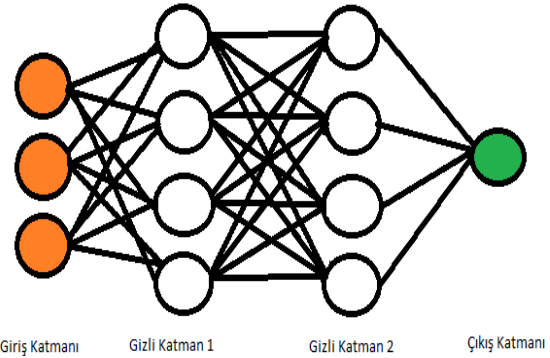
Tablo 1’de görüldüğü üzere veri setinde, 200 adet kuş pisiği, 202 adet temiz, 220 adet tozlu, 98 adet elektriksel hasarlı 66 adet fiziksel hasarlı, 122 adet karlı ve 80 adet gölgelenmiş panel görüntüsü vardır. Bu çalışmada kullanılan veri setindeki panel görüntüsü örnekleri Şekil 1’de gösterilmiştir.

**Şekil 1.** Veri setinde bulunan örnek panel görüntüleri

Tablo 1’ de görüldüğü üzere veri seti, görüntü sayısı açısından yetersizdir ve sınıflandırma elemanları arasındaki sayı dengesizliği dikkat çekmektedir. Ayrıca, .png ve .jpg olarak bulunan görüntülerin çözünürlükleri farklılık göstermektedir. Bunun önüne geçmek için veri seti çözünürlükleri 256x256 hale getirilmiş ve farklı veri çoğaltma metotları (ölçeklendirme, döndürme, yakınlaştırma, gürültü ekleme) kullanılarak veri setinin her sınıfı için yaklaşık 1000’er ve toplamda 6097 adet görüntü elde edilmiştir. Çoğaltılan veri seti ile modelin aşırı öğrenmesinin önüne geçilmiştir. Yeni veri setinin görüntü sayısı Tablo 2’de gösterilmiştir.

2.3. Derin Öğrenme

Derin öğrenme, temeli yapay sinir katmanlarından oluşan bir ağdır. Çoklu nöron bağlantıları birleşerek katmanları oluşturur. Derin sinir ağları, katmanların üst üste istiflenmesiyle oluşturulan yapay sinir ağlarının diğer adıdır. Burada oluşan ağız derinliği katman sayısının az veya çok olmasıyla belirlenir. Katman sayısı arttıkça ağ yapısı derinleşmektedir. Benzer şekilde katman sayısının azalması, ağ yapısının ya derin olmadığını ya da derinleştiğini gösterir [22]. Şekil 2’de örnek bir derin öğrenme modeli verilmiştir.

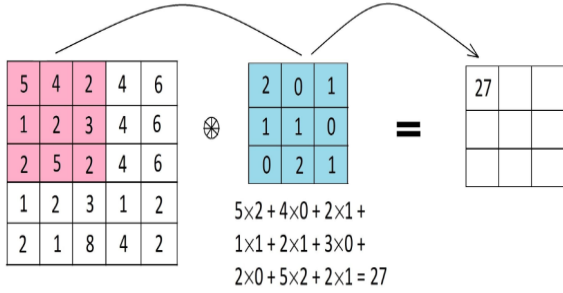
**Şekil 2.** Derin öğrenme adımları

ESA; giriş, evrişim, havuzlama, düzleştirme, aktivasyon, seyreltme, tam bağlantı ve sınıflandırma katmanları olmak üzere sekiz katmandan oluşmaktadır.

Giriş katmanı, adından da anlaşılacağı gibi ESA'nın en üst katmanıdır. Performans ve maliyet açısından doğru giriş görsel boyutunun kullanılması gerekir. Görsel boyutunun artması başarı oranını arttıracak gibi işlem sayısını da artırır, bu durum da performansı olumsuz etkiler. Aynı şekilde görsel boyutunun küçülmesi başarı oranını azaltacağı gibi işlem sayısını da azaltır, bu durum da performansı olumlu etkileyebilmektedir.

Evrişim katmanı ESA'ların temel yapı taşıdır [23]. Bu katman, dönüşüm katmanı olarak da bilinir ve bu dönüşüm filtrenin bütün görüntü üzerinde dolaştırılmasıdır [24]. Filtreler 2x2, 3x3, 5x5 gibi farklı

boyutlarda olabilir. Filtreler, önceki katmandaki görüntüler üzerinde evrişim işlemi kullanarak çıktı verilerini üretir. Bu işlem sonucu Özellik Haritası oluşur.

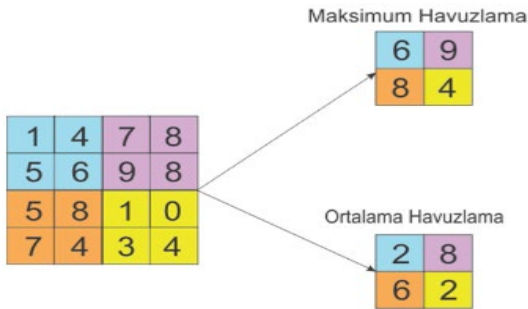


Şekil 3. Konvolüsyon işlemi uygulanma örneği

Evrişim katmanında üretilen her özellik haritası, bir ESA'ya doğrusal olmama özelliği sağlamak amacıyla aktivasyon fonksiyonu kullanır. ReLU (Rectified Linear Unit) en popülerleridir [24].

Bir ESA tasarımında, havuzlama katmanı evrişim katmanları arasında sıkıştırılmıştır. Havuzlama katmanının temel amacı, ağırlık hesaplamasını ve parametre sayısını azaltmak için düzeltilmiş özellik haritalarının boyutunu azaltmaktır, bu da eğitim süresini kısaltır ve aşırı uyumu önler.

Havuzlamayı gerçekleştirmek için sıklıkla ortalama veya maksimum havuzlama gibi basit bir yöntem kullanılır. Maksimum havuzlama diğer havuzlama yöntemleriyle karşılaştırıldığında, daha yüksek performans ve daha hızlı yakınsama gösterdiği görülmüştür [25].



Şekil 4 Maksimum ve ortalama havuzlama örneği

Düzleştirme katmanı, 2 veya 3 boyutlu gibi çok boyutlu formattaki verileri tek boyutlu bir vektöre dönüştürür. Tamamen bağlı katmanlar, bir ESA'da girişin bir boyutlu bir vektör olmasını beklediklerinden, bu yeniden şekillendirme işlemi, evrişim ve havuzlama katmanlarından tamamen bağlı katmanlara geçişte gereklidir.

Bir ESA tasarımında, tam bağlantılı katman genellikle en sonda bulunur [22]. Tam bağlantılı katmanda nöronlar, geleneksel sinir ağlarındakine benzer şekilde gruplandırılır. Önceki evrişimli veya havuzlama katmanının çıktısından elde edilen düzleştirilmiş bir vektör, girdi olarak kullanılır.

Aşırı uyumu azaltmak için derin öğrenmede ve sinir ağlarında seyreltme katmanı adı verilen bir düzenleme yöntemi kullanılır. Bir model, eğitim verileri üzerinde iyi performans göstermeyi öğrendiğinde ancak yeni, denetlenmemiş verilere genelleme yapmakta zorlandığında, modelin aşırı uyumlu olduğu anlaşılır. Seyreltme, bu soruna basit ama etkili bir çözümdür. Tamamen bağlantılı katmanın ardından bu katman gelir. Derin öğrenme mimarisinin bu katmanında sınıflandırma gerçekleşir. Bu katmanın çıkış değeri sınıflandırılacak nesne sayısı kadardır. Farklı sınıflandırıcılar olsa da başarısından dolayı genellikle softmax kullanılır [24].

III. SONUÇLAR VE TARTIŞMA

Bu çalışmada, güneş paneli kusurlarını yüksek doğrulukta sınıflandırabilmek için model yapısında ve parametrelerinde düzenlemeler yapılarak en iyi sonuca ulaşılmaya çalışılmıştır. Deneylerde 2 farklı model yapısı kullanılmıştır. Model özetleri Şekil 5 ve Şekil 6' da verilmiştir.

sequential (Sequential)	(32, 256, 256, 3)	0
conv2d (Conv2D)	(32, 254, 254, 32)	896
max_pooling2d (MaxPooling2D)	(32, 127, 127, 32)	0
conv2d_1 (Conv2D)	(32, 125, 125, 64)	18496
max_pooling2d_1 (MaxPooling2D)	(32, 62, 62, 64)	0
conv2d_2 (Conv2D)	(32, 60, 60, 64)	36928
max_pooling2d_2 (MaxPooling2D)	(32, 30, 30, 64)	0
conv2d_3 (Conv2D)	(32, 28, 28, 64)	36928
max_pooling2d_3 (MaxPooling2D)	(32, 14, 14, 64)	0
conv2d_4 (Conv2D)	(32, 12, 12, 64)	36928
max_pooling2d_4 (MaxPooling2D)	(32, 6, 6, 64)	0
conv2d_5 (Conv2D)	(32, 4, 4, 64)	36928
max_pooling2d_5 (MaxPooling2D)	(32, 2, 2, 64)	0
flatten (Flatten)	(32, 256)	0
dense (Dense)	(32, 64)	16448
dropout (Dropout)	(32, 64)	0
dense_1 (Dense)	(32, 7)	455

Şekil 5. Denenen ilk model yapısı

sequential (Sequential)	(32, 256, 256, 3)	0
conv2d (Conv2D)	(32, 254, 254, 32)	896
max_pooling2d (MaxPooling2D)	(32, 127, 127, 32)	0
conv2d_1 (Conv2D)	(32, 125, 125, 64)	18496
max_pooling2d_1 (MaxPooling2D)	(32, 62, 62, 64)	0
conv2d_2 (Conv2D)	(32, 60, 60, 128)	73856
max_pooling2d_2 (MaxPooling2D)	(32, 30, 30, 128)	0
conv2d_3 (Conv2D)	(32, 28, 28, 128)	147584
max_pooling2d_3 (MaxPooling2D)	(32, 14, 14, 128)	0
conv2d_4 (Conv2D)	(32, 12, 12, 128)	147584
max_pooling2d_4 (MaxPooling2D)	(32, 6, 6, 128)	0
conv2d_5 (Conv2D)	(32, 4, 4, 256)	295168
max_pooling2d_5 (MaxPooling2D)	(32, 2, 2, 256)	0
flatten (Flatten)	(32, 1024)	0
dense (Dense)	(32, 64)	65600
dropout (Dropout)	(32, 64)	0
dense_1 (Dense)	(32, 7)	455

Şekil 6. Denenen ikinci model yapısı

Şekil 5' te görüldüğü üzere, ilk modelde 6 konvolüsyon katmanı bulunmaktadır. Bu katmanlardaki filtre sayıları sırasıyla 32, 64, 64, 64, 64, 64'tür. Şekil 6' da görülen ikinci modelde de 6 konvolüsyon katmanı bulunmaktadır ve katmanlardaki filtre sayıları sırasıyla 32, 64, 128, 128, 128, 256' dir. Tablo 3' te parametre değişikliklerinin başarı oranı ve eğitim süresine etkisi görülmektedir.

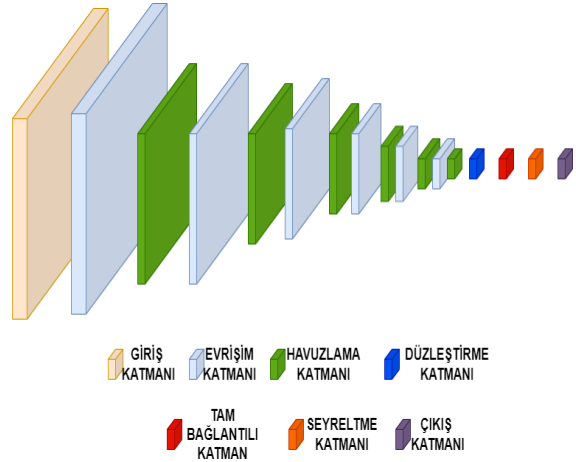
Tablo 3. Parametre değişimlerini ve sonuçları

Parametre	Model 1	Model 2	Model 3	Model 4
Epok sayısı	50	50	50	50
Kümeleme sayısı	32	32	32	16
Seyreltme miktarı	0.5	0.5	Yok	Yok
Model yapısı	1.yapı	2.yapı	1.yapı	1.yapı
Başarı oranı	96.56	95.94	95.78	91.03
Eğitim süresi	57 dakika	63 dakika	56 dakika	51 dakika

Tablo 3' te denenen modeller 10'ar kez çalıştırılıp ortalamaları alınmıştır. Bunun sonucunda görüldüğü gibi denenen 4 farklı model arasından başarı oranı ve eğitim süresi gibi faktörler göz önüne alınarak Model 1 seçilmiştir.

Tablo 3' te denenen modeller 10'ar kez çalıştırılıp ortalamaları alınmıştır. Bunun sonucunda görüldüğü gibi denenen 4 farklı model arasından başarı oranı ve

eğitim süresi gibi faktörler göz önüne alınarak Model 1 seçilmiştir.



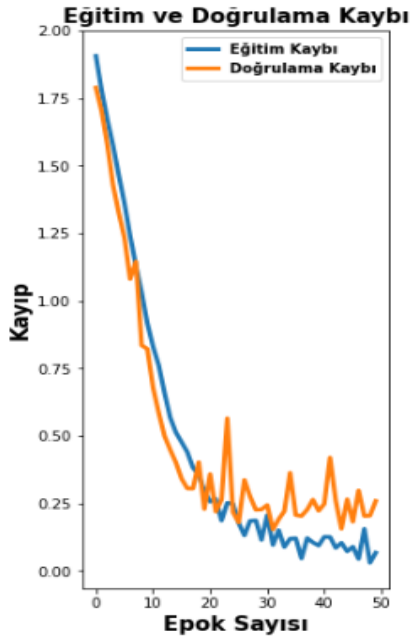
Şekil 7. Önerilen evrişimli sinir ağı modeli

Önerilen mimarinin eğitimi sırasında en hızlı ve en iyi yakınsama yaptığından dolayı Adam optimizasyonu kullanılarak epok başına ağırlıklar sürekli olarak güncellenmiştir. Önerilen modelde kullanılan parametreler Tablo 4'te verilmiştir.

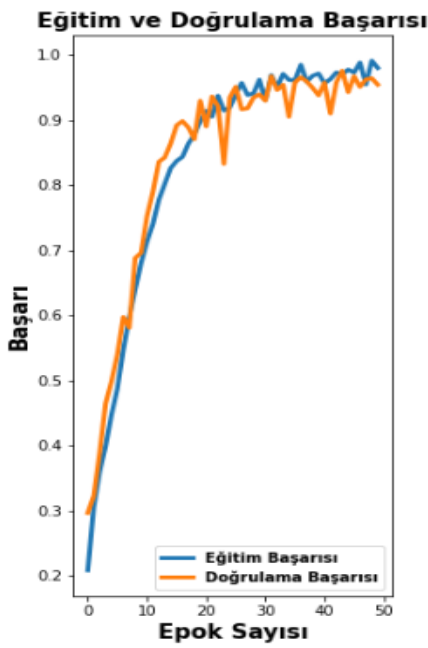
Tablo 4. Önerilen model parametreleri

Epok sayısı	50
Kümeleme(batch)	32
Öğrenme oranı	10 ⁻⁵
Görsel boyutları	256x256
Evrişim	
Aktivasyon fonksiyonu	ReLU
Sınıflandırma	
Aktivasyon fonksiyonu	Softmax
Kayıp fonksiyonu	Losses.SparseCategorical Crossentropy
Seyreltme katsayısı	0.5

Güneş paneli kusurlarının sınıflandırılmasına yönelik yapılan bütün çalışmalar, Intel(R) Core(TM) i5-7200U CPU @ 2.50GHz 2.71 GHz işlemci, 2 GB NVIDIA GeForce 940 MX ekran kartı ve 12 GB RAM'e sahip bilgisayarda Jupyter Notebook kullanılarak gerçekleştirilmiştir. Eğitim sonucu epok başına hata grafiği Şekil 8' de görülmektedir. Şekil 8'den de görüldüğü üzere eğitim ve doğrulama kayıpları 0'a yakınsamakta ve bu da modelin aşırı uyuma düşmediğini göstermektedir. Önerilen modelin eğitim süresi epok başına 68 saniyedir. Eğitim toplamda 57 dakikada tamamlanmıştır.



Şekil 8. Eğitim ve doğrulama kaybı grafiği



Şekil 9. Eğitim ve doğrulama başarıları grafiği

Önerilen modelin eğitim ve doğrulama başarıları Şekil 9’da gösterilmiştir. Şekil 9’da görüldüğü üzere önerilen model, veri setini %96,56 gibi yüksek bir doğrulukta eğitmiştir.

3.1. Performans Metrikleri

Önerilen model tarafından yapılan tahminlerin veri kümesindeki gerçek sınıf etiketleriyle ne kadar iyi eşleştiğinin belirlenmesi amacıyla geri çağırma, kesinlik ve f1-skoru performans metrikleri kullanılmıştır.

Kesinlik: Tüm gerçek olumsuz örnekler arasında yanlış pozitif tahminlerin oranıdır.

$$\frac{TP}{(TP + FP)} \quad (1)$$

Geri Çağırma: Tüm gerçek olumlu örnekler arasında gerçek olumlu tahminlerin oranıdır.

$$\frac{TP}{(TP + FN)} \quad (2)$$

F1-Skoru: İki ölçüm arasında denge sağlayan hassaslık ve hatırlamanın harmonik ortalamasıdır.

$$\frac{2 * \text{Geri Çağırma} * \text{Kesinlik}}{(\text{Kesinlik} + \text{Geri Çağırma})} \quad (3)$$

Eşitlik (1), (2) ve (3) ’te TP modelin pozitif bir sınıfın bir örneğini pozitif olarak doğru bir şekilde tanımladığı örnekleri gösteren gerçek pozitifler; TN modelin negatif sınıfın bir örneğini negatif olarak doğru bir şekilde tanımladığı örnekleri gösteren gerçek negatifler; FP modelin negatif bir sınıf örneğini hatalı olarak pozitif olarak yansıttığı örnekleri gösteren yanlış pozitifler; FN modelin pozitif bir sınıf örneğini olumsuz olarak yanlış yorumladığı örnekleri gösteren yanlış negatifler anlamına gelmektedir.

Buna göre sırasıyla eşitlik (1), (2) ve (3) ile hesaplanan performans metrik değerleri Tablo 5’te verilmiştir.

Tablo 5. Performans metrikleri

	Kesinlik	Geri Çağırma	F1 Skoru
Kuş Pislği	0.95	0.96	0.96
Temiz	0.98	0.94	0.96
Tozlu	0.97	0.94	0.95
Elektriksel-Hasarlı	0.96	0.99	0.97
Fiziksel-Hasarlı	0.97	0.97	0.97
Karlı	1	0.97	0.98
Gölgelenmiş	0.92	0.97	0.95
Ortalama	0.97	0.97	0.97

Tablo 5’te görüldüğü üzere ortalama kesinlik değeri 0.97, geri çağırma değeri 0.97 ve f1-skoru 0.97 olarak hesaplanmıştır.

Gerçek	0-Kuş Pislği	79	1	0	0	3	0	0
	1-Temiz	1	97	0	0	1	0	2
	2-Tozlu	7	1	87	3	0	0	2
	3-Elektriksel-Hasarlı	0	1	0	95	0	0	0
	4-Fiziksel-Hasarlı	2	0	0	0	73	0	0
	5-Karlı	3	1	0	0	0	94	2
	6-Gölgelenmiş	0	1	0	1	0	0	83
	Tahmin	0-Kuş Pislği	1-Temiz	2-Tozlu	3-Elektriksel-Hasarlı	4-Fiziksel-Hasarlı	5-Karlı	6-Gölgelenmiş

Şekil 10. Eğitim sonucu oluşan karışıklık matrisi

Şekil 10' da modelin karışıklık matrisi görülmektedir. Bu matris eğitimin doğruluğunun görülebilmesi açısından önemlidir. Örneğin, model 100 adet tozlu panel görüntüsünün 87'sini doğru tahmin etmiştir. 1 adet görüntü tozlu olmasına rağmen temiz olarak, 7 tanesi kuş pislği olarak, 3 adet görüntü elektriksel hasarlı olarak, 2 adet görüntü ise gölgelenmiş olarak tahmin edilmiştir.

Tablo 6' da önerilen modelin yapılan çalışmalarla karşılaştırılması gösterilmiştir. Önerilen model, çok sınıflı hasarları kısa bir sürede yüksek doğrulukta sınıflandırma konusunda diğer çalışmaların önündedir.

Tablo 6. Önerilen modelin mevcut çalışmalarla karşılaştırılması

	Sınıf Sayısı	Başarı Oranı	Eğitim süresi
Korkmaz ve Ark. [6]	11	93.5	-
Espinosa ve Ark. [7]	4	70	-
Pierdica ve Ark. [9]	2	70	-
Li ve Ark. [10]	6	97.9	8 saat

Vankatesh ve Arkadaşları [13]	6	95.4	-
Kurukuru ve Arkadaşları [17]	8	91.7	-
Önerilen model	7	96.56	57 Dakika

IV. SONUÇ

Yenilenemez enerji kaynaklarının tükenmesi ve çevreye verdikleri zarar, başta güneş enerjisi olmak üzere yenilenebilir enerji kaynaklarına olan ilginin artmasına neden olmuştur. Yenilenebilir enerji kaynaklarının en yaygını, doğada en çok bulunan güneştir. Güneş panelleri, güneş enerjisini elektrik enerjisine çeviren sistemlerdir. Güneş panellerinin yaygınlığı günümüzde giderek artmaktadır.

Güneş panellerinden iyi performans alabilmek için panel bakımı düzenli yapılmalıdır. Ancak panel bakımları maliyet ve zaman gerektirmektedir.

Bu çalışmada panel kusurları, "Kuş Pislği, Temiz, Tozlu, Elektriksel Hasarlı, Fiziksel Hasarlı, Karlı ve Gölgelenmiş" şeklinde sınıflandırılan veri seti kullanılmış ve kusurların tespit edilerek sınıflandırılabilmesi için derin öğrenme tabanlı bir ESA modeli önerilmiştir. Önerilen modelin kesinlik, geri çağırma ve f1-skoru değerleri sırasıyla %97, %97, %97 olarak ölçülmüştür. Elde edilen sonuçlar, panel kusurlarının sınıflandırılması için önerilen modelin diğer modellere kıyasla çok sınıflı hasarları kısa bir sürede yüksek doğrulukta sınıflandırma konusunda önde olduğunu göstermektedir. Çalışmada önerilen model sayesinde, panel kusurları kısa sürede yüksek bir doğrulukla belirlenebilecek ve panellerden istenilen verim alınabilecektir.

KAYNAKLAR

- [1] "Times of 1500 PV system has come" URL: <https://www.mornsun-power.com/html/news-detail/blog-posts/213.html>
- [2] Platon, R., Martel, J. T., Woodruff, N., & Chau, T. Y. (2015b). Online fault detection in PV systems. IEEE Transactions on Sustainable Energy, 6(4), 1200–1207. <https://doi.org/10.1109/tste.2015.2421447>
- [3] Li, B., Delpha, C., Diallo, D., & Migan Dubois, A. (2021). Application of artificial neural networks to photovoltaic fault detection and diagnosis: A review. Renewable & Sustainable Energy

- Reviews, 138, 110512. <https://doi.org/10.1016/j.rser.2020.110512>
- [4] Tang, W., Yang, Q., Xiong, K., & Yan, W. (2020). Deep learning based automatic defect identification of photovoltaic module using electroluminescence images. *Solar Energy*, 201, 453–460. <https://doi.org/10.1016/j.solener.2020.03.049>
- [5] Jordan, D., Kurtz, S., VanSant, K., & Newmiller, J. (2016). Compendium of photovoltaic degradation rates. *progress in photovoltaics*, 24(7), 978–989. <https://doi.org/10.1002/pip.2744>
- [6] Korkmaz, D., & Açıköz, H. (2022). An efficient fault classification method in solar photovoltaic modules using transfer learning and multi-scale convolutional neural network. *Engineering Applications of Artificial Intelligence*, 113, 104959. <https://doi.org/10.1016/j.engappai.2022.104959>
- [7] Espinosa, A. R., Bressan, M., & Giraldo, L. F. (2020). Failure signature classification in solar photovoltaic plants using RGB images and convolutional neural networks. *Renewable Energy*, 162, 249–256. <https://doi.org/10.1016/j.renene.2020.07.154>
- [8] Kayci, B., Demir, B. E., & Demir, F. (2022). İHA tarafından elde edilen termal görüntüler kullanılarak fotovoltaik sistemde derin öğrenme tabanlı arıza tespiti ve teşhisi. *Politeknik Dergisi*, 1, 1. <https://doi.org/10.2339/politeknik.1094586>
- [9] Pierdicca, R., Malinverni, E. S., Piccinini, F., Paolanti, M., Felicetti, A., & Zingaretti, P. (2018). Deep convolutional neural network for automatic detection of damaged photovoltaic cells. *The International Archives of the Photogrammetry, Remote Sensing and Spatial Information Sciences*, XLII-2, 893–900. <https://doi.org/10.5194/isprs-archives-xlii-2-893-2018>
- [10] Li, X., Yang, Q., Lou, Z., & Yan, W. (2019). Deep learning based module defect analysis for large-scale photovoltaic farms. *IEEE Transactions on Energy Conversion*, 34(1), 520–529. <https://doi.org/10.1109/tec.2018.2873358>
- [11] S. Wei, X. Li, S. Ding, Q. Yang and W. Yan, (2019). Hotspots Infrared detection of photovoltaic modules based on hough line transformation and faster-rcnn approach, 2019 6th International Conference on Control, Decision and Information Technologies (CoDIT), pp. 1266-1271, <https://doi.org/10.1109/codit.2019.8820333>
- [12] Herráiz, Á. H., Marugán, A. P., & Márquez, F. P. G. (2020). Photovoltaic plant condition monitoring using thermal images analysis by convolutional neural network-based structure. *Renewable Energy*, 153, 334–348. <https://doi.org/10.1016/j.renene.2020.01.148>
- [13] Venkatesh, S., & Sugumaran, V. (2021). Fault detection in aerial images of photovoltaic modules based on deep learning. *IOP Conference Series*, 1012(1), 012030. <https://doi.org/10.1088/1757-899x/1012/1/012030>
- [14] Xie, X., Wei, X., Wang, X., Guo, X., Ju, L., & Cheng, Z. (2020). Photovoltaic panel anomaly detection system based on unmanned aerial vehicle platform. *IOP Conference Series*, 768(7), 072061. <https://doi.org/10.1088/1757-899x/768/7/072061>
- [15] Díaz, J. J. V., Vlaminc, M., Lefkaditis, D., Vargas, S. a. O., & Luong, H. (2020). Solar panel detection within complex backgrounds using thermal images acquired by UAVs. *Sensors*, 20(21), 6219. <https://doi.org/10.3390/s20216219>
- [16] Akram, M. W., Li, G., Jin, Y., Xiao, C., Zhu, C., & Ahmad, A. (2020). Automatic detection of photovoltaic module defects in infrared images with isolated and develop-model transfer deep learning. *solar energy*, 198, 175–186. <https://doi.org/10.1016/j.solener.2020.01.055>
- [17] Kurukuru, V. S. B., Haque, A., Khan, M. A., & Tripathy, A. K. (2019). Fault classification for photovoltaic modules using thermography and machine learning techniques, 2019 International Conference on Computer and Information Sciences (ICCIS), pp. 1-6, <https://doi.org/10.1109/iccisci.2019.8716442>
- [18] Zaki, S. A., Zhu, H., Fakhri, M. A., Sayed, A. R., & Yao, J. (2021). Deep learning-based method for faults classification of PV system. *Iet Renewable Power Generation*, 15(1), 193–205. <https://doi.org/10.1049/rpg2.12016>
- [19] Deitsch, S., Christlein, V., Berger, S., Buerhop Lutz, C., Maier, A., Gallwitz, F., & Rieß, C. (2019). Automatic classification of defective photovoltaic module cells in electroluminescence images. *Solar Energy*, 185, 455–468. <https://doi.org/10.1016/j.solener.2019.02.067>
- [20] Tang, W., Yang, Q., Xiong, K., & Yan, W. (2020b). Deep learning based automatic defect identification of photovoltaic module using electroluminescence images. *Solar Energy*, 201, 453–460. <https://doi.org/10.1016/j.solener.2020.03.049>
- [21] Solar panel clean and faulty images. (2023, May 16). Kaggle. <https://www.kaggle.com/datasets/pythonafroz/solar-panel-clean-and-faulty-images>
- [22] LeCun, Y., Bengio, Y., & Hinton, G. E. (2015b). Deep learning. *nature*, 521(7553), 436–444. <https://doi.org/10.1038/nature14539>
- [23] Krizhevsky, A., Sutskever, I., & Hinton, G. E. (2017). ImageNet classification with deep convolutional neural networks. *Communications of the ACM*, 60(6), 84–90. <https://doi.org/10.1145/3065386>
- [24] İnik, Ö. & Ülker, E. (2017). Derin öğrenme ve görüntü analizinde kullanılan derin öğrenme modelleri, *Gaziosmanpaşa Bilimsel Araştırma Dergisi*, c. 6, sayı. 3, ss. 85-104. <http://dergipark.gov.tr/download/article-file/380999>

- [25] Scherer, D., Müller, A., & Behnke, S. (2010). Evaluation of pooling operations in convolutional architectures for object recognition. in proceedings of the International Greece, Springer: Berlin/Heidelberg, Germany, 2010; pp. 92–101.

Green Synthesis, Characterization and Antibacterial Activities of Silk Sericin Capped Zinc Oxide Nanoparticles

Aleyna TEMEL ¹, Zehra GÜN GÖK ¹

¹ Kırıkkale Üniversitesi, Mühendislik ve Doğa Bilimleri Fakültesi, Biyomühendislik Bölümü, Kırıkkale, Türkiye

Abstract

In recent years, interest in metal-based antibacterial materials has increased due to microorganisms gaining resistance to antibiotics. Silk sericin obtained from *Bombyx mori* cocoon has found use in many different areas thanks to its biocompatibility, hydrophilic character and biodegradability. Zinc oxide nanoparticles (ZnONPs) obtained in various zinc salts exhibit broad-spectrum antibacterial properties. In this study, to be produce metal based antibacterial materials, synthesis of silk sericin-coated ZnONPs (SS-ZnONPs) in a green and scalable method was investigated by using silk sericin protein as both reducing and capping agent to obtain ZnONPs. For producing SS-ZnONPs, 2% silk sericin solution was mixed with Zn(NO₃)₂ solution and the blend solution was heated at 100 °C for a certain period of time. Observing surface plasmon resonance (SPR) peak specific at 380 nm in the UV-vis spectrum of SS-ZnONPs represented the formation of ZnONPs. Then, the chemical, morphological, crystalline, thermal, and antibacterial properties of the synthesized SS-ZnONPs were examined. Characteristic peak of the Zn-O band was found in fourier transform infrared spectroscopy (FTIR) analysis of SS-ZnONPs. According to scanning electron microscopy (SEM) analyses, ZnONPs had morphology similar to cubic/hexagonal shape, showed a uniform structure, and did not represent any agglomerations. In energy dispersive spectroscopy (EDS) analyses of SS-ZnONPs, peaks belonging to carbon, nitrogen, oxygen, sulphur, and zinc elements were observed. The formation of Zn peak indicated that the zinc ions were transformed into ZnONPs. In addition, characteristic peaks of zinc were seen in the X-ray diffractometer (XRD) result of SS-ZnONPs. Thermogravimetric analysis (TGA) showed that the thermal stability and remaining amount of SS-ZnONPs was higher compared to pure silk sericin powder due to the formation of ZnONPs. Lastly, agar well diffusion test was carried out with *Staphylococcus aureus* (ATCC 6538) and *Escherichia coli* (ATCC 25922) bacteria and SS-ZnONPs showed antibacterial action against *S. aureus*. It has been observed that the obtained SS-ZnONPs can be used as antibacterial agents. However, it was also understood that the ZnONPs concentration in this study was low for high antibacterial activity.

Keywords: Green synthesis, Silk sericin, Zinc oxide nanoparticles, Antibacterial materials

I. INTRODUCTION

Nanoparticles (NPs) are atomic level particles having 1-100 nm size and they can be produced from a wide variety of materials. NPs are categorized as metallic NPs (for example; Ag, Zn and Au), metal and non-metal oxides NPs (for example; ZnO, FeO and AlO); semiconductor NPs (for example; CdS, ZnS and ZnSe) and carbon NPs [1,2]. Compared to bulk materials, NPs have different advanced features in size, distribution and morphology [3]. The quantum effect, surface and heterogeneity of NPs play a significant role in the chemical reactivity, optical, mechanical, electrical and even magnetic features of NPs. Heterogeneity and surface area of NPs can also affect other properties such as antimicrobial activity [2,3].

In the field of nanotechnology, there have been spectacular developments in recent years, with various advanced methodologies to synthesize NPs of certain forms and sizes. NPs can be obtained by physical, chemical and biological and green procedures. Various physical and chemical techniques such as sol-gel synthesis, laser ablation, hydrothermal and lithography have been developed. However, these methods may have disadvantages such as requiring special equipment and skilled labour, and may have toxic effects due to the use of harmful chemicals [4]. Increasing demands for environmentally friendly NPs have increased the interest in obtaining NPs with green synthesis methods instead of physical and chemical methods [5]. Many metal and metal oxide NPs have been synthesized by green synthesis methods, by using natural molecules as both stabilizing and reducing agents [5-7].

One of the excellent metallic nanomaterials is zinc NPs (ZnNPs) and ZnONPs. Zinc is a highly active element and also a powerful reducing agent [8]. Zinc is one of the most essential microelements in human beings and is existed in all of tissues, especially muscle, skin and bone [2,9,10]. ZnONPs are obtained from zinc salts by various methods such as chemical or chemical vapor deposition, hydrothermal synthesis technique, laser vaporization condensation technique, precipitation and green synthesis technique [13]. ZnONPs have a wide range of usages areas in different industrial areas [2,11]. With wide band gap (3.37 eV), ZnO has good transparency at room temperature and it is used as semiconductor materials [11,12]. Due to the strong pharmacological properties of ZnO, ZnONPs has usage areas in health fields as an anticancer, antimicrobial and antioxidant agent [2,11]. Additionally, ZnONPs are less toxic to the human body compared to other NPs and Zn ions, which are the dissolved form of ZnO, are substances found in normal human physiological system [13].

Silk cocoons are formed two main proteins called sericin and fibroin [14]. Fibroin is a fibrous protein that forms the structure of the cocoon and has been used for years in different application areas [15]. On the other hand, sericin is a globular water-soluble protein that keeps the fibroin proteins in the cocoon together. Sericin has 18 distinct amino acids in its structure and mostly contains amino acids containing polar groups [14]. After obtaining fibroin in silk processing plants, the sericin protein is disposed of together with the wastewater. However, sericin is a cheap, readily available, biodegradable and biocompatible material [5,7]. Many valuable biological activities of silk sericin have been reported in the literature and silk sericin has wide applications areas in tissue engineering [16,17], wound healing material synthesis [18,19], drug delivery [20,21], cosmetics [22,23] and food additives [24]. After the studies showing the usability of sericin in these important areas, many researchers continue to make new studies on sericin. Although sericin is mostly used in the production of wound dressing materials due to its increase in cell proliferation and biocompatibility, it is a protein with different uses, such as a reducing agent in the production of various NPs [25-28], in the synthesis of packaging materials [29] and in the production of adsorbent materials [30].

There are a few studies in the literature using sericin protein for ZnONPs synthesis [8,31]. However, to our knowledge, there is no study in the literature on the production of stable ZnONPs using only silk sericin as reducing and stabilizing material. However, in these studies, sericin protein was not used alone as a reducing and coating agent. In the current our study, stable ZnONPs were obtained by a simple, green method using only silk sericin solution as reducing and stabilizing agent and the chemical, morphological,

thermal and antibacterial properties of the obtained SS-ZnONPs were investigated.

II. MATERIALS AND METHODS

2.1. Materials

Silk sericin in solid powder form (obtained from *Bombyx mori* silkworm, CAS no. 60650-88-6; 60650-89-7, MA: ca. 138 kDa) was taken from Nembri Industrie Tessili. All other chemical and the bacterial cultures mediums were supplied from Merck (Germany) and Across Bio, respectively.

2.2. Synthesis of SS-ZnONPs

Silk sericin and zinc solutions were prepared for the obtaining of SS-ZnONPs. To prepare sericin solution, 2 grams of sericin were taken and added to 100 mL of water. After heating the mixture, pH of sericin mixture was raised to above 7 with NaOH, ensuring complete dissolution of sericin [5]. Then, the prepared 10 mM $Zn(NO_3)_2$ solution (30 mL) was added to the boiling silk sericin solution (30 mL) in a controlled manner. When $Zn(NO_3)_2$ were added to the silk sericin solution, a white-cloud-like solution was formed. The mixture was heated in a controlled manner for 2 hours and in continuation, it was stirred for 24 hours at room temperature. For FTIR, XRD, SEM-EDS analyses, liquid mixture of SS-ZnONPs was poured into petri dishes and the mixture was dried in an oven (50 °C, 1 day). Finally, powders of SS-ZnONPs were collected as solids from petri dishes.

2.3. Characterization of SS-ZnONPs

With a UV-Vis spectrophotometer (Biochrom, UK), UV-Vis absorption spectra of SS-ZnONPs solution was measured between 300 and 500 nm wavelength range. For chemical characterization of SS-ZnONPs, the FTIR spectra of the silk sericin and SS-ZnONPs were obtained with a FTIR device (Bruker Vertex 70 V). The morphologies and elemental analysis of the SS-ZnONPs were investigated with a SEM device and EDS analysed were obtained on SEM images (QUANTA 400F Field Emission SEM). After mixing the SS-ZnONPs homogeneously, with a ZetaSizer instrument (Malvern Instruments, Malvern, UK), the zeta size and potential of the SS-ZnONPs were recorded. The crystal structure of SS-ZnONPs was examined with a XRD device (Rigaku Ultima-IV brand) in the 0-80° scanning range. The thermal properties of SS-ZnONPs and original silk sericin were determined by TGA (PerkinElmer) between 25-950 °C with 10 °C/min heating rate.

2.4. Evaluation of Antibacterial Properties of SS-ZnONPs

Agar well diffusion test procedure was carried out in solid medium by using *E. coli* and *S. aureus* bacteria according to our previous works [5,7,32]. For the test, liquid cultures of *E. coli* and *S. aureus* bacteria were prepared and the number of cells in cell suspensions for bacterial cultures was adjusted to 10^8

microorganisms/mL by measuring optical densities of the bacterial cultures. 100 μL bacterial samples from these suspensions were poured to Mueller Hinton agar plate (prepared in 20 mm petri dish) and the cells were spread over the entire surface with sterile cotton swab. After 10 minutes of bacterial plating, wells were opened in solid media with 7 mm diameter with 1 mL pipette tip back on each agar surfaces. 100 μL of SS-ZnONPs samples (sterilized by keeping under UV-light at 254 nm in a cabinet for 1 hour) were placed to the opened wells and the petri dishes were incubated for 24 hours at 37 $^{\circ}\text{C}$. For the antibacterial test performed, autoclave sterilized water and gentamicin antibiotic discs were used as negative and positive control, respectively. After 24 hours of incubation, it was checked whether there were inhibition zone areas around the wells and the resulting inhibition zone diameters were measured with the help of a ruler.

III. RESULTS AND DISCUSSION

3.1. Production of SS-ZnONPs

For production of SS-ZnONPs, solutions of silk sericin and $\text{Zn}(\text{NO}_3)_2$ were blended and solution of sericin- $\text{Zn}(\text{NO}_3)_2$ was heated at 100 $^{\circ}\text{C}$ after NaOH addition (Figure 1). As time passed, sericin- $\text{Zn}(\text{NO}_3)_2$ solution colour turned from yellow to cloudy white. The occurrence of color change was proof that silk sericin converted zinc ions to ZnONPs. Because, sericin can reduce the zinc ions to ZnONPs due to its functional groups found its structure. This color change observed due to ZnO formation has been reported in many studies in the literature [33,34].

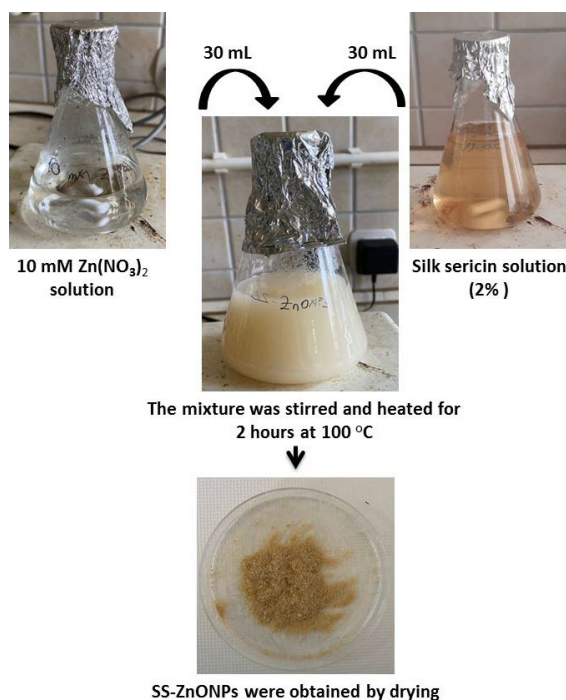


Figure 1: Obtaining SS-ZnONPs with silk sericin solution

Afterwards, the absorbances of solutions of silk sericin, $\text{Zn}(\text{NO}_3)_2$ SS-ZnONPs were recorded between 300-500 nm and the results were given in Figure 2. SPR peak specific to ZnONPs around 380 nm was observed while $\text{Zn}(\text{NO}_3)_2$ and sericin solution did not show any SPR peak. There are many studies in the literature showing that ZnONPs have SPR peaks in the range of approximately 350-400 nm [35,36]. This peak formation represent formation of hexagonal wurtzite ZnO and according to the literature, the result we obtained was compatible [37,38].

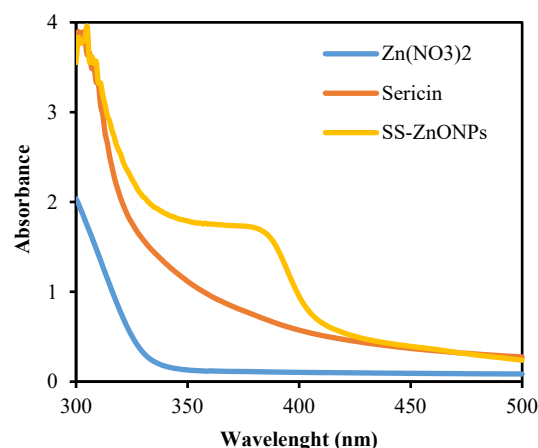


Figure 2: UV-Vis analyses of $\text{Zn}(\text{NO}_3)_2$, silk sericin, and SS-ZnONPs sample between 300-500 nm

3.2. Characterization of SS-ZnONPs

For the SS-ZnONPs samples, zeta size and zeta potential was found as 316.4 and -22.4 mV, respectively (Figure 3 (a) and 3(b)). The zeta potentials of the synthesized SS-ZnONPs were found to be negative. This result shows that the synthesized SS-ZnONPs were stable and had homodispersed distribution since the negatively charged ZnONPs repelled each other in aqueous solution [32,39]. The fact that NPs had a negative zeta potential is because of the use of sericin protein as a coating agent. Because, ZnONPs were synthesized at a pH that was above the isoelectric point of the sericin (isoelectric point of silk sericin is 3.7) [5]. When we look at the zeta size distribution plot of the synthesized NPs, it was seen that the ZnONPs have different size distributions.

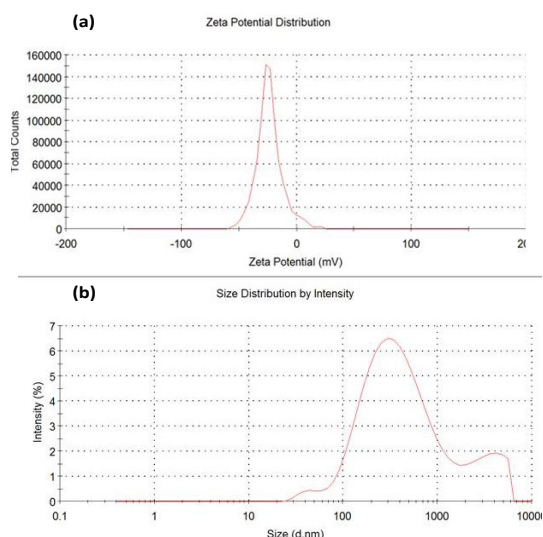


Figure 3: Zeta potential (a) and size distribution (b) of SS-ZnONPs sample

The FTIR analyses of silk sericin and SS- ZnONPs powders were given in Figure 4. In the FTIR result of pure silk sericin, amide I (at 1634 cm^{-1}), amide II (at 1515 cm^{-1}) and amide III (at 1236 cm^{-1}) peaks were clearly seen. In addition, the peaks around at 3266, 2927 and 1404 cm^{-1} were observed due to the O-H stretching vibration, C-H groups and symmetrical-asymmetrical stretching of the methyl group, respectively [5,7]. It was also observed that all peaks

belonging to sericin protein were present in the FTIR analysis of NPs. These findings proved that SS-ZnONPs were coated with sericin. Although there were peaks related to sericin in the spectrum of SS-ZnONPs compared to pure sericin, shifts in these peaks have occurred. These shifts resulted from the interaction of sericin with ZnO. Mumtaz et al. [40] synthesized ZnONPs using chitosan and silk fibroin, and by FTIR analysis, they observed that there were shifts in the peaks of chitosan and fibroin in the spectrum of coated ZnONPs. The authors attributed the reason for these shifts in the peaks to the interaction of chitosan and fibroin with ZnO. In the FTIR analysis of SS-ZnONPs, in addition to sericin-related peaks, a new peak observed at 618 cm^{-1} , which is the characteristic peak of the Zn-O band [41]. The formation of this peak proved the formation of ZnONPs in the presence of sericin as reducing agent. In addition, peaks associated with carboxylate ions (at 1593 cm^{-1}) and amine salt (at 847 cm^{-1}) were seen as the synthesis was performed in alkaline conditions using the sericin solution. These new peaks found in the SS-ZnONPs group represented that the amide bonds of silk sericin were hydrolyzed at alkaline conditions during the synthesis [5]. Moreover, in SS-ZnONPs FTIR result, a new peak formation observed at 1119 cm^{-1} indicated the presence of C-O around ZnONPs [42].

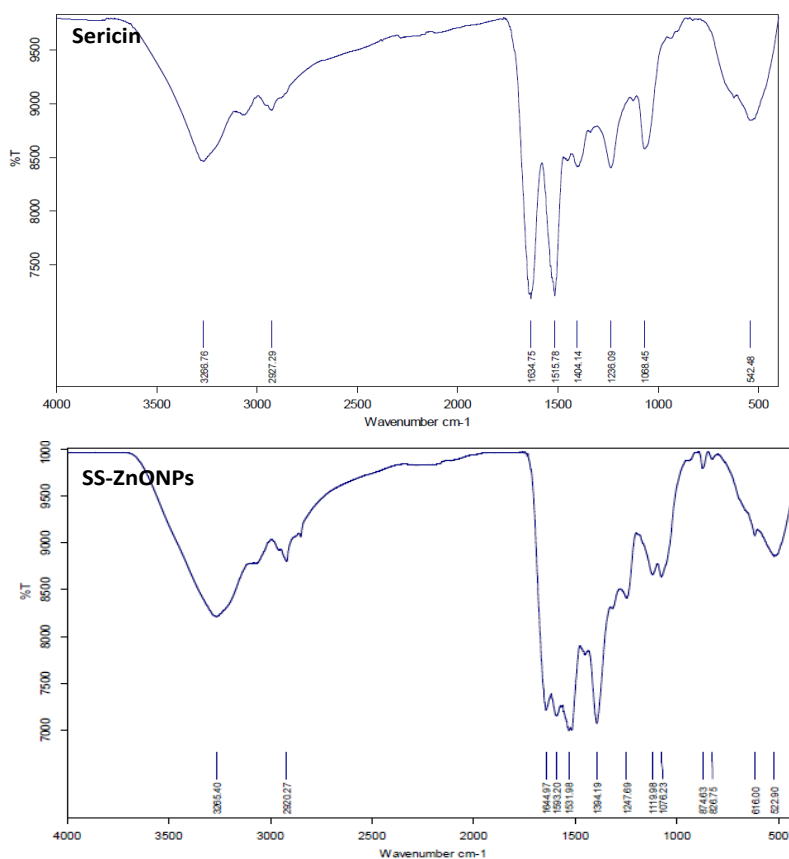


Figure 4: FTIR spectra of silk sericin and SS-ZnONPs sample

The SEM illustrations of SS-ZnONPs at different magnification were shown in Figure 5 (a) and (b). As seen from the images, the synthesized SS-ZnONPs have a cubic/hexagonal appearance and did not come together and form agglomerates. The high stability of particles with negative surface charge in zeta potential measurements has also been proven with SEM analysis. In addition, these images showed that by using silk sericin as a stabilizing and coating agent, NPs that were stable and did not form aggregates were obtained. In the literature, it has been shown that

stable ZnONPs were synthesized in ZnONPs synthesis studies using various substances as coating agents [33,34,40]. EDS analysis taken on the SEM pictures of SS-ZnONPs was given in Figure 5 (c). In the EDS analyses of SS-ZnONPs, peaks belonging to carbon, nitrogen, oxygen and sulfur elements as well as zinc peaks were observed. The existence of Zn peaks represented the formation ZnO from zinc salt. Due to the sericin protein, which was found as a coating agent around the obtained NPs, elemental structures belonging to the protein were seen in their structure.

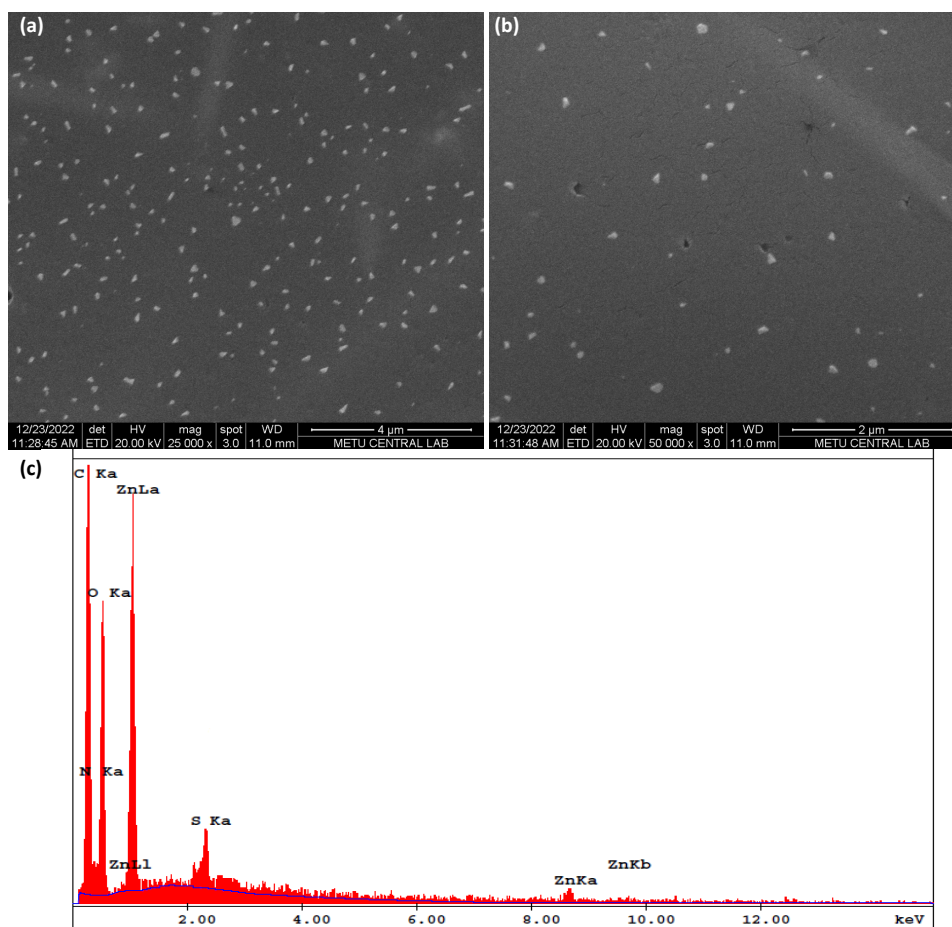


Figure 5: SEM images of SS-ZnONPs sample at different magnifications ((a) x25.000, (b) 50.000 magnification) and EDS analysis of SS-ZnONPs powder (c)

The XRD examination results of pure silk sericin and SS-ZnONPs were given in Figure 6. According to XRD result, sericin had contained both crystalline and amorphous structures. The sharp and wide peak, between 15-25°, showed the semi-crystalline structure of silk sericin with crystal and amorphous regions. In the XRD result of SS-ZnONPs, this broad peak belonging to the sericin was also found due to coating of ZnONPs with sericin. In ZnONPs synthesis studies

carried out with different coating agents, characteristic peaks belonging to the hexagonal structure of the ZnO formed have been reported in many previous studies [8,41]. As in these studies, in the XRD analysis of SS-ZnONPs, characteristic peaks of zinc oxide were found. The diffraction peaks found at 31.57, 34.032, 36.01, 47.515, 56.63, 62.68 and 67.83 ° associated with the 100, 002, 101, 102, 110, 103 and 112 hexagonal crystallographic planes of ZnO [42,43].

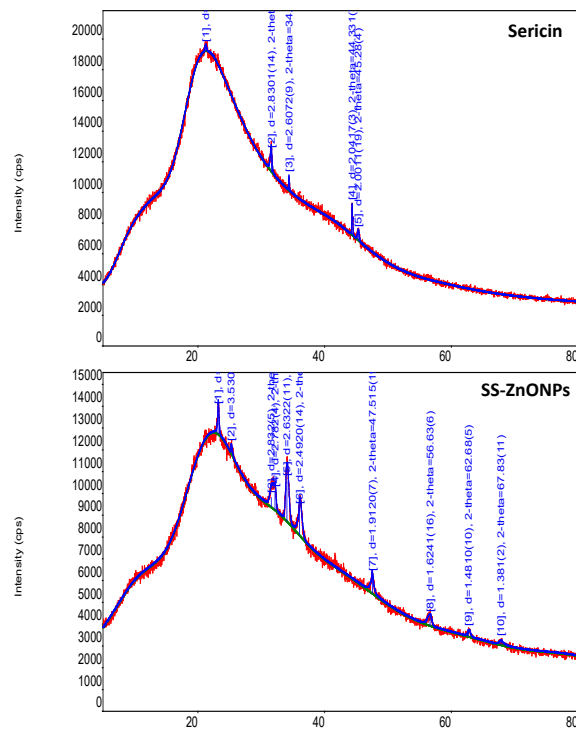


Figure 6: XRD spectra of silk sericin and SS-ZnONPs sample

The thermal degradation properties of pure silk sericin and SS-ZnONPs were investigated with TGA analysis and the results were given in Figure 7. According to TGA analysis, sericin degraded in 3 steps. In the first degradation step, sericin has lost moisture found its structure. In other degradation steps, organic structures of silk sericin were degraded [25] and the remaining mass of the silk sericin was found to be 20.276% at the end of 950 °C. According to TGA thermograms of SS-ZnONPs, SS-ZnONPs degraded in 4 steps. In the first step, it had lost the moisture in its structure, but the weight loss was more than the mass loss of silk sericin. ZnONPs are able to retain water in their structure and, compared to pure silk sericin, therefore, the mass loss due to moisture loss in the first step was increased. In the second and third degradations steps, the organic sections of silk sericin found around the ZnONPs degraded. In the 4th step, residual materials that may be on the surface of SS-ZnONPs have been degraded [44]. The amount remaining of SS-ZnONPs was found to be 29.922% at 950 °C. TGA analysis results showed that the amount of remaining substance in ZnONPs samples increased at 950 °C in comparison with pure sericin. The increment in the amount of remaining residue compared to the pure sericin was due to the formation of ZnONPs.

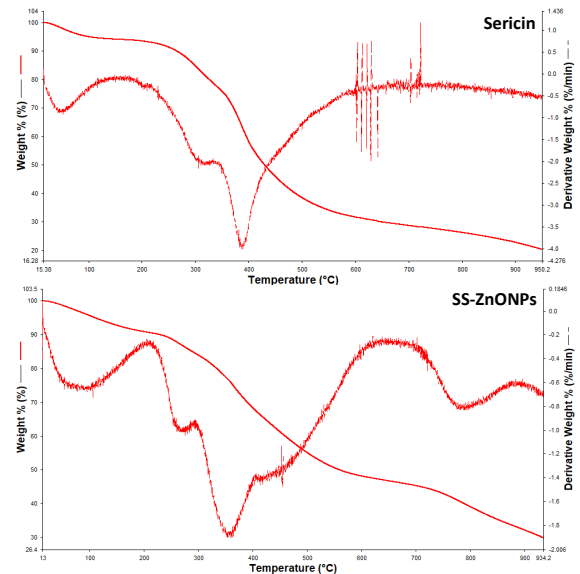


Figure 7: TGA results of silk sericin and SS-ZnONPs powder

3.3. Antibacterial Properties of SS-ZnONPs

NPs are seen as substitutes for antibiotics due to their low toxicity to the human body and broad-spectrum lethal effects against pathogenic microorganisms [45,46]. Bacterial cell walls are negatively charged because of teichoic acid found in gram-positive and phospholipid found in gram-negative bacteria. Therefore, it is thought that the ions released from NPs interact with the negatively charged cell wall and NPs show antibacterial activity [2,8]. The antimicrobial effects of NPs can be determined by growing microorganisms in culture media containing NPs or by establishing a direct interaction medium by electrospinning [47,48].

Bacteria are divided into two main groups, gram positive and gram negative, according to differences in their cell wall structures. The cell wall differences of gram-positive and gram-negative bacteria create differences in the behaviour of bacteria against antibacterial materials [32]. In our study, in antibacterial test, we used *S. aureus* bacteria as gram-positive bacteria and *E. coli* bacteria as gram-negative bacteria, which are frequently used in antibacterial tests.

There are studies showing that ZnONPs synthesized with different coating agents have antibacterial activity on many microorganisms [40,49,50]. In the present study, antibacterial properties of the produced SS-ZnONPs was investigated against gram-positive *S. aureus* and gram-negative *E. coli* with performed agar well-diffusion test. The measured inhibition diameters for the samples and agar images of test were represented in Table 1 and Figure 8, respectively. For *E. coli*, it was observed that no zones of inhibition were formed around the wells in which SS-ZnONPs were added. These results showed that the obtained NPs did not show any antibacterial effect on *E. coli*,

which is in the gram-negative bacteria. In addition, in experiments with *S. aureus*, inhibition zones were found around the wells and this result showed that SS-ZnONPs have antibacterial activities for *S. aureus*. Previous studies have shown that ZnONPs own more lethal influence on gram-positive bacteria [51,52].

This is an acceptable result, because, in general, gram-negative bacteria show high resistance to antibacterial agents compared to gram-positive bacteria, due to the outer membrane structure found in their cell walls [32].

Table 1. Measured inhibition zone values for positive, negative control, and SS-ZnONPs sample

Samples	Zone of Inhibition for <i>E. coli</i> (mm)	Zone of Inhibition for <i>S. aureus</i> (mm)
Posicitive control (PC, Gentamicin,10 µg)	19.67±0.41	22.67±0.82
Negative control (NC, sterilized water)	0	0
SS-ZnONPs	0	12.42±0.33

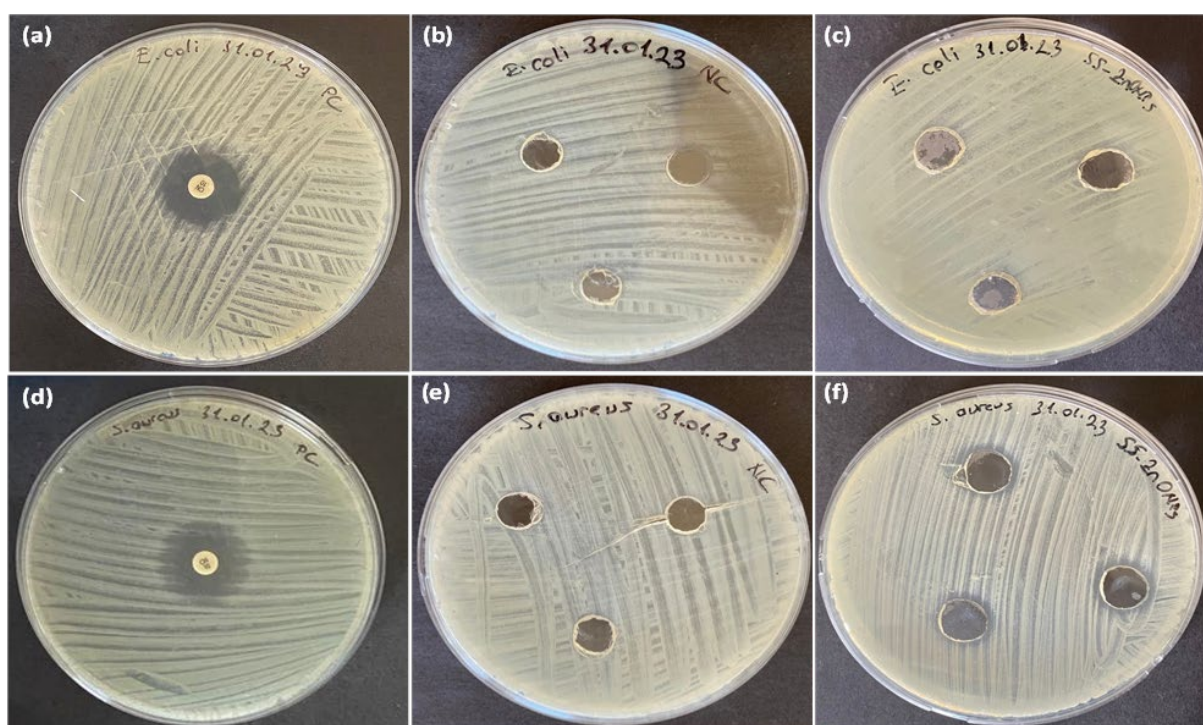


Figure 8: Agar images of the applied antibacterial test (for *E. coli*; positive control (a), negative control (b), SS-ZnONPs sample (c), for *S. aureus* positive control (a), negative control (b), SS-ZnONPs sample (c)).

IV. CONCLUSIONS

In the current work, green synthesis method was applied for producing of SS-ZnONPs. The synthesis of the obtained SS-ZnONPs was confirmed both by colour change and UV-Vis analysis. The chemical feature of the obtained SS-ZnONPs were examined by FTIR, and the Zn-O peak formed in the FTIR analysis was shown chemically to form ZnONPs. Looking at the SEM photographs, it is understood that the synthesized NPs have a cubic/hexagonal appearance and did not come together and form agglomerates. EDS analysis performed on SEM photographs showed that there were oxygen, carbon, sulphur, and nitrogen peaks in the structure of NPs, originating from the

coating agent sericin. Moreover, Zn peak was seen in EDS analysis and this result proved that the elemental form of Zn was formed. In XRD analysis, crystallographic peaks belonging to the hexagonal structure of Zn were observed. With TGA analysis, it was observed that, compared to the pure sericin, there was an increase in the amount of remaining mass of SS-ZnONPs without degradation at the end of 950 °C due to the formation of Zn-O. Finally, it was confirmed that the synthesized NPs had an antibacterial effect on *S. aureus*, a gram-positive bacterium.

ACKNOWLEDGMENTS

This study was carried out at Kırıkkale University. We would like to thank Kırıkkale University for providing us with every opportunity to carry out our study.

REFERENCES


- [1] Railean-Plugaru, V., Pomastowski, P., Wypij, M., Szultka-Mlynska, M., Rafinska, K., Golinska, P., Dahm, H., Buszewski, B. (2016). Study of silver NPs synthesized by acidophilic strain of Actinobacteria isolated from the of *Picea sitchensis* forest soil. *J. Appl. Microbiol.*, 120, 1250-1263. <https://doi.org/10.1111/jam.13093>
- [2] Krol, A., Pomastowski, P., Rafinska, K., Railean-Plugaru, V., Buszewski, B. (2017) Zinc oxide NPs: Synthesis, antiseptic activity and toxicity mechanism. *Adv. Colloid Interface Sci.*, 249, 37-52. <https://doi.org/10.1016/j.cis.2017.07.033>
- [3] Buzea, C., Pacheco, I.I., Robbie, K. (2007) Nanomaterials and NPs: sources and toxicity. *Biointerphases*, 2, 17-71. <https://doi.org/10.1116/1.2815690>
- [4] Jayachandran, A., Aswathy. T.R., Achuthsankar, S.N. (2021) Green synthesis and characterization of zinc oxide NPs using *Cayratia pedata* leaf extract. *Biochem. Biophys. Rep.*, 26, 100995. <https://doi.org/10.1016/j.bbrep.2021.100995>
- [5] Gün Gök, Z., Günay, K., Arslan, M., Yiğitoğlu, M., Vargel, İ. (2020) Coating of modified poly(ethylene terephthalate) fibers with sericin-capped silver NPs for antimicrobial application. *Polym. Bull.*, 77, 649-1665. <https://doi.org/10.1007/s00289-019-02820-0>
- [6] Bozkaya, O., Arat, E., Gün Gök, Z., Yiğitoğlu, M., Vargel, İ. (2022) Production and characterization of hybrid nanofiber wound dressing containing *Centella asiatica* coated silver NPs by mutual electrospinning method. *Eur. Polym. J.*, 166, 111023. <https://doi.org/10.1016/j.eurpolymj.2022.111023>
- [7] Gün Gök, Z. (2022), Synthesis and characterization of polyvinyl alcohol–silk sericin nanofibers containing gelatin-capped silver NPs for antibacterial applications. *Polym. Bull.*, 79, 10357-10376. <https://doi.org/10.1007/s00289-022-04455-0>
- [8] Chauhan, N., Thakur, B., Kumari, A., Khatana, C., Sharma, R. (2023) Mushroom and silk sericin extract mediated ZnONPs for removal of organic pollutants and microorganisms. *S. Afr. J. Bot.*, 153, 370-381. <https://doi.org/10.1016/j.sajb.2023.01.001>
- [9] Sadhasivam, S., Shanmugam, M., Umamaheswaran, P.D., Venkattappan, A., Shanmugam, A. (2021) Zinc Oxide NPs: Green Synthesis and Biomedical Applications. *J. Clust. Sci.*, 32, 1441-1455. <https://doi.org/10.1007/s10876-020-01918-0>
- [10] Tapiero, H., Tew, K.D. (2003) Trace elements in human physiology and pathology: zinc and metallothioneins. *Biomed Pharmacother.*, 57, 299-411 (2003). [https://doi.org/10.1016/s0753-3322\(03\)00081-7](https://doi.org/10.1016/s0753-3322(03)00081-7)
- [11] Dulta, K., Koşarsoy Ağçeli, G., Chauhan, P., Jasrotia, R., Chauhan, P.K. (2021) A Novel Approach of Synthesis Zinc Oxide NPs by *Bergenia ciliata Rhizome* Extract: Antibacterial and Anticancer Potential. *J. Inorg. Organomet. Polym. Mater.*, 31, 180-190. <https://doi.org/10.1007/s10904-020-01684-6>
- [12] Calestani, D., Zha, M., Mosca, R., Zappettini, A., Carotta, M.C., Di Natale, V., Zanotti, L. (2010) Growth of ZnO tetrapods for nanostructure-based gas sensors. *Sens. Actuators B*, 144(2), 472-478. <https://doi.org/10.1016/j.snb.2009.11.009>
- [13] Mandal, A.K., Katuwal, S., Tettey, F., Gupta, A., Bhattarai, S., Jaisi, S., Bhandari, D.P., Shah, A.K., Bhattarai, N., Parajuli, N. (2022) Current Research on Zinc Oxide NPs: Synthesis, Characterization, and Biomedical Applications. *Nanomaterials*, 12, 3066. <https://doi.org/10.3390/nano12173066>
- [14] Aramwit, P., Siritientong, T., Srichana, T. (2012) Potential applications of silk sericin, a natural protein from textile industry by-products. *Waste Manag. Res.*, 30, 212-224. <https://doi.org/10.1177/0734242X11404733>
- [15] Akturk, O., Kismet, K., Yasti, A.C., Kuru, S., Duymus, M.E., Kaya, F., Caydere, M., Hucumenoglu, D., Keskin, D. (2016) Wet electrospun silk fibroin/gold nanoparticle 3D matrices for wound healing applications. *RSC Adv.*, 6, 13234-13250. <https://doi.org/10.1039/C5RA24225H>
- [16] Aramwit, P., Keongamaroon, O., Siritientong, T., Bang, N., Supasynhdh, O. (2012) Sericin cream reduces pruritus in hemodialysis patients: a randomized, double-blind, placebo-controlled experimental study. *BMC Nephrol.*, 13, 119. <https://doi.org/10.1186/1471-2369-13-119>
- [17] Yang, M., Mandal, N., Shuai, Y., Zhou, G., Min, S., Zhu, L. (2014) Mineralization and Biocompatibility of *Antheraea pernyi* (A. pernyi) Silk Sericin Film for Potential Bone Tissue Engineering. *Bio-Med. Mater. Eng.*, 24, 815-824 (2014). <https://doi.org/10.3233/bme-130873>
- [18] Tao, G., Cai, R., Wang, Y., Liu, L., Zuo, H., Zhao, P., Umar, A., Mao, C., Xia, Q., He, H. (2019) Bioinspired design of AgNPs embedded silk sericin-based sponges for efficiently combating bacteria and promoting wound healing. *Mater. Des.*, 180, 107940. <https://doi.org/10.1016/j.matdes.2019.107940>
- [19] Liu, L., Cai, R., Wang, Y., Tao, G., Ai, L., Wang, P., Yang, M., Zuo, H., Zhao, P., He, H. (2018) Polydopamine-Assisted Silver Nanoparticle Self-Assembly on Sericin/Agar Film for Potential Wound Dressing Application. *Int. J.*

- Mol. Sci., 19(10), 2875. <https://doi.org/10.3390%2Fijms19102875>
- [20] Li, X., Hou, S., Chen, J., He, C.E., Gao, Y.E., Lu, Y., Jia, D., Ma, X., Xue, P., Kang, Y. (2021) Engineering silk sericin decorated zeolitic imidazolate framework-8 nanoplatfrom to enhance chemotherapy. *Colloids Surf. B*, 200, 111594. <https://doi.org/10.1016/j.colsurfb.2021.111594>
- [21] Zhang, Y., Liu, J., Huang, L., Wang, Z., Wang, L. (2015) Design and performance of a sericin alginate interpenetrating network hydrogel for cell and drug delivery. *Sci. Rep.*, 5, 12374. <https://doi.org/10.1038/srep12374>
- [22] Sheng, J.Y., Xu, J., Zhuang, Y., Sun, D.Q., Xing, T.L., Chen, G.Q. (2013) Study on the application of sericin in cosmetics. *Adv. Mater. Res.*, 796, 416-423. <https://doi.org/10.4028/www.scientific.net/AMR.796.416>
- [23] Padamwar, M.N., Pawar, A.P., Daithankar, A.V., Mahadik, K. (2005) Silk sericin as a moisturizer: an *in vivo* study. *J. Cosmet. Dermatol.*, 4(4), 250-257. <https://doi.org/10.1111/j.1473-2165.2005.00200.x>
- [24] Takechi, T., Takamura, H. (2014) Development of bread supplemented with the silk protein sericin. *Food Sci. Technol. Res.*, 20(5), 1021-1026. <https://doi.org/10.3136/fstr.20.1021>
- [25] Gün Gök, Z., Yiğitoğlu, M., Vargel, İ., Sahin, Y., Alçıgır, M.E. (2021) Synthesis, characterization and wound healing ability of PET based nanofiber dressing material coated with silk sericin capped-silver NPs. *Mater. Chem. Phys.*, 259, 124043. <https://doi.org/10.1016/j.matchemphys.2020.124043>
- [26] Akturk, O., Gün Gök, Z., Erdemli, Ö., Yiğitoğlu, M. (2019) One-pot facile synthesis of silk sericin-capped gold NPs by UVC radiation: investigation of stability, biocompatibility, and antibacterial activity. *J. Biomed. Mater. Res.*, 107A, 2667-2679. <https://doi.org/10.1002/jbm.a.36771>
- [27] Akturk, O., Gün Gök, Z., Daş, M.T., Erdemli, Ö. (2018) Synthesis and characterization of sericin-capped gold NPs. *J. Fac. Eng. Archit. Gazi Univ.*, 33, 675-684. <https://doi.org/10.17341/gazimmfd.416377>
- [28] Aramwit, P., Bang, N., Ratanavaraporn, J., Ekgasit, S. (2014) Green synthesis of silk sericin-capped silver NPs and their potent anti-bacterial activity. *Nanoscale Res. Lett.*, 9, 79-86 (2014). <https://doi.org/10.1186/1556-276X-9-79>
- [29] Purwar, R., Sharma, S., Sahoo, P., Srivastava, C.M. (2015) Flexible sericin/polyvinyl alcohol/clay blend films. *Fibers Polym.*, 16, 761-768. <https://doi.org/10.1007/s12221-015-0761-y>
- [30] Kwak, H.W., Lee, K.H. (2018) Polyethylenimine-functionalized silk sericin beads for high-performance remediation of hexavalent chromium from aqueous solution. *Chemosphere*, 207, 507-516. <https://doi.org/10.1016/j.chemosphere.2018.04.158>
- [31] Chuang, C.C., Prasanna, A., Huang, B.R., Hong, P.D., Chiang, M.Y. (2017). Simple synthesis of eco-friendly multifunctional silk-sericin capped zinc oxide nanorods and their potential for fabrication of hydrogen sensors and UV photodetectors. *ACS Sustain. Chem. Eng.* 5(5), 4002-4010. <https://doi.org/10.1021/acssuschemeng.7b00012>
- [32] Gün Gök, Z., Karayel, M., Yiğitoğlu, M. (2021) Synthesis of carrageenan coated silver NPs by an easy green method and their characterization and antimicrobial activities. *Res. Chem. Intermed.*, 47, 1843-1864. <https://doi.org/10.1007/s11164-021-04399-6>
- [33] Santhoshkumar, J., Kumar, S.V., Rajeshkumar, S. (2017) Synthesis of zinc oxide nanoparticles using plant leaf extract against urinary tract infection pathogen. *Resour.-Effic. Technol.*, 3(4), 459-465. <https://doi.org/10.1016/j.reffit.2017.05.001>
- [34] Suresh, D., Nethravathi, P.C., Rajanaika, H., Nagabhushana, H., Sharma, S.C. (2015) Green synthesis of multifunctional zinc oxide (ZnO) nanoparticles using *Cassia fistula* plant extract and their photodegradative, antioxidant and antibacterial activities. *Mater. Sci. Semicond. Process.*, 31, 446-454. <https://doi.org/10.1016/j.mssp.2014.12.023>
- [35] Rajapriya, M., Sharmili, S.A., Baskar, R., Balaji, R., Alharbi, N.S., Kadaikunnan, S., Khaled, J.M., Alanzi, K.F., Vaseeharan, B. (2020) Synthesis and characterization of zinc oxide nanoparticles using *Cynara scolymus* Leaves: Enhanced hemolytic, antimicrobial, antiproliferative, and photocatalytic activity. *J. Cluster Sci.*, 31, 791-801. <https://doi.org/10.1007/s10876-019-01686-6>
- [36] Karthik, S., Siva, P., Balu, K.S., Suriyaprabha, R., Rajendran, V., Maaza, M. (2017) Acalypha indica-mediated green synthesis of ZnO nanostructures under differential thermal treatment: Effect on textile coating, hydrophobicity, UV resistance, and antibacterial activity. *Adv. Powder Technol.*, 28(12), 3184-3194. <https://doi.org/10.1016/j.apt.2017.09.033>
- [37] Wooten, A.J., Werder, D.J., Williams, D.J., Casson, J.L., Hollingsworth, J.A. (2009) Solution-liquid-solid growth of ternary Cu-In-Se semiconductor nanowires from multiple- and single-source precursors. *J. Am. Chem. Soc.*, 131, 16177-1618. <https://doi.org/10.1021/ja905730n>
- [38] Pudukudy, M., Yaakob, Z. (2015) Facile Synthesis of Quasi Spherical ZnO NPs with Excellent Photocatalytic Activity. *J. Clust. Sci.*, 26, 1187-1201. <https://doi.org/10.1007/s10876-014-0806-1>
- [39] Farhadi, S., Ajerloo, B., Mohammadi, A. (2017) Green Biosynthesis of Spherical Silver NPs by

- Using Date Palm (*Phoenix Dactylifera*) Fruit Extract and Study of Their Antibacterial and Catalytic Activities. *Acta. Chim. Slov.*, 64, 129-143. <https://doi.org/10.17344/acsi.2016.2956>
- [40] Mumtaz, S., Ali, S., Tahir, H.M., Mumtaz, S., Mughal, T.A., Kazmi, S.A.R., Hassan, A., Summer, M., Zulfiqar, A., Kazmi, S. (2024) Biological applications of biogenic silk fibroin–chitosan blend zinc oxide nanoparticles. *Polym. Bull.*, 81, 2933-2956. <https://doi.org/10.1007/s00289-023-04865-8>
- [41] Patrón-Romero, L., Luque, P.A., Soto-Robles, C.A., Nava, O., Vilchis-Nestor, A.R., Barajas-Carrillo, V.W., Martínez-Ramírez, C.E., Chávez Méndez, J.R., Alvelais Palacios, J.A., Leal Ávila, M.A., Almanza-Reyes, H. (2020) Synthesis, characterization and cytotoxicity of zinc oxide NPs by green synthesis method. *J. Drug Deliv. Sci. Technol.*, 60, 101925. <https://doi.org/10.1016/j.jddst.2020.101925>
- [42] Indubala, E., Dhanasekar, M., Sudha, V., Padma Malar, E.J., Divya, P., Sherine, J., Rajagopal, R., Bhat, S.V., Harinipriya, S. (2018) l-Alanine capping of ZnO nanorods: increased carrier concentration in ZnO/CuI heterojunction diode. *RSC Adv.*, 8, 5350-5361. <https://doi.org/10.1039/C7RA12385J>
- [43] Stankovic' A., Dimitrijevic', S., Uskokovic', D. (2013) Influence of size scale and morphology on antibacterial properties of ZnO powders hydrothermally synthesized using different surface stabilizing agents. *Colloids Surf., B*, 102, 21-28. <https://doi.org/10.1016/j.colsurfb.2012.07.033>
- [44] Menazea, A.A., Ismail, A.M., Samy, A. (2021) Novel Green Synthesis of Zinc Oxide NPs Using Orange Waste and Its Thermal and Antibacterial Activity. *J. Inorg. Organomet. Polym. Mater.*, 31, 4250-4259. <https://doi.org/10.1007/s10904-021-02074-2>
- [45] Maleki Dizaj, S., Mennati, A., Jafari, S., Khezri, K., Adibkia, K. (2015) Antimicrobial Activity of Carbon-Based NPs. *Adv. Pharm. Bull.*, 5, 19-23. <https://doi.org/10.5681/apb.2015.003>
- [46] Akbar, S., Tauseef, I., Subhan, H., Sultana, N., Khan, I., Ahmed, U., Syed Haleem, K. (2020) An overview of the plant-mediated synthesis of zinc oxide NPs and their antimicrobial potential. *Inorg. Nano-Met. Chem.*, 50, 257-271. <https://doi.org/10.1080/24701556.2019.1711121>
- [47] Rana, S., Kalaichelvan, P. (2011) Antibacterial Activities of Metal NPs. *Adv. Bio. Tech.*, 11, 21-23.
- [48] Yamamoto, O. (2001) Influence of particle size on the antibacterial activity of zinc oxide. *Int. J. Inorg. Mater.*, 3, 643-646. [https://doi.org/10.1016/S1466-6049\(01\)00197-0](https://doi.org/10.1016/S1466-6049(01)00197-0)
- [49] Wahab, R., Siddiqui, M.A., Saquib, Q., Dwivedi, S., Ahmad, J., Musarrat, J., Al-Khedhairi, A.A., Shin, H.-S. (2014) ZnO nanoparticles induced oxidative stress and apoptosis in HepG2 and MCF-7 cancer cells and their antibacterial activity. *Colloids Surf., B*, 117, 267-276. <https://doi.org/10.1016/j.colsurfb.2014.02.038>
- [50] Babayevska, N., Przysiecka, Ł., Iatsunskyi, I., Nowaczyk, G., Jarek, M., Janiszewska, E., Jurga, S. (2022) ZnO size and shape effect on antibacterial activity and cytotoxicity profile. *Scientific Reports*, 12(1), 8148. <https://doi.org/10.1038/s41598-022-12134-3>
- [51] Yusof, N.A.A., Zain, N.M., Pauzi, N. (2019) Synthesis of ZnO nanoparticles with chitosan as stabilizing agent and their antibacterial properties against Gram-positive and Gram-negative bacteria. *Int. J. Biol. Macromol.*, 124, 1132-1136. <https://doi.org/10.1016/j.ijbiomac.2018.11.228>
- [52] Yu, Y.C., Hu, M.H., Zhuang, H.Z., Phan, T.H.M., Jiang, Y.S., Jan, J.S. (2023) Antibacterial Gelatin Composite Hydrogels Comprised of In Situ Formed Zinc Oxide Nanoparticles. *Polymers*, 15(19), 3978. <https://doi.org/10.3390/polym15193978>

Enzymatic Bioregeneration of Activated Carbon by Laccase

Aktif Karbonun Lakkaz ile Enzimatik Biyorejenerasyonu

Özgür Aktaş^{1,2}, Zeynep Merve Tiryaki², Işık Çoban^{1,2}

¹Department of Bioengineering, Istanbul Medeniyet University, 34700, Istanbul, Turkey

²Environmental and Energy Systems Engineering Program, Istanbul Medeniyet University, 34700, Istanbul, Turkey

Abstract

Activated carbon is widely used in combination with biological treatment systems for the treatment of organic compounds, which are refractory or toxic in conventional biological treatment systems. In these systems, compounds adsorbed on activated carbon may desorb within time due to a concentration gradient between adsorbent and the bulk liquid caused by the biodegradation of substrates in the liquid phase by microorganisms. The desorbed compounds are further biodegraded by microorganisms. This mechanism is called bioregeneration of activated carbon. Previous studies showed that bioregeneration percentages could be higher than the concentration gradient-driven desorbability. This was attributed to exoenzymatic bioregeneration occurring due to the activity of extracellular enzymes secreted by microorganisms in these systems. These extracellular enzymes can diffuse into the activated carbon pores where they can react with the previously adsorbed compounds resulting in their desorption from the carbon surface and degradation. However, the effect of extracellular enzymes on bioregeneration was not conclusively proven in any of the literature studies on bioregeneration because extracellular enzymes were not directly used for the purpose of bioregeneration. In this study, enzymatic bioregeneration of activated carbon was investigated by directly using an extracellular enzyme, laccase, which is known from the literature to catalyze the oxidation reactions of phenolic substances and is commercially available in its pure form. Therefore phenol, 2-nitrophenol, and bisphenol-A were used as the target compounds. For this purpose, batch adsorption, abiotic desorption, enzymatic degradation and enzymatic bioregeneration experiments were performed using two different activated carbon types; thermally and chemically activated ones. The results showed that there was a significant difference between the total enzymatic bioregeneration efficiencies and abiotic desorption efficiencies for each phenolic compound depending on the activated carbon type. Thereby, exoenzymatic bioregeneration has been quantitatively shown for the first time in the literature.

Key Words: activated carbon, phenol, 2-nitrophenol, bisphenol-A, bioregeneration, laccase

Öz

Aktif karbon, geleneksel biyolojik arıtma sistemlerinde refrakter veya toksik olan organik bileşiklerin arıtımında biyolojik arıtma sistemleriyle kombinasyon halinde yaygın olarak kullanılmaktadır. Bu sistemlerde, aktif karbon üzerinde adsorbe edilen bileşikler, mikroorganizmaların sıvı fazındaki substratları degrades etmesi neticesinde oluşan konsantrasyon gradyanı nedeniyle desorbe olabilir ve daha sonrasında biyolojik olarak parçalanabilir. Bu mekanizmaya aktif karbonun biyorejenerasyonu denir. Önceki çalışmalar, biyorejenerasyon yüzdelerinin konsantrasyon gradyanı kaynaklı desorplanabilirlikten daha yüksek olabileceğini gösterdi. Bu durum bu sistemlerde mikroorganizmalar tarafından salgılanan hücre dışı enzimlerin aktivitesiyle gerçekleşen ekzoenzimatik biyorejenerasyona atfedildi. Bu hücre dışı enzimler, aktif karbon gözeneklerine girerek, daha önce adsorbe edilen bileşiklerle reaksiyona girebilmekte ve bunların karbon yüzeyinden desorpsiyonuna ve degrades olmasına neden olabilmektedir. Ancak literatürde biyorejenerasyon üzerine yapılan çalışmaların hiçbirinde enzimlerin biyorejenerasyon üzerindeki etkisi kesin olarak kanıtlanamamıştır. Çünkü hücre dışı enzimler bu amaçla doğrudan kullanılmamıştır. Bu çalışmada, literatürde fenolik maddelerin oksidasyon reaksiyonlarını katalize ettiği bilinen hücre dışı bir enzim olan ve ticari olarak saf haliyle temin edilebilen lakkaz enzimi kullanılarak aktif karbonun enzimatik biyorejenerasyonu araştırılmıştır. Hedef bileşikler olarak fenol, 2-nitrofenol ve bisfenol-A kullanılmıştır. Bu amaçla termal ve kimyasal olarak aktive edilmiş iki farklı aktif karbon tipi kullanılarak kesikli adsorpsiyon, abiyotik desorpsiyon, enzimatik biyodegradasyon ve enzimatik biyorejenerasyon deneyleri yapılmıştır. Sonuçlar, aktif karbon tipine bağlı olarak her bir fenolik bileşik için toplam enzimatik biyorejenerasyon verimleri ile abiyotik desorpsiyon verimleri arasında önemli bir fark olduğunu göstermiştir. Böylece literatürde ilk kez ekzoenzimatik biyorejenerasyon niceliksel olarak da gösterilmiştir.

Anahtar Kelimeler: aktif karbon, fenol, 2-nitrofenol, bisfenol-A, biorejenerasyon, lakkaz

I. INTRODUCTION

In the activated carbon process, adsorbed pollutants fill the activated carbon pores over time and the adsorption capacity of the activated carbon decreases. For this reason, activated carbon must be disposed of or regenerated at the end of the process. However, regeneration techniques using chemical and thermal methods are often expensive. Biological regeneration, or in other words bioregeneration, of activated carbon is suggested as an alternative method in the literature [1]. In activated carbon applications combined with biological processes, the lifetime of activated carbon increases significantly due to bioregeneration. Biofilm development on the surface of activated carbon in biological activated carbon filters enables bioregeneration of the adsorbent and extends its lifetime, particularly in the treatment of micropollutants [2]. Therefore, increasing the extent of bioregeneration in these applications is expected to decrease the costs related to the following regeneration techniques [3].

Bioregeneration is defined as the regeneration of the adsorption capacity of activated carbon as a result of the biodegradation of previously adsorbed organic materials [1]. Literature studies showed high bioregeneration efficiencies for activated carbon reaching up to 90 % in the biological treatment of phenolic compounds with a mixed microbial culture of acclimated activated sludge [4,5,6]. A more recent study showed about 80 % bioregeneration of phenol and paranitrophenol-loaded GACs, when phenol-acclimated biomass was used [7]. On the other hand, Immobilized pure bacterial culture of *Pseudomonas aeruginosa* could achieve 33-66 % bioregeneration of activated carbon in the treatment of phenolic compounds [8]. Another study obtained 98 % bioregeneration of activated carbon loaded with phenolics by using a pure fungus culture of *Scedosporium apiospermum*. This amount of bioregeneration was reported to be higher than conventional regeneration methods such as thermal treatment or solvent extraction [9].

The bioregeneration mechanism includes the desorption of adsorbed organic substances due to the concentration gradient between the activated carbon surface and the bulk liquid, and the following biological decomposition of these desorbed organic compounds by microorganisms [3]. The second hypothesis about bioregeneration is that extracellular enzymes produced by bacteria diffuse into the activated carbon pores and form an enzyme-substrate complex with adsorbed compounds, and as a result, the adsorption energy of the degraded or hydrolyzed organic compound decreases and empties the activated carbon pores to which it is bound to. This enzyme-substrate complex can be transformed into a degraded form by the extracellular enzymes or further degraded by the microorganisms in the bulk liquid [1]. A more

recent study based on meta-omics analysis also indicated that bioregeneration was mostly caused by the enzyme reactions mechanism, i.e., the metabolism-related enzymes secreted by bacteria degraded the organic matter adsorbed by activated carbon into small molecules for further metabolism [10].

However, although the studies in the literature indicated the occurrence of exoenzymatic bioregeneration [4,5,6,11], the exoenzymatic bioregeneration could not be conclusively proven in any of these studies because the bioregeneration was provided with the microbial mixture in the activated sludge. In order to qualitatively show and quantitatively calculate the exoenzymatic bioregeneration, it was recommended to use the extracellular enzymes directly in bioregeneration experiments in the absence of microorganisms [3]. In addition, previous studies have shown that enzymatic bioregeneration may depend on the chemical properties of the activated carbon surface [1]. In literature studies, it was found that thermally activated carbons were more suitable for chemical adsorption, while chemically activated carbons led to physical adsorption. Therefore, it has been argued that occurrence of exoenzymatic bioregeneration is more probable in thermally activated carbons, where the activation energy is higher due to chemical adsorption [3].

The ability of microorganisms to adapt to micropollutants more easily when they are attached to activated carbon and to provide suitable enzymes for their degradation also increases the biodegradability of adsorbed xenobiotics, which are difficult to decompose in conventional biological treatment systems. In addition, the degradation of such compounds with purified enzymes has recently gained importance [12]. Although phenolic compounds can be removed to some extent in conventional activated sludge plants, advanced chemical oxidation methods are often needed [13] because they are quite difficult to completely biodegrade [14]. In this respect, treatment studies with various phenolic compounds in biological systems enhanced by the addition of enzymes combined with physicochemical methods such as adsorption to activated carbon gain importance.

Laccase enzyme is of increasing interest due to its ecological importance in biological remediation of soils and waters, applications in the food and textile industry, and chemical synthesis reactions [15]. Important laccase-producing microorganisms, such as white rot fungi, are used for the biological removal of different pollutants [13]. In literature, there are so many studies on the biological degradation of phenolic compounds by laccase-producing microorganisms. For example, Uhnakova et al. (2009) investigated the biodegradation of brominated phenols by *Trametes versicolor* fungus and the laccase enzyme it produces [16]. Besides, Zhang et al. (2008) studied the

degradation of 2,4-dichlorophenol (2,4-DCP), 4-chlorophenol and 2-chlorophenol with the laccase enzyme produced by *Coriolus versicolor* fungus [17]. Studies on the use of purified enzymes for the degradation of organic substances in wastewater which are difficult to biodegrade have been increasing in recent years. There are many studies in the literature on the use of laccase as an oxidoreductase enzyme for the removal of phenols, chlorophenols, endocrine disruptors, hormones, micropollutants, PAHs and textile dyes [12]. For example, it was determined that the laccase enzyme (5 U/mL) degrades phenol and bisphenol-A (BPA) at pH 5 and 35°C by 80% and 60%, respectively, during 30 minutes of mixing [13]. Another study examined the degradation of bisphenol-A with the laccase enzyme. In that study, under optimum conditions (pH: 7, 30°C, initial BPA concentration: 20 mg/L, laccase concentration >0.12 U/mL) laccase provided over 95% BPA biotransformation during the 3 hours of contact period [14].

Studies on the degradation of phenolic compounds such as bisphenol-A and similar xenobiotics with enzymes immobilized on activated carbon or nanoparticles have also started to take place in the literature [18,19]. However, bioregeneration of activated carbon was not studied in these studies and it was not determined quantitatively. Although their purpose and methods are very different, Nguyen et al. (2016) showed that micropollutants can be oxidized by enzymes immobilized on the activated carbon surface after adsorbing to the activated carbon [19]. In this study in the literature, it has been shown that electron transfer between the substrate and oxygen occurs more easily with the catalyst effect of laccase on the activated carbon surface compared to free enzymes.

This study aimed to qualitatively and quantitatively show the occurrence of exoenzymatic bioregeneration in activated carbon adsorption processes combined with biological systems. The extent of enzymatic bioregeneration was not quantified in the literature by the use of exoenzymes. For this purpose, laccase enzyme was selected as an example of exoenzyme owing to its ability to transform phenolic substances. The present study does suggest the use of purified enzymes in full-scale-bioregeneration applications due to their high costs, but tries to understand the mechanism and extent of enzymatic bioregeneration. The study mainly investigates the extent of bioregeneration that could occur due to the presence of an exoenzyme, considering that various exoenzymes are naturally present in biological wastewater treatment systems. In the literature, it has been suggested that the bioregeneration extent could be increased by increasing the activity of exoenzymes [3]. The results of the study are expected to open new perspectives in the engineered use of enzymes for the purpose of maximized bioregeneration, particularly in the

presence of toxic and inhibitory organic compounds. For this reason, in this study, besides phenol, which has inhibitory effects in biological systems and is relatively easy to biodegrade in high concentrations in classical biological systems, 2-nitrophenol (2-NP) and bisphenol-A (BPA), which are difficult to degrade and also inhibitory, were chosen as the target compounds. Within the scope of the study, first of all, adsorption and desorption studies of these compounds were carried out on thermally and chemically activated carbons in abiotic environment, and their adsorption and desorption capacities were calculated. Then, suitable conditions were determined for bisphenol-A to be degraded by laccase, and finally, the biological regeneration potential of both activated carbon types was determined using laccase as an extracellular enzyme.

II. MATERIALS AND METHODS

Experimental studies include adsorption studies, desorption studies, enzymatic biodegradation and enzymatic bioregeneration studies with phenol, 2-nitrophenol (2-NP) and bisphenol-A (BPA). Two different types of activated carbon, which are thermally and chemically activated (Norit PKDA and Norit CAgan, respectively) were used in the studies. In order to determine enzymatic bioregeneration, laccase enzyme purified from *Trametes Versicolor* fungus was used. All studies were carried out in batch systems. The applied methods and the measured parameters are explained below.

2.1 Adsorption Experiments

Adsorption studies were carried out in a temperature-regulated shaker at 150 RPM at 25°C. The adsorption capacities of activated carbons for the phenolic compounds (phenol, 2-nitrophenol and bisphenol-A) were determined by contacting 200 mg/L concentration of the phenolic compound with 1 g/L dose of granular activated carbon (GAC) in 100 mL capacity flasks. In adsorption studies, the pH value of the thermally activated carbon PKDA increased to around 8-8.5 due to its basic properties, while the pH value of CAgan activated with phosphoric acid decreased to about 5.5 due to acidic functional surface groups. Adsorption studies were also performed with 250 mg/L $\text{KH}_2\text{PO}_4 + \text{K}_2\text{HPO}_4$ buffer solution to adjust pH between 6.5-7.5. By measuring the concentrations of the target compound at the beginning and end of the adsorption, the adsorption capacities were calculated according to Equation (1).

$$q_{\text{ads}} = (C_b - C_f) / M \quad (1)$$

q_{ads} : adsorption capacity (mg compound/g GAC)

C_b : Initial concentration (mg/L)

C_f : Final concentration (mg/L)

M : Activated Carbon Dose (g/L)

2.2 Desorption Experiments

Activated carbons used in desorption studies were initially saturated with the target phenolic compounds as in Section 2.1. In 100mL flasks, phenolic compound at a concentration of 200 mg/L and activated carbon (1 g/L) were contacted to ensure that the activated carbons were completely saturated with the phenolic compound. Then, desorption studies were also carried out at 25°C and 150 RPM in a temperature-regulated shaker. Desorption of phenolic compounds was achieved by contacting the previously saturated activated carbon with distilled water. During the desorption studies, the pH value was measured between 6 and 7 for both types of activated carbon. Desorption studies were also performed in the presence of 250 mg/L $\text{KH}_2\text{PO}_4 + \text{K}_2\text{HPO}_4$ buffer solution to adjust pH around 7. At the end of each desorption step, the concentration of the phenolic compound was measured and the amount of desorbed phenolic compound was calculated from the difference. The total desorption capacity cannot be determined with a single desorption step since sorption equilibrium between the activated carbon surface and bulk liquid will be quickly reached in a single abiotic desorption test. Therefore, in order to keep the concentration gradient high, the desorption tests were repeated by periodically refreshing the distilled water (every day) after measuring the concentration of the desorbed phenolic compound at the end of each desorption step. These step-wise desorption tests were continued until the phenolic compound was not desorbed from the activated carbon any more, or the desorbed amount was below measurable levels. Total desorption from activated carbon was calculated according to Equation (2) [1].

$$q_{\text{des}} = \sum (C_i/M) \quad (2)$$

q_{des} : desorption capacity (mg phenolic compound/g GAC)

C_i : Concentration in the water phase after each desorption step (mg/L)

M : Activated carbon dose (g/L)

Accordingly, abiotic regeneration efficiencies (R_{des}) of each activated carbon type were calculated according to Equation (3).

$$R_{\text{des}} = (q_{\text{des}} / q_{\text{ads}}) \times 100 \quad (3)$$

R_{des} : desorption efficiency (%)

2.3 Enzymatic Biodegradation Experiments

In order to determine the oxidation properties of phenolic compounds by the purified free laccase enzyme, different doses of enzymes were contacted with phenol, 2-nitrophenol or bisphenol-A at a concentration of 200 mg/L for each compound at 2 different pH (4.7 and 7.2) conditions in a temperature-regulated shaker at 25°C and 50°C for three days. In

both biodegradation and bioregeneration studies, pH was adjusted to about 7.2 with phosphate buffer, or adjusted to pH value of about 4.7 with sodium acetate buffer. With enzymatic biodegradation studies, it was aimed to determine the conditions (enzyme dose, pH and temperature) where phenol, 2-nitrophenol and bisphenol-A oxidation activities of laccase enzyme are high.

The laccase enzyme used in the study is a product with activity ≥ 0.5 U/mg purified from *Trametes versicolor* fungus, obtained from Sigma Aldrich (Product Code: 34829). The reason for using this enzyme was that it is an extracellular enzyme well known for its ability to degrade phenolic substances and is commercially available in its pure form. The activity of the enzyme was tested by the methods specified in the literature. Laccase enzyme activity was determined by color change at 420 nm as a result of contacting the enzyme with ABTS (2,2'-Azibonis-(3-ethylbenzthiazoline-6-sulphonate) under certain conditions [13]. In enzymatic degradation experiments, laccase enzyme was applied with activities of 0.2, 1 and 5 U/mL in batch tests.

2.4 Enzymatic Bioregeneration Experiments

Bioregeneration studies were carried out with enzymes under suitable conditions. As in abiotic desorption tests, the activated carbons to be used were first saturated with the target phenolic compound. Enzymatic bioregeneration studies were carried out at 25°C (and 50°C when necessary) at pH 7.2 and pH 4.7 in a temperature regulated shaker at 150 RPM. In these studies, desorption and oxidation of phenolic compounds in pre-saturated activated carbon were provided by contacting them with free enzymes dissolved in 25 mL distilled water. Thus, enzymatic bioregeneration was achieved in these flasks. Laccase enzyme was added to have an activity of 0.2 or 1 U/mL in the flasks. During the enzymatic bioregeneration tests, concentrations of the phenolic compound in the liquid phase were also measured at regular intervals, and thereby the part that desorbed but could not be oxidized by the enzymes was also followed. However, the percent enzymatic bioregeneration was determined by applying post-adsorption tests to the regenerated activated carbon at the end of each enzymatic bioregeneration test. The post-adsorption tests were carried out under the same conditions as the pre-adsorption tests and the amount of the adsorption area that was regenerated at the end of enzymatic bioregeneration was calculated according to Equation (4).

$$R_{\text{enz}} = (q_{\text{postads}} / q_{\text{ads}}) \times 100 \quad (4)$$

R_{enz} : Percentage of enzymatic bioregeneration (%)

q_{ads} : Adsorption capacity of unused GAC (mg compound/g GAC)

q_{postads} : Adsorption capacity of enzymatic bioregenerated GAC (mg compound/g GAC)

The difference ($R_{enz} - R_{des}$) between the regeneration capacities due to enzymatic bioregeneration and abiotic desorption indicates regeneration that is not dependent on the concentration gradient and is only caused by the activity of exoenzymes. Thus, it has been possible to quantitatively determine enzymatic bioregeneration for different types of activated carbon.

2.5 Analyses

The analyzes of phenolic substances were made by the direct spectrophotometric method (5530D) of 4-Aminoantipyrine (4-AAP) defined as a standard method [20]. Phenol, 2-NP and BPA concentrations were also measured by HPLC (High-performance Liquid Chromatography) method for some selected samples, and the reliability of the method and the possibility of interference by by-products were evaluated. In the case of biodegradation and bioregeneration experiments of 2-NP, the 4-AAP method measurements were interfered by the formation of a phenolic product upon oxidation of 2-NP by laccase. Therefore, only HPLC measurements were considered for determination of 2-NP concentrations in biodegradation and bioregeneration experiments.

For HPLC measurements, Dionex Ultimate 3000 HPLC device and C18 column (3 μ m 4.6 X 150 mm Dionex Bonded Silica Products) were used. For the measurements, BPA standard solutions and samples diluted 50 times were prepared in volumes between 0.5 and 1 mL with 10% methanol and put into HPLC sample tubes. During the measurement, 30% methanol and 70% distilled water were given to the column as the carrier phase and during the washing of the column between samples. Each injection took 25 minutes, with a flow rate of 0.5 mL/min. During the studies, the column temperature was kept constant at 30 °C and the pressure was kept between 100 -130 bar. In the measurements, the peaks were monitored with the DAD detector at 280 nm, and the peaks were observed at 19.1, 20.4 and 19.4 minutes respectively for phenol, 2-NP and bisphenol-A.

III. RESULTS AND DISCUSSIONS

3.1 Adsorption and Desorption of Phenolic Compounds at Abiotic Conditions

Adsorption capacities were calculated according to Equation (1) as shown in Table 1 for each phenolic compound at initial concentrations of about 200 mg/L.

Table 1. Adsorption capacities of GACs for the target phenolic compounds

q_{ads} (mg/g)	phenol	2-NP	BPA
PKDA	103.6	176.7	98.9
CAgran	85.8	164.1	193.0

As shown in Table 1, phenol and 2-NP adsorption capacities of thermally activated PKDA were higher than those of CAgran. However, the difference in 2-NP adsorption capacities between the two carbon types was less compared to the case of phenol. For both types of activated carbon, 2-NP adsorption capacity was much higher than phenol adsorption capacity. In addition, it was determined that the adsorption capacity of both activated carbons decreased somewhat as a result of balancing the pH with the buffer solution (data not shown). But the difference was not noteworthy. On the other hand, for bisphenol-A, it was determined that CAgran activated carbon adsorbed almost twice as much BPA than PKDA. The reason for this difference is that, unlike the other two phenolic compounds, BPA has a larger molecule because it contains two benzene rings, and therefore it is more amenable to physical adsorption on chemically activated CAgran. Physical adsorption was determined as the dominant adsorption mechanism for adsorption of phenol and 2-NP on chemically activated carbons in previous studies [4,6].

Cumulative desorption capacities were calculated according to Equation (2) as shown in Table 2 for each phenolic compound. Desorption efficiencies were calculated according to Equation (3). The desorption efficiencies obtained by succeeding adsorption-desorption studies are given in Table 3. These cumulative desorption efficiencies were obtained in 9 steps for phenol, 30 steps for 2-NP and 74 steps, i.e. 74 days for BPA until reaching a non-measurable concentration of the phenolic compound in the bulk liquid.

As can be seen in Tables 2 and 3, the desorption capacity and efficiency of chemically activated GAC CAgran were much higher than those of thermally activated PKDA for each compound. Desorbability of phenolic compounds were highly dependent on the activation type of activated carbon. This showed that the carbon activation type eventually affects the occurrence of physical and chemical adsorption. For CAgran, high amounts of physical adsorption of 2-NP and BPA molecules led to higher desorption efficiencies, whereas chemisorption of all three compounds on the thermally activated PKDA led to much lower desorption capacities for this carbon.

Table 2. Desorption capacities of GACs for the target phenolic compounds

q_{des} (mg/g)	phenol	2-NP	BPA
PKDA	9.8	13.4	8.9
CAgran	19.2	70.4	89.8

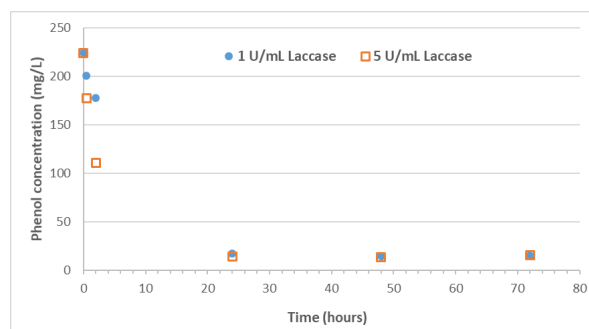
Table 3. Desorption efficiencies (%) of each phenolic compound from the two GAC types

	phenol	2-NP	BPA
PKDA	9.5 %	7.6 %	9.0 %
CAgran	22.4 %	42.9 %	46.6 %

In each case, these desorption efficiencies obtained are not sufficient for long-term use of activated carbon, and it is suggested that desorption itself is not an efficient method for regeneration of activated carbon under abiotic conditions. These abiotic desorption efficiencies obtained will be compared with enzymatic bioregeneration efficiencies in Section 3.3.

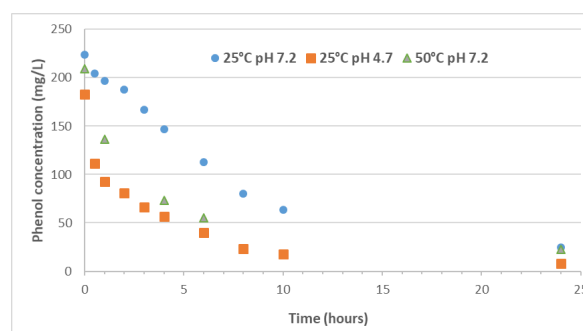
3.2 Enzymatic Oxidation of Phenolic Compounds

Firstly, the powdered laccase enzyme was dissolved in 25 mL tubes to have activities of 1 U/mL and 5 U/mL and contacted with phenol at a concentration of approximately 200 mg/L at a fixed pH of 7.2. The change in phenol concentration was observed with respect to time and the obtained results are given in Figure 1. As can be seen, the laccase enzyme led to oxidation of phenol by 93% in less than 24 hours at both enzyme doses. However, phenol degradation rate was slightly higher at 5 U/mL enzyme dose. This is an expected result. In a literature study, it was determined that laccase enzyme (5 U/mL) degraded phenol at an efficiency of 80% during 30 minutes of mixing at pH 5 and 35°C [13]. These results are consistent with our study. In the present study, 15 mg/L phenol remained nondegradable in both tubes with 1 and 5 U/mL enzyme doses. This shows that laccase enzyme lost its activity in less than 24 hours and therefore could not degrade some of the phenol. For this reason, in the following enzymatic bioregeneration studies of phenol-saturated GAC, the duration time of bioregeneration tests were applied as 24 hours.

**Figure 1.** Phenol degradation by laccase enzyme at 1 U/mL and 5 U/mL doses at 25°C and pH:7,2.

pH can be an important parameter in enzymatic reactions [14]. In order to determine the effect of pH on enzymatic degradation with laccase, phenol degradation studies were carried out with 1 U/mL

enzyme at 25 °C at 2 different pH values (7.2 and 4.7) (Figure 2). pH 7.2 was achieved with phosphate buffer and pH 4.7 with sodium acetate buffer. While the initial phenol concentration was 224 mg/L at pH 7.2, it decreased to 25 mg/L after 24 hours resulting in 89% phenol removal. On the other hand, the initial phenol concentration of 183 mg/L at pH 4.7 decreased to 8 mg/L during 24 hours resulting in 96% phenol removal. The efficiency of enzymatic degradation at pH 4.7 was slightly higher than at pH 7.2. It was also understood that at pH 4.7, the phenol concentration decreased with a greater removal rate. While the phenol concentration was halved in approximately 6 hours at pH 7.2, it was halved within 2 hours at pH 4.7 in an acidic environment. As can be seen, it is not possible to say that there was a significant difference between pH 4.7 and 7.2 in terms of degradation efficiency, but it is clear that the degradation rate for the laccase enzyme was higher at pH 4.7. This result was not surprising since the laccase enzyme used in our study is produced by fungi which usually have higher enzyme activities at lower pH values compared to bacteria.

**Figure 2.** Phenol degradation by laccase enzyme at a dose of 1 U/mL at pH 4.7 and 7.2 at 25 °C and 50 °C.

To determine the effect of temperature on the activity of the laccase enzyme, enzymatic degradation studies were also carried out at 50°C. The time-dependent variation of the degradation of phenol and 2-NP with 1U/mL laccase enzyme at 50°C and at pH of 7.2 are given in Figure 2. Compared to the phenol removal profile for 25 °C and 7.2 pH, it is seen that the removal rate was much higher at 50 °C. While approximately 25 mg/L phenol was degraded after 1 hour at 25 °C and 115 mg/L after 6 hours, approximately 70 mg/L phenol was degraded after 1 hour at 50 °C, and 150 mg/L phenol after 6 hours. At the end of 24 hours, phenol concentration of around 20-25 mg/L remained in the environment without being oxidized by laccase at both temperatures.

In order to find out whether phenol removal also occurred due to mechanisms other than enzymatic degradation, 200 mg/L phenol was shaken under the same conditions without adding enzyme and phenol concentration was followed with respect to time for 4

days. These experiments were performed both at 25°C and 50°C at both pH values of 4.7 and 7.2. Phenol concentration did not decrease by time (data not shown) showing that phenol was not measurably removed by any mechanism other than enzymatic reaction, such as evaporation or adsorption to the glass surface, etc. Hence, enzymatic degradation was identified as the only phenol removal mechanism in these studies. Brown precipitate observed at the end of the biodegradation experiments indicated that the polymerized phenols, which were produced as a result of oxidation process catalyzed by laccase, were removed from the bulk by precipitation. Phenol, which is oxidized by the enzyme laccase, turns into phenoxy radicals. Phenoxy radicals react with each other and form polymers by covalently bonding via C bonds [1].

2-NP degradation studies were also carried out at 25 °C at pH 7.2 and pH 4.7, by adding approximately 527 and 348 mg/L 2-NP, respectively and 1 U/mL laccase enzyme to each flask. Also, 166 mg/L initial 2-NP concentration was tested with 1 U/mL enzyme at pH 7.2. In the samples of adsorption and desorption experiments in which only 2-NP and GAC were present in the medium, 2-NP concentrations had been successfully measured with the 4-AAP method. But parallel HPLC measurements showed that 4-AAP method was interfered by a by-product of 2-NP oxidation by laccase in the biodegradation experiments. Therefore, HPLC measurements were used in biodegradation and bioregeneration experiments performed with 2-NP.

To monitor the 2-NP removal in degradation experiments, 2-NP concentrations were measured by taking samples at certain time intervals within 24 hours (data not shown). It was found that 1 U/mL laccase decreased 527 mg/L 2-NP down to 329 mg/L and 166 mg/L 2-NP to 3 mg/L at pH 7.2 within 24 hours. At pH 4.7 conditions, 1U/mL laccase decreased 348 mg/L 2-NP down to 4 mg/L. Enzymatic degradation efficiencies reached up to 99 % except in the case of high initial 2-NP concentration of 527 mg/L at pH 7.2, where degradation efficiency was only 38 %. The reason for this was high initial 2-NP concentration and the fact that activity of the suspended enzyme lasted for less than 24 hours and therefore was not able to further oxidize 2-NP. These results showed that 1 U/mL enzyme dose and a 24-hour contact period were sufficient for effective oxidation of 2-NP, and they will be also sufficient for the following bioregeneration studies. To determine whether 2-NP removal occurs by evaporation, it was shaken at 25°C, pH 4.7 and without adding enzyme, and 2-NP concentration was followed for 5 days. It was also monitored at 50°C and pH 7.2 and pH 4.7 conditions. 2-NP was not removed by any mechanism other than enzymatic reaction as in the case of phenol.

In the enzymatic degradation experiments performed with bisphenol-A, laccase enzyme at a dose of 1 U/mL

was contacted with bisphenol-A at concentrations of approximately 10, 50 and 100 mg/L at pH of 7.2 in 25 mL tubes. These tests lasted for 24 hours and the concentration change was observed. The results obtained are given in Figure 3 on a logarithmic scale.

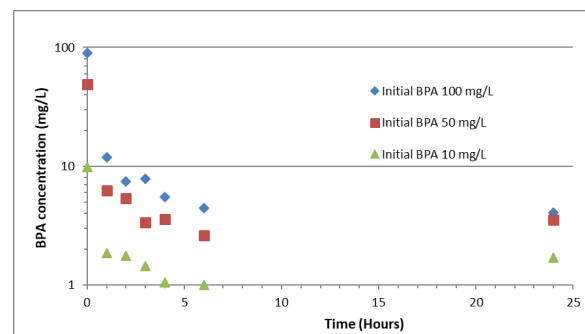


Figure 3. Degradation of BPA by laccase enzyme (1 U/mL) at pH 7.2 and 25°C conditions.

Laccase enzyme achieved most of the bisphenol-A oxidation within the first hour, and bisphenol-A concentration in the water phase stabilized within the first 5-6 hours. Laccase was able to oxidize bisphenol-A at a concentration of 100 mg/L by 90% in the first hour. The removal efficiency reached 95% within 5-6 hours. This enzymatic degradation efficiency was very similar to the 93% removal that was obtained for phenol. This showed that laccase was able to degrade BPA in a manner similar to phenol and at a relatively high rate, although BPA is known to be much more difficult to be biodegraded by microorganisms compared to phenol. In this sense, it is understood that bisphenol-A degradation with laccase and similar oxidoreductive exoenzymes will be an effective method. After the first 5-6 hours, BPA concentrations remained almost constant. This shows that the activity of the suspended laccase enzyme did not exceed a few hours. When the initial BPA concentration was 50 and 100 mg/L, the final BPA concentration decreased to 3 and 4 mg/L, respectively, at the end of the enzymatic treatment. When the initial concentration was 10 mg/L, the final concentration ranged between 1-2 mg/L (Figure 3).

In order to determine the effect of pH, degradation of BPA was also studied at an initial concentration of 50 mg/L at the pH values kept around 4.7-5 with sodium acetate buffer, again at 1 U/mL laccase enzyme activity and at a temperature of 25°C (Figure 4). As can be seen, decreasing the pH from 7.2 to 4.7 did not cause a significant difference in the degradation of BPA. However, under pH 4.7 conditions, the final BPA concentration decreased to 1 mg/L as it was around 3 mg/L under pH 7.2 conditions. Although this may not seem like a significant difference at first glance, even this small difference can be very significant, since Bisphenol-A is among the primary pollutants and even very low concentrations may cause endocrine

disrupting effects in nature. For this reason, applying low pH (around 5) in enzymatic degradation with laccase will reduce the effluent values. Also in another study, higher BPA removal was found at pH 6 compared to neutral conditions [14].

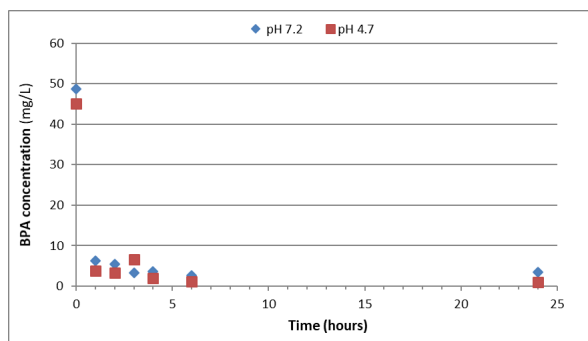


Figure 4. Degradation of BPA by 1 U/mL laccase enzyme activity at different pH conditions at 25°C.

The studies have shown that laccase enzyme provides a very effective BPA removal at an activity dose of 1 U/mL. Exceeding this dose will increase the cost of the enzyme, but will not provide any significant benefit. Therefore, it was decided to try a lower enzyme dose (0.2 U/mL). Figure 5 shows BPA removal with laccase at 2 different enzyme doses. 95% removal was observed in the case of 1 U/mL laccase dose, resulting in final BPA concentration of around 4 mg/L. The removal efficiency decreased to 70% at 0.2 U/mL laccase dose, and the final BPA concentration remained at a very high level of around 30 mg/L. In addition, bisphenol-A degradation rate was higher at 1 U/mL enzyme dose. In the first hour, 1 U/mL laccase degraded approximately 90% of 100 mg/L BPA, while laccase at 0.2 U/mL was only able to degrade approximately 30% of the initial concentration. These studies have shown that the enzyme activity has a very important effect on BPA removal, and should be optimized.

In order to see whether the removal of BPA took place by evaporation, 200 mg/L BPA was shaken at 25 °C under the same conditions without adding enzyme, and BPA concentration was followed for 4 days depending on time. No decrease in BPA concentration was observed during 4 days (data not shown). Since the enzymatic bioregeneration studies will also be carried out at 50 °C, the change in the initial concentration of 120 mg/L BPA was monitored for 3 days in the absence of enzymes at two different pH conditions (pH 4.7 and 7.2) to see if BPA would be removed by evaporation at this relatively high temperature (data not shown). There was again no decrease in BPA concentration at 50 °C. These studies have shown that BPA was not removed by any mechanism other than enzymatic reaction, such as evaporation or adsorption to the glass surface, etc., at conditions of 25 and 50 °C and pH 4.7 and 7.2. For this reason, enzyme activity has been

identified as the only effective BPA removal mechanism in our enzymatic degradation studies.

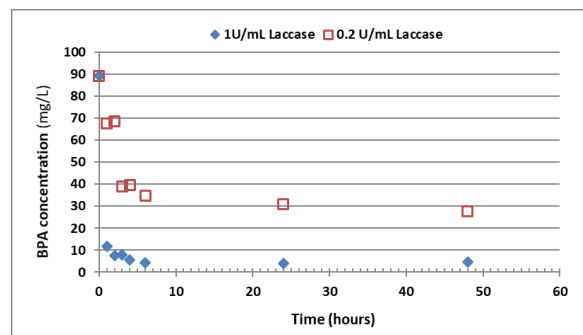


Figure 5. BPA degradation at pH 7.2 and 25°C by different laccase enzyme activities (1 U/mL and 0.2 U/mL).

To determine the effect of temperature on the activity of the laccase enzyme, enzymatic degradation studies were also carried out at 50°C. The time-dependent variation of the concentration of BPA at 50°C with 1U/mL laccase enzyme at pH 7.2 and pH 4.7 conditions are given in Figure 6. BPA oxidation took place in the first 1 hour at 50°C as well as at 25°C. However, at 25 °C, the BPA removal efficiency was around 90% and an additional 5% removal occurred in the next few hours, while at 50 °C this rate reached around 95% in the first hour and there was no further degradation in the following hours. This shows that the degradation of BPA by laccase at 50°C occurred slightly faster than at 25°C, but the enzyme activity was lost more quickly. On the other hand, no difference was observed at pH 7.2 and pH 4.7 conditions in studies performed at 50°C (Figure 6).

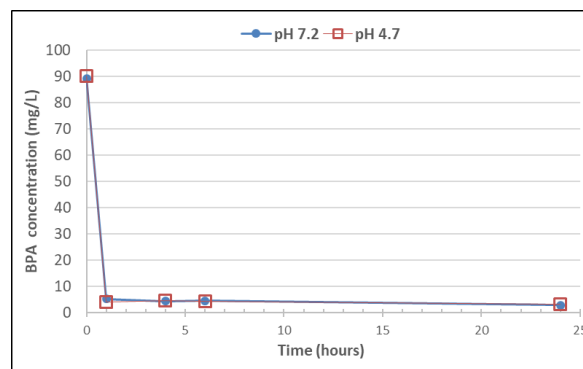


Figure 6. BPA degradation at pH 7.2 and pH 4.7 and at 50°C conditions at laccase enzyme activity of 1 U/mL.

A literature study examining the removal of BPA using crude laccase solution obtained from *Trametes versicolor* showed that the degradation yield in 24 hours reached 88.76% [21]. In another study, it was determined that laccase enzyme (5 U/mL) degraded bisphenol-A by 60% at pH 5 and 35°C during 30

minutes of contact [13]. The degradation efficiencies obtained in all degradation experiments with laccase in our study were consistent with the values obtained in the literature [13,14,19].

3.3 Bioregeneration with Laccase Enzyme

In bioregeneration experiments, 1 U/mL laccase enzyme dose was used since it was found to be sufficient in enzymatic degradation experiments. Bioregeneration studies were carried out in two different solutions such that pH was adjusted to 7.2 with a phosphate buffer or pH was fixed to 4.7 with sodium acetate buffer. The initial abiotic adsorption capacities (q_{ads}) obtained for approximately 200 mg/L of phenol and the post-adsorption capacities ($q_{postads}$) obtained after enzymatic regeneration as well as the bioregeneration efficiencies calculated from these values are shown in Table 4 for phenol as the target compound.

While the maximum total desorption efficiency was around 10% in thermally activated PKDA carbon under abiotic conditions in Section 3.1, this efficiency was increased to around 40% with laccase enzyme (Table 4). This has shown that activated carbon saturated with phenol can be enzymatically regenerated partially with laccase enzyme, the amount of which is much higher than the maximum desorption (regeneration) that could be achieved under abiotic conditions. In the case of chemically activated CAgran, the bioregeneration efficiency was much higher. The desorption capacity of CAgran, which was around 26% under abiotic conditions at pH 7, increased to 82% with the laccase enzyme. The very high bioregeneration efficiency differences between the two types of activated carbon indicate the importance of the activated carbon type. Although enzymatic bioregeneration was also valid for the thermally activated carbon, the results indicated that it will provide a more realistic solution for bioregeneration of chemically activated carbons.

Table 4. Enzymatic bioregeneration efficiencies of phenol-loaded GACs by laccase (1 U/mL).

GAC	pH	T (°C)	q_{ads} (mg/g)	$q_{postads}$ (mg/g)	Bioregeneration efficiency (%)
1 g/L PKDA	7.2	25	131.0	51.2	39.1
1 g/L CAgran	7.2	25	40.2	33.1	82.3
1 g/L PKDA	4.7	25	86.5	38.1	44.0
1 g/L CAgran	4.7	25	39.9	49.1	123.2
1 g/L PKDA	7.2	50	132.0	39.9	30.2
1 g/L CAgran	7.2	50	58.0	26.7	46.0

At pH 4.7, higher bioregeneration efficiencies were observed for both activated carbon types compared to pH 7.2. In the previous section, it was observed that degradation of phenolic compounds with laccase was higher at pH 4.7. Therefore, higher bioregeneration was an expected result. Surprisingly, after the contact of laccase enzyme with CAgran at pH 4.7, the adsorption capacity exceeded that of unused activated carbon, and accordingly, the bioregeneration efficiency was found to be higher than 100%. This was probably because the enzymes attached to the activated carbon surface continued their activity for a while and resulted in further enzymatic degradation during post-adsorption tests. It has been shown in another study in the literature that the laccase enzyme immobilized on the activated carbon surface maintains its activity longer than the suspended enzyme [19]. In bioregeneration studies, after 1 day of contact with the enzyme, the phenol concentration remaining in the water phase was only between 3 and 5 mg/L in each of the 4 reactors (data not shown). This indicated that, as predicted from previous degradation studies, most of the desorbed phenol was further degraded by suspended laccase enzymes within 24 hours.

Bioregeneration experiments were also performed with phenol at 50°C in order to see the effect of high temperature at pH 7.2. Bioregeneration efficiencies were obtained as 30.2 % for PKDA and 46.0 % for CAgran (Table 4). These bioregeneration efficiencies were lower compared to the values obtained at 25 °C. At 25 °C, bioregeneration occurred at 39.1 and 82.3 % efficiencies, respectively for PKDA and CAgran. This decrease in bioregeneration efficiency was attributed to the loss of enzymatic activity at higher temperature, although enzyme activity duration increased with immobilization on GAC.

In enzymatic bioregeneration experiments with 2-NP as the target compound, bioregeneration studies were carried out in a solution containing 1 U/mL laccase enzyme and 2-NP at a concentration of approximately 140 mg/L at pH adjusted to 7.2 with phosphate buffer. In the biodegradation studies for phenol, it was observed that degradation rate was higher at 50 °C, but the final efficiencies were comparable. Based on this, the bioregeneration of 2-NP was monitored at 50°C. The adsorption capacities before and after enzymatic regeneration and the bioregeneration efficiencies calculated from these values are given in Table 5.

Table 5. Enzymatic bioregeneration efficiencies of 2-NP-loaded GACs by laccase (1 U/mL) at 50 °C.

GAC	pH	q_{ads} (mg/g)	$q_{postads}$ (mg/g)	Bioregeneration efficiency (%)
1 g/L PKDA	7.2	135.1	116.4	86.2
1 g/L CAgran	7.2	104.6	69.2	66.2

While the maximum total desorption efficiency was around 7% in thermally activated PKDA carbon with high adsorption capacity under abiotic conditions (Table 3), this efficiency was increased to around 86% with laccase enzyme (Table 5). This showed that activated carbon saturated with 2-NP was regenerated 12 times more than the case in abiotic conditions when laccase enzyme was provided. The regeneration capacity for CAgran, which was around 42% under abiotic conditions, increased to 66% with laccase enzyme. When the desorption efficiencies and bioregeneration efficiencies are compared, it is obvious that bioregeneration efficiencies are considerably higher than desorption efficiencies for both GAC types. These bioregeneration efficiencies for 2-NP were higher than the 25-30 % efficiencies obtained by a biomass mixture in a literature study [22]. However, in another study, 65-90 % bioregeneration efficiencies were obtained by an activated sludge mixture, which was previously acclimated to 2-NP [6]. The laccase enzyme, when it was used in the absence of other biological agents in the present study, was able to achieve comparable bioregeneration efficiencies with an acclimated biomass that was used in the previous study [6]. This indicates that acclimation may provide the necessary exoenzymes for the degradation of xenobiotics adsorbed on activated carbon.

The bioregeneration efficiency differences between the two activated carbon types showed the importance of the activated carbon type. It appears that PKDA was more bioregenerated, although 2-NP was desorbed much more from CAgran at abiotic conditions. Considering the higher adsorption capacity and lower abiotic desorption efficiency of PKDA, it can be concluded that laccase was very effective in bioregeneration of PKDA with high 2-NP saturation. Therefore, in terms of high adsorption and high bioregeneration efficiency, the use of thermally activated carbons should be considered to be more appropriate for 2-NP removal. This finding is totally opposite to the results obtained with phenol. Since thermal activation is carried out without oxygen, it leads to a reactive surface and chemical adsorption takes place, forming strong irreversible bonds. In chemical activation, since the activated carbon has a surface with fully oxidized active sites, its interaction with oxygen does not affect the surface, and more physical adsorption takes place and more reversible weak bonds are formed [1]. In the case of phenol, it seems that laccase enzyme could not oxidize most of the chemically adsorbed phenol and could open less new adsorption sites via enzymatic bioregeneration on the thermally activated PKDA. But on the other hand, chemically adsorbed 2-NP could be oxidized to a higher amount by laccase leading to higher bioregeneration efficiencies. This is because most of the phenolics including phenol participate in oxidative polymerization on the surface of oxygen-sensitive thermal activated carbons. However, 2-NP does not

participate in oxidative polymerization reactions. It is known that oxidative coupling reactions of phenolic compounds other than nitrophenols reduces the reversibility of adsorption [1].

Bioregeneration experiments were also performed for bisphenol-A (BPA) at an initial bulk concentration of 200 mg/L in the pre-adsorption process. These experiments were performed at laccase activity doses of 0.2 U/mL and 1 U/mL and at pH values of 4.7 and 7.2. The studies were first carried out under 25°C temperature conditions. The initial adsorption capacities and the adsorption capacities obtained by post-adsorption after enzymatic regeneration and the bioregeneration efficiencies calculated from these values are given in Table 6 for the enzyme activity dose of 0.2 U/mL.

While the maximum total desorption efficiency was around 45% in chemically activated CAgran carbon under abiotic conditions in Section 3.1, this efficiency was increased to around 90% with laccase enzyme (Table 6). Moreover, while only one day of contact time was sufficient for enzymatic bioregeneration, the 45% cumulative abiotic desorption took place in 74 steps, i.e. 74 days, as discussed in Section 3.1. The rate of abiotic desorption, which took place in one day, was only around 3%. In other words, this has shown that CAgran activated carbon saturated with BPA was regenerated by laccase enzyme, at least 2 times the maximum total desorption (regeneration) that can be possible only with water under abiotic conditions.

Table 6. Enzymatic bioregeneration efficiencies of 200 mg/L BPA at 25°C with laccase at 0.2 U/mL activity

GAC	pH	q _{ads} (mg/g)	q _{postads} (mg/g)	Bioregeneration efficiency (%)
1 g/L PKDA	7.2	73.7	156.7	212.5
1 g/L CAgran	7.2	167.2	154.4	92.3
1 g/L PKDA	4.7	89.1	157.3	176.5
1 g/L CAgran	4.7	174.9	156.9	89.7

The bioregeneration efficiencies were much higher with thermally activated PKDA as in the case of phenol. In section 3.1, the regeneration capacity for PKDA, which was around 9% under abiotic conditions, increased to over 100% with laccase enzyme (Table 6). Efficiencies above 100% show that the activity of enzymes attached to activated carbon lasted much longer and continued to degrade BPA during post-adsorption. However, in Section 3.2, the enzyme

activity had lasted for only a few hours in the degradation experiments without activated carbon. Enzymes attached to carbon surface should have kept their activity longer compared to the enzymes, which were totally suspended in the previous biodegradation experiments. As a result of this, the calculated bioregeneration efficiencies were much higher than the total desorbabilities. It has also been observed in another study with BPA and laccase, that the activity of enzymes held on activated carbon is much longer than those of suspended enzymes [19]. It can be said that these findings obtained in our study showed that the amount of enzymatic bioregeneration could be much more than the sum of abiotic desorption and enzymatic degradation because of a synergistic effect, and therefore it was more effective than expected. In other words, it is understood that, as a treatment application, enzymatic bioregeneration may have much more efficient effects than sole enzymatic degradation of phenolic compounds.

The bioregeneration efficiency differences between the two activated carbon types also show the importance of the activated carbon type. Although CAgran activated carbon gave higher bioregeneration efficiencies in our study with phenol, the opposite was true in our experiments performed with BPA. This can be attributed to the chemical structure of BPA molecule, which has two benzene rings and much larger compared to phenol. Bioregeneration studies showed no noteworthy effect of pH on the enzymatic bioregeneration of BPA. In bioregeneration studies, after 1 day of contact with enzyme, BPA concentration remaining in the water phase was only around 2 mg/L in each of the 4 reactors. This showed that, as predicted from previous degradation studies, desorbed BPA was largely degraded by the suspended laccase enzymes within 24 hours.

Bioregeneration studies were also repeated at 1 U/mL laccase activity to see how increasing the enzyme dose would affect bioregeneration efficiency. As seen in Table 7, increasing the enzyme dose did not further increase the bioregeneration efficiency. In section 3.2, it was shown that enzymatic degradation increased with increasing enzyme dose from 0.2 to 1 U/mL. However, this increase was not observed in enzymatic bioregeneration. In other words, a dose of 0.2 U/mL enzyme activity was sufficient for enzymatic bioregeneration. This shows that the enzymes immobilized on activated carbon remain active for longer than suspended enzymes and can oxidize more BPA. Therefore, enzymatic bioregeneration can be achieved with a much lower enzyme addition compared to sole enzymatic degradation.

Table 7. Enzymatic bioregeneration efficiencies of 200 mg/L BPA at 25°C with laccase at 1 U/mL activity.

GAC	pH	q _{ads} (mg/g)	q _{postads} (mg/g)	Bioregeneration efficiency (%)
1 g/L PKDA	7.2	92.2	159.1	172.6
1 g/L CAgran	7.2	178.2	168.1	94.3
1 g/L PKDA	4.7	106.7	86.6	81.1
1 g/L Cagran	4.7	174.3	137.1	78.7

To determine the effect of temperature, bioregeneration studies were also carried out at 50 °C at pH 7.2 and pH 4.7 with 1 U/mL enzyme activity doses. In these studies, unlike the previous ones, 100 mg/L BPA was used in pre- and post-adsorption. As seen in Table 8, bioregeneration efficiencies decreased at 50 °C compared to 25 °C. The immobilized enzymes may have lost their activity at 50 °C much faster than the case at 25 °C. A similar situation was also detected in the previous studies with phenol. The fact that this decrease is more pronounced especially in PKDA indicates the possibility that the activated carbon type may also affect the enzyme immobilization. It is suggested that the enzyme immobilization was higher on PKDA and therefore the decrease in bioregeneration efficiency at high temperature was higher than that of Cagran.

Table 8. Enzymatic bioregeneration efficiencies of 100 mg/L BPA at 50°C with laccase at 1 U/mL activity.

GAC	pH	q _{ads} (mg/g)	q _{postads} (mg/g)	Bioregeneration efficiency (%)
1 g/L PKDA	7.2	92.4	65.9	71.3
1 g/L Cagran	7.2	90.0	65.2	72.5
1 g/L PKDA	4.7	97.9	26.0	26.5
1 g/L Cagran	4.7	95.8	70.2	73.3

In addition, as seen in Tables 6-8, PKDA bioregeneration was found to be much lower at pH 4.7 than the values obtained at pH 7.2 in all cases. This difference did not exist for CAgran. This can be attributed to the fact that PKDA, which was activated thermally by steam, has more basic surface functional groups, while CAgran, activated by phosphoric acid, has acidic surface functional groups [1].

IV. CONCLUSIONS

The results obtained in the study showed by which mechanisms and to what extent extracellular enzymes were able to bioregenerate activated carbon to fill an important gap in the scientific literature. With this study, extracellular enzymatic bioregeneration was demonstrated quantitatively for the first time in the literature by directly using purified exoenzymes. Phenol, 2-nitrophenol and bisphenol-A were degraded to a large extent with the laccase enzyme. Depending on the pH, 40-45% of thermally activated PKDA carbon and 80-100% of chemically activated CAgran carbon loaded with phenol were bioregenerated at 25 °C between pH 5-7. However, the bioregeneration efficiencies decreased at 50 °C. In the case of 2-NP, bioregeneration efficiencies as high as 86 and 66 % were achieved at 50 °C for PKDA and CAgran, respectively. At an enzyme activity of 0.2-1 U/mL, bisphenol-A was greatly degraded by the laccase enzyme and 80-100% of PKDA and 80-95% of CAgran could be bioregenerated at 25 °C between pH 5-7. The study showed that both the activation type of activated carbon and the chemical structure of the target compound affect the extent of bioregeneration. In all cases, the bioregeneration efficiencies were much higher than the abiotic total desorption efficiencies. This showed that extracellular enzymes such as laccase take an active role in the bioregeneration of activated carbon.

ACKNOWLEDGMENT








This study was funded by The Scientific and Technological Research Council of Turkey (TUBITAK) (Project No: 118Y010) and Istanbul Medeniyet University Scientific Research Projects Fund (Project No: F-GAP-2018-1270). We are also thankful to Dr. Songül Yaşar Yıldız for her help in HPLC measurements.

REFERENCES

- [1] Aktaş, O., Çeçen, F. Bioregeneration of activated carbon: a review. *Int. Biodeterior. Biodegradation*, 59, 257-272. (2007). <https://doi.org/10.1016/j.ibiod.2007.01.003>
- [2] Gutkovski, J.P., Schneider, E.E., Michels, C. How effective is biological activated carbon in removing micropollutants? A comprehensive review. *J. Environ. Manage.*, 349, 1-15. (2024). <https://doi.org/10.1016/j.jenvman.2023.119434>
- [3] Çeçen, F., Aktaş, Ö. Activated Carbon for Water and Wastewater Treatment: Integration of Adsorption and Biological Treatment. *Wiley-VCH Verlag GmbH&Co. KgaA, Weinheim, Germany*. (2011). ISBN: 978-3-527-32471-2
- [4] Aktaş, Ö., Çeçen, F. "Effect of activation type on bioregeneration of various activated carbons loaded with phenol", *Journal of Chemical Technology and Biotechnology*, 81, 1081-1092. (2006). <https://doi.org/10.1002/jctb.1472>.
- [5] Aktaş, Ö., Çeçen, F. "Cometabolic bioregeneration of activated carbons loaded with 2-chlorophenol", *Bioresource Technology*, 100, 4604-4610. (2009). <https://doi.org/10.1016/j.biortech.2009.04.053>
- [6] Aktaş, Ö., Çeçen, F. "Adsorption and cometabolic bioregeneration in activated carbon treatment of 2-nitrophenol", *Journal of Hazardous Materials*, 177, 956-961. (2010). <https://doi.org/10.1016/j.jhazmat.2010.01.011>.
- [7] Chan, P.Y., Lim, P.E., Ng, S.L., Seng, C.E. Bioregeneration of granular activated carbon loaded with phenolic compounds: effects of biological and physico-chemical factors. *Int. J. Environ. Sci. Technol.*, 15, 1699-1712. (2018). <https://doi.org/10.1007/s13762-017-1527-4>
- [8] Jain, D.M., Singh, V. Biodegradation of phenolic compounds using immobilized *Pseudomonas aeruginosa* on granular activated carbon: Effect of immobilization, kinetic study and microbial regeneration. *Indian J. Chem. Technol.*, 28, 402-411. (2021). <https://doi.org/10.56042/ijct.v28i4.31179>
- [9] Acevedo, Y.S.M., Mancera, L.T.M., Moreno-Piraján, J.C., Florez M.V. Regeneration of activated carbon by applying the phenolic degrading fungus *Scedosporium apiospermum*. *J. Environ. Chem. Engineer.*, 8, 1-10. (2020). <https://doi.org/10.1016/j.jece.2020.103691>
- [10] Lu, Z., Li, C., Jing, Z., Ao, X., Chen, Z., Sun, W. Implication on selection and replacement of granular activated carbon used in biologically activated carbon filters through meta-omics analysis. *Water Res.*, 198, 1-13. (2021). <https://doi.org/10.1016/j.watres.2021.117152>
- [11] Ilyasoglu, G., Vergili, I., Aktas, O., Kaya, Y., Gonder, Z.B., Yilmaz, G. Effect of sludge retention time on bioregeneration of powdered activated carbon loaded with paracetamol. *Int. J. Environ. Sci. Technol.*, 20, 7353-7366. (2023). <https://doi.org/10.1007/s13762-023-04861-5>
- [12] Demarche, P., Junghanns, C., Nair, R.R., Agathos, S.N. Harnessing the power of enzymes for environmental stewardship. *Biotechnol. Adv.*, 30, 933-953. (2012). <https://doi.org/10.1016/j.biotechadv.2011.05.013>
- [13] Asadgol, Z., Forootanfar, H., Rezai, S., Mahvi, A.H., Faramarzi, M.A. Removal of phenol and bisphenol-A catalyzed by laccase in aqueous solution. *J. Environ. Health Sci. Engineer.*, 12, 93-97. (2014). <https://doi.org/10.1186/2052-336X-12-93>

- [14] Escalona, I., de Grooth, J., Font, J., Nijmeijer, K. Removal of BPA by enzyme polymerization using NF membranes. *J. Membr. Sci.* 468, 192-201. (2014). <https://doi.org/10.1016/j.memsci.2014.06.011>
- [15] Otto, B., Schlosser, D. First laccase in green algae: purification and characterization of an extracellular phenol oxidase from *Tetracystis aeria*, *Planta*, 240, 1225-1236. (2014). <https://doi.org/10.1007/s00425-014-2144-9>
- [16] Uhnakova, B., Petrickova, A., Biedermann, D., Homolka, L., Vejvoda, B., Bendnar, P., Papouskova, B., Sulk, M., Martinkova, L. Biodegradation of brominated aromatics by cultures and laccase of *Trametes versicolor*. *Chemosphere*, 76, 826-832. (2009). <https://doi.org/10.1016/j.chemosphere.2009.04.016>
- [17] Zhang, J., Liu, X., Xu, Z., Chen, H., Yang, Y. Degradation of chlorophenols catalyzed by laccase. *Int. Biodeterior. Biodegradation*, 61, 351-356. (2008). <https://doi.org/10.1016/J.IBIDOD.2007.06.015>
- [18] Arca-Ramos, A., Ammann, E.M., Gasser, C.A., Nastold, P., Eibes, G., Feijoo, G., Lema, J.M., Moreira, M.T., Corvini, P.F.X. Assessing the use of nanoimmobilized laccases to remove micropollutants from wastewater. *Environ. Sci. Pollut. Res.*, 23, 3217-3228. (2016). <https://doi.org/10.1007/s11356-015-5564-6>
- [19] Nguyen, L.N., Hai, F.I., Dosseto, A., Richardson, C., Price, W.E., Nghiem, L.D. Continuous adsorption and biotransformation of micropollutants by GAC-bound laccase in a packed-bed enzyme reactor. *Bioresour. Technol.*, 210, 108-116. (2016). <https://doi.org/10.1016/j.biortech.2016.01.014>
- [20] APHA-AWWA-WFC, Standard methods for the examination of water and wastewater, 21st ed., Washington, USA. (2005).
- [21] Hongyan, L., Zexiong, Z., Shiwei, X., He, X., Yinian, Z., Haiyun, L., Zhongsheng, Y. Study on transformation and degradation of bisphenol A by *Trametes versicolor* laccase and simulation of molecular docking. *Chemosphere*, 224, 743-750. (2019). <https://doi.org/10.1016/j.chemosphere.2019.02.143>
- [22] Smolin, S.K., Vasenko, L.V., Klymenko, N.A., Smolin, Y.S. Desorption of 2-Nitrophenol from Activated Carbon Under the Action of Biotic and Abiotic Factors, *J. Water Chem. Technol.*, 41, 158-163. (2019). <https://doi.org/10.3103/S1063455X19030044>

Morphological and molecular diagnosis of the pine processionary moth in Marmara University Göztepe Campus¹

Semanur YAZICI ² , İrem Sülüm AYDOĞAN ² , Berfin Ece DALKIRAN ² , Hilal CODUR ² ,
Tunahan Irmak BAŞARAN ³ , Barış GÖKALSIN ² , Nüzhet Cenk SESAL ² , Yavuz TURAN ² 

²Marmara University, Faculty of Science, Department of Biology, 34722, İstanbul, Türkiye

³Marmara University, Institute of Science and Technology, Department of Biology, 34722, İstanbul, Türkiye

Abstract

Pine processionary moth are known as oligophagous forest pests, usually found in cocoons on *Pinus* trees. While these moths are found in the south of Europe and the north of Africa worldwide, in Turkey they are found in the Mediterranean, Aegean, Black Sea and Marmara regions. *Thaumetopoea pityocampa* (Den. & Schiff.) and *Thaumetopoea wilkinsoni* (Tams) species have been observed in the coastal regions of Turkey. Identification of the species is an important step in the development of biological control strategies. The starting point of this study is the desire to control the pine processionary moth in Marmara University Göztepe Campus. However, since both of these species are found in Turkey, especially in the Marmara Region, the main aim of this study is to determine which species the pine processionary moth in the campus belong to. Morphological and molecular methods were used. As a result of the study, based on both morphology and molecular data, it was determined that the species found on the campus was *Thaumetopoea wilkinsoni*.

Keywords: Marmara University, Molecular Systematics, Morphology, Pine Processionary Moth, *Thaumetopoea wilkinsoni*

I. INTRODUCTION

The genus *Thaumetopoea* belongs to the subfamily Thaumetopoeinae (Lepidoptera: Notodontidae) [1]. Pine processionary moths have four stages are observed in the life cycle of pine processionary insects: Egg, larva, pupa and adult. After emerging from their pupae, pine processionary moths mate approximately one week later, and eggs are laid on the leaves of the pine tree a few hours following copulating [2]. While the egg laying process occurs at the end of summer, the eggs hatch approximately 25 days later, at the beginning of autumn [3]-[5]. While pine processionary larvae are 1-2 mm long when they hatch, they can reach 3-4 cm in length at the end of the larval stage [2]. Under normal conditions, the larval stage is the longest phase in the life cycle of the pine processionary moth. The pine processionary larva molts its skin four times and completes its larval stage in five stages [5]. When the larvae hatch, they are white and covered with fine hairs. Among larvae at the same stage, female larvae are larger than male larvae [6].

After spending the winter in the larval stage, pine processionary moths larvae begin to burrow underground in the morning hours in the spring. Pupae spend the summer months underground. Oval cocoons of chestnut color, 20-25 mm in length and 8-10 mm in width are formed [2]. Generally, female pupae are 4 mm longer and 1.5-2 mm thicker than male pupae [5]. The pupal stage, which takes place underground, can last between 1.5 and 7 months [7].

The adult, which completes its development at the end of the pupal period, emerges from the soil in the afternoon at the beginning of the summer. Adult pine processionary moths have bipectinate type antennae and a thin pectinate thorax covered with gray hairs. The forewings are grayish-white, the edges and nerves of the wing are darker, and there are three black transverse bands on the wings. The hind wings are white with gray corners [2]. Pine processionary females are univoltine; they produce offspring only once in their lifetime. Females often die within 24 hours of spawning [3]. Just like the female, the male makes a long flight after mating, falls to the ground and dies when his energy runs out [2], [5].

¹ This study was supported by The Scientific and Technological Research Council of Türkiye (TÜBİTAK) 2209-A University Students Research Projects Support Program

Corresponding Author: YAVUZ TURAN, Tel: 0212 777 32 80, E-posta: yavuz.turan@marmara.edu.tr

Submitted: 27.02.2024, **Revised:** 14.05.2024, **Accepted:** 07.06.2024

The pine processionary moth has adapted to the Mediterranean climate depending on the amount of sunlight and the lowest winter temperature, and accordingly, it plays a very important role in temperature development and dispersion [2]. The most suitable temperature for the development of the pine processionary moth is 20–25°C [8]. Recently, the excessive planting of pine trees in Southern Europe has caused the pine processionary moth to spread over large areas [9]. The increase in average temperature values due to global warming allows the pine processionary larva to live at altitudes where it would not normally survive [4].

The pine processionary moth is found worldwide in the south of Europe and north of Africa [10]. Although there are suitable habitats for the survival of the pine processionary moth throughout the world, their distribution is limited because the female individuals that lay eggs have a weak ability to fly [11]. Countries where pine processionary moth is seen are Germany, Albania, Austria, Bosnia and Herzegovina, Bulgaria, Algeria, Denmark, Morocco, Palestine, France, Croatia, Spain, Israel, Switzerland, Italy, Libya, Lebanon, Hungary, Macedonia, Egypt, Portugal, Romania, Syria, Tunisia, Turkey and Greece [12].

In Turkey, the pine processionary moth has spread to the Mediterranean, Aegean, Marmara and Black Sea regions. Additionally, two species, *T. pityocampa* and *T. wilkinsoni*, are found in Turkey; It has been reported that *T. pityocampa* is distributed in Thrace, Northern Aegean and Western Marmara, and *T. wilkinsoni* is distributed in the Central and Southern Aegean, Eastern Marmara, Mediterranean and Black Sea [13].

The pine processionary moth is an oligophagous insects. Pine processionary moth larvae begin to become harmful when they emerge from their pouches and begin to consume the leaves around them, and the damage they cause in the last larval stage can reach high levels (Devkota and Schmidt, 1990). In a study, it was observed that young Scots pine trees (*Pinus sylvestris* L.) with damaged leaves produced 50% fewer seeds and grew approximately 50% slower than trees without damage [4].

It has been determined that the pine processionary moth also damages *Pinus brutia*, *P. halepensis*, *P. nigra*, *P. pinea*, *P. radiata*, *P. strobus*, *P. sylvestris*, *Cedrus atlantica*, *C. deodara* and *C. libani* trees throughout Turkey. Although the pine processionary larvae weaken the host by eating its leaves, short-term damages can be tolerated by the tree because this damage occurs during periods when tree development slows down [2]. Despite this, trees that are constantly under attack by pine processionary larvae enter the new vegetation period with fewer leaves, slowing down their growth rate [14].

The pine processionary moth not only damages forests but also causes allergic reactions in humans and most other homoiterm animals [15]. "Caterpillar dermatitis" occurs when contact with pine processionary larvae occurs; local symptoms of redness, swelling, itching and pain are observed on the skin [16].

When determining the control method, the interaction of the pine processionary moth with biotic and abiotic factors should be examined, and the method to be followed should be prevented from harming these factors [17]. Fighting against the pine processionary moth can be achieved by biological, chemical, mechanical and cultural means [2]. Among the alternatives, biological control is the most effective method, while chemical method is the most dangerous, therefore it has been observed that biological control methods are mostly preferred. Biological control is carried out through species-specific competing populations, the main purpose of which is to reduce the density of the species being combated and make it less harmful [18].

When it comes to biological control, all forms of the pine processionary moth can have enemies. As a result of an experiment, it was observed that the pine processionary moth attack was reduced by 19.3% after the egg parasites were used in biological control [19]. In Europe and Israel, *Ooencyrtus pityocampae* (Mercet) (Hymenoptera: Encyrtidae) and *Baryscapus servadeii* (Domenichini, 1965) (Hymenoptera: Eulophidae) have been recorded as primary *T. pityocampa* egg parasitoids [2]. In another study, *O. pityocampae* and *B. servadeii* species were identified as the most common pine processionary parasitoids in Isparta [20].

The continuous presence of the pupa in the soil and the formation of pupae heaps as the larvae move together increases the effectiveness of biological control through the enemies of the pine processionary moth pupae (Battisti et al., 2000). In this context, *Formica rufa* (Hymenoptera: Formicidae) (Red forest ant) was used to combat the pine processionary moth and the results were found to be successful [21].

In addition to biological control, it is aimed to reduce the population density within the scope of biotechnical control: Establishing pheromone traps by synthetically producing secreted pheromones so that adults can find each other is one of these methods [2].

In this study carried out within the scope of the TÜBİTAK 2209/A project, it was aimed to determine the species of pine processionary moth found in Marmara University Göztepe Campus using morphological and molecular methods. The results obtained through the study are intended to contribute to the determination of methods to combat the pine processionary moth.

II. MATERIALS AND METHOD

2.1 Sample Collection from the field

On 02.02.2023, sacs of the pine processionary moth were observed on *P. brutia* species in Marmara University Göztepe Campus (40.987252; 29.053699, 44 m) (Figure 1). Sacs were collected by pruning-shears from three *P. brutia* trees distributed in different areas in this campus and larvae were obtained from the sacs (Figure 2). Then all sacs were brought to the laboratory.



Figure 1. The pine processionary moth pouches seen in Marmara University Göztepe Campus



Figure 2. Larvae of the pine processionary moth collected at Marmara University Göztepe Campus

2.2 Species Identification of Specimens According to Morphological Characteristics

Twelve of the larvae collected from three different trees were placed in 90% alcohol (in 2 ml sterilized cryo tubes) and stored at -20°C for molecular species identification. The larvae in the remaining sacs were kept in glass aquariums (with soil underneath) at 25°C and 60% RH humidity conditions and reared under 12:12 hours light:dark photoperiod conditions for morphological identification. Larvae then moved into the soil to enter the pupal stage. Pupated larvae were kept at 25°C, 60% RH humidity and continuous dark conditions. After about 3 months, adults emerging from the pupae were collected and necessary dissection procedures were carried out in the laboratory for species identification.

Although classical systematic studies in insects are based on external body morphology, in some cases this method is not sufficient. For example, it is very difficult or even impossible to make a morphological species

identification in sibling species. For this reason, genitalia are an important morphological character used for species identification.

Morphological diagnoses of species belonging to the genus *Thaumetopoea* are usually made according to canthus structure. Adult specimens were killed with ethyl acetate species identifications were made according to the structure of the removed canthus.

2.3 Species Identification of Specimens by Molecular Systematic Methods

DNA isolation was performed from the larvae collected for molecular species determination. DNA isolation was performed manually. DNA quality and quantity were determined with Take3 plate and Cytation3 (Biotek, USA) device. Approximately 810 bp of the cytochrome oxidase I (COI) gene region in mtDNA was amplified by PCR from the samples in 90% ethyl alcohol. Primer pairs given in Table 1 were used to amplify the gene region to be studied. The prepared mixtures were loaded into microplate wells and placed in a thermal cycler. PCR reactions were performed in a Biorad (USA) brand thermal cycler. Amplicons were visualized by agarose gel electrophoresis and purified by gel recovery kit. The pure amplicon was then sequenced by outsourced sequencing. The sequences obtained were compared with GenBank data by BLAST algorithm and species determinations were performed.

Table 1. Primers used to amplify the gene region to be sequenced

Gene	Series	Source
COI	Jerry(forward)C1-J-2183	Simon et al., 1994
	5'-CAACATTTATTTTGATTTTTTG	
	G-3'	
	Pat(reverse)TL2N-3014	
	5'-TCCAATGCACTAATCTGCCAT	
	ATTA-3'	

The head of the larvae in 90% ethyl alcohol was dissected and the samples were taken into 1.5 ml sterile ependorfs. Sterile glass beads (for sample disintegration) and 300 µl KCL buffer were added to the same ependorfs. These samples were then physically lysed in a MagNa Lyser at 5000 rpm for 1 minute. Then 300 µl of chloroform was added to the ependorfs and vortexed for 30 seconds. The ependorfs were then centrifuged at 12000 rpm for 3 minutes at +4°C. After centrifugation, 200 µl of the supernatants of the centrifuged samples were taken and transferred into 1.5 ml sterile ependorfs. Then 120 µl of cold isopropanol was added to the samples. For 30 seconds, the samples were mixed by hand movement. The

samples were then centrifuged at 12000 rpm for 2 minutes at +4°C. The supernatant was gently discarded and 200 µl of 96% cold ethanol was added to the samples. Centrifugation was again performed at 12000 rpm for 2 minutes at +4°C. The liquid phase was slowly poured off and the tubes were allowed to dry upright to evaporate the ethyl alcohol. Then 100 µl of TE buffer was added and stored at +4°C until NanoDrop processing. DNA quality and quantity were determined on a Take3 plate with Cytation3 (Biotek, USA).

A mitochondrial nuclear gene region (cytochrome oxidase subunit I (COI)) was amplified from the isolated DNA using the following primers and PCR protocol. Prepared mixtures (PCR Mix) and samples were loaded into microplate wells and placed in a thermal cycler. PCR reactions were performed in a Biorad (USA) brand thermal cycler.

PCR protocol for the COI gene region [22]: 1 cycle: 94°C 5 min; 35 cycles: 94°C 45 s, 45°C 30 s, 72°C 1 min; 1 cycle: 72°C, 2 min

The Cytochrome Oxidase I gene region amplified by PCR from the samples was run on 2% agarose gel electrophoresis using non-toxic electrophoresis dye (Safeview etc.) for each sample and the results of the PCR were checked according to the amplicon lengths. The PCR products were then purified using a gel recovery kit. The pure amplicons were then sequenced by the Sanger method by outsourcing.

The raw data obtained by Sanger sequencing were opened with SnapGene 7.0.2 software and analyzed based on base quality scores. Regions of 20-30 nucleotides with low quality scores at the beginning of the sequence were deleted with trim and bases with a quality score (Phred) above 20 were preferred. The two-way reads obtained with Sanger were then merged with NCBI Blast to obtain a consensus sequence. The NCBI BLASTN algorithm was applied to compare the consensus sequence with the reference database of COI gene sequences from various species. The best BLAST result was used to assign a taxonomic identity based on the COI gene sequence. At the same time, the consensus sequence was also searched in the BOLD database using the Identification Engine and the identification report was obtained.

III. RESULTS AND DISCUSSION

As a result of species identification made from adult pine processionary moth taken from three different trees, it was determined that the pine processionary moth found on campus were *Thaumetopoea wilkinsoni* species. Since it is difficult to identify species from the larvae of the species belonging to the genus, species identification was made using adult pine processionary moth. The canthus structure of male pine processionary moth was examined (Figure 3). The studies were

compared with the existing literature [23]-[25]. According to the canthus structure, it has been determined that the pine processionary moth detected in Marmara University Göztepe Campus are *Thaumetopoea wilkinsoni* species.

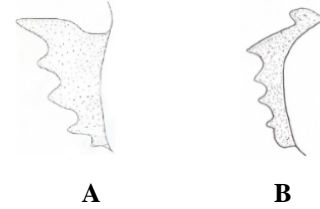


Figure 3. Canthus structure: A. *Thaumetopoea pityocampa* [26] B. *Thaumetopoea wilkinsoni* (drawed by authors)

ACKNOWLEDGMENT

We thank The Scientific and Technological Research Council of Turkey (TÜBİTAK) for supporting this research through the 2209-A project application number 1919B012205571. We would like to express our special thanks to Furkan YENEROĞLU, who helped us in collecting data for our research, and Kahraman İPEKDAL, who inspired us with his valuable work. We are also grateful to our valuable friends and colleagues who supported us in the realization of this study, and to the administrative staff of Marmara University for their assistance.

REFERENCES

- [1] Demirsoy, A. (1997). Yaşamın Temel Kuralları, Omurgasızlar/Böcekler, Entomoloji, Meteksan A.Ş., Ankara, 941 s.
- [2] İpekdal, K. (2005). Çam Kese Böceği *Thaumetopoea* (Denis & Schiff, 1775) (Lepidoptera: Thaumetopoeidae)'nin Biyo-Ekolojisi ve Mücadelesi Üzerine Araştırmalar. Yüksek Lisans Tezi, Hacettepe Üniversitesi, 116 sayfa.
- [3] Schmidt, G.H. (1990). The egg-batch of *Thaumetopoea pityocampa* (Den. & Schiff.) (Lep., Thaumetopoeidae): Structure, hatching of the larvae and parasitism in southern Greece. *Journal of Applied Entomology*, 110, 217–228.
- [4] Hódar, J.A., Zamora, R. ve Castro, J. (2002). Host utilisation by moth and larval survival of pine processionary caterpillar *Thaumetopoea pityocampa* in relation to food quality in three *Pinus* species. *Ecological Entomology*, 27, 292–301.
- [5] Özkazanç, O. (2002). Çam kese böceği *Thaumetopoea pityocampa* Schiff. (Lepidoptera: Thaumetopoeidae)'nin Akdeniz Bölgesi'ndeki biyo-ekolojisi. Ülkemiz Ormanlarında Çam Keseböceği Sorunu ve Çözüm Önerileri Sempozyumu Bildiri Kitabı, 1–11.

- [6] Fitzgerald, T.D. (2003). Role of the trail pheromone in foraging and processionary behavior of pine processionary caterpillars *Thaumetopoea pityocampa*. *Journal of Chemical Ecology*, 29(3), 513–532.
- [7] Mendel, Z. (1990). On the origin of the pine processionary caterpillar, *Thaumetopoea wilkinsoni* Tams (Lep., Thaumetopoeidae) in Israel. *Journal of Applied Entomology*, 109, 311–314.
- [8] Blas, X.P. (2000). An initial study of the building of the *Thaumetopoea pityocampa* communal nest. (Web address: http://www.acs.bolton.ac.uk/~xp1pls/T_PITYOCAMPAPANADES2000.PDF), (Date accessed: July 2023).
- [9] Battisti, A. (1988). Host-plant relationships and population dynamics of the pine processionary caterpillar *Thaumetopoea pityocampa* (Denis & Schiffermüller). *Journal of Applied Entomology*, 105, 393–402.
- [10] Battisti, A., Bernardi, M. ve Ghirardo, C. (2000). Predation by the hoopoe (*Upupa epops*) on pupae of *Thaumetopoea pityocampa* and the likely influence on other natural enemies. *BioControl*, 45(3), 311–323.
- [11] Devkota, B. ve Schmidt, G.H. (1990). Larval development of *Thaumetopoea pityocampa* (Den. & Schiff.) (Lep., Thaumetopoeidae) from Greece as influenced by different host plants under laboratory conditions. *Journal of Applied Entomology*, 109(4), 321–330.
- [12] Öymen, T. ve Küçükosmanoğlu, A. (2002). *Thaumetopoea pityocampa* (Den. & Schiff.) ile biyolojik, kimyasal ve fiziksel savaşın popülasyon üzerindeki etkileri. Ülkemiz Ormanlarında Çam Keseböceği Sorunu ve Çözüm Önerileri Sempozyumu Bildiri Kitabı, 152–157.
- [13] İpekdal, K. (2012). Çam Kese Böceği, *Thaumetopoea pityocampa* (Dennis&Schiffermüller, 1775) ve *Thaumetopoea wilkinsoni* Tams, 1924 (Lepidoptera: Notodontidae), Türlerinde Ayrılma ve Filocoğrafya. Doktora Tezi, Hacettepe Üniversitesi, Türkiye, 194 sayfa.
- [14] Carus, S., (2004). Impact of defoliation by the pine processionary moth (*Thaumetopoea pityocampa*) on radial, height and volume growth of Calabrian pine (*Pinus brutia*) trees in Turkey. *Phytoparasitica*, 32(5), 459–469.
- [15] Triggiani, O. ve Tarasco, E. (2002). Efficacy and persistence of entomopathogenic nematodes in controlling larval populations of *Thaumetopoea pityocampa* (Lepidoptera: Thaumetopoeidae). *Biocontrol Science and Technology*, 12, 747–752.
- [16] Ekerbiçer, H., Çelik, M., Aral, M. ve Şaşmaz, S. (2002). Çam kese böceğinin (*Th. pityocampa*) insan sağlığı üzerine olumsuz etkileri. Ülkemiz Ormanlarında Çam Keseböceği Sorunu ve Çözüm Önerileri Sempozyumu Bildiri Kitabı, s. 203–211.
- [17] Krebs, C. (1990). Ecology: The Experimental Analysis of Distribution and Abundance. Harper&Row Publishers, New York, 800 p.
- [18] Van Driesche, R.G. ve Bellows, Jr. T.S. (1996). Biological Control, Chapman&Hall, New York, 539 p.
- [19] Tsankov, G., Schmidt, G.H. ve Mirchev, P. (1998). Studies on the egg parasitism in *Thaumetopoea pityocampa* over a period of four years (1991-1994) at Marikostino/Bulgaria. *Anzeiger für Schädlingskunde, Pflanzenschutz, Umweltschutz*, 71: 1–7.
- [20] Mirchev, P., Schmidt, G.H., Tsnakov, G. ve Avcı, M. (2004). Egg parasitoids of *Thaumetopoea pityocampa* (Den. & Schiff.) (Lep., Thaumetopoeidae) and their impact in SW Turkey. *Journal of Applied Entomology*, 128(8), 533–542.
- [21] Avcı, M., Morkoyunlu, M. ve Yılmaz, A. (2000). Kırmızı orman karıncası ve Isparta yöresinde transplantasyon çalışmaları. *T.C. Orman Bakanlığı Teknik Bülteni*, 1(2), 22–26.
- [22] Chatzimanolis, S., Cohen, I.M., Schomann, A.S. ve Solodovnikov, A. (2010). Molecular phylogeny of the mega-diverse rove beetle tribe Staphylinini (Insecta, Coleoptera, Staphylinidae). *Zoologica Scripta*, 39, 436–449.
- [23] Basso, A., Simonato, M., Cerretti, P., Paolucci, P. ve Battisti, A. (2016). A review of the “summer” *Thaumetopoea* spp. (Lepidoptera: Notodontidae, Thaumetopoeinae) associated with *Cedrus* and *Pinus*. *Turkish Journal of Forestry*, 17, 31-39.
- [24] Basso, A., Negrisol, E., Zilli, A., Battisti, A. ve Cerretti, P. (2017). A total evidence phylogeny for the processionary moths of the genus *Thaumetopoea* (Lepidoptera: Notodontidae: Thaumetopoeinae). *Cladistics*, 33, 557–573.
- [25] Trematerra, P., Scalercio, S. ve Scalercio, M. (2017). *Thaumetopoea hellenica* sp. n. and *Thaumetopoea mediterranea* sp. n. New Taxa From Southern Europe (Lepidoptera Notodontidae Thaumetopoeinae). *Redia*, 100, 3-10.
- [26] Trematerra, P. ve Colacci, M. (2018). Morphology and ethology of *Thaumetopoea hellenica* and *Thaumetopoea mediterranea* (Lepidoptera Notodontidae Thaumetopoeinae). *Redia*, 101, 13-22.
- [27] Simonato, M., Mendel, Z., Kerdelhué, C., Rousselet, J., Magnoux, E., Salvato, P., Roques, A., Battisti, A. ve Zane, L. (2007). Phylogeography of the pine processionary moth *Thaumetopoea wilkinsoni* in the Near East. *Molecular Ecology*, 16, 2273–2283.